



**FIRST UNIVERSITY OF NAPLES “ FEDERICO II”**

PHD SCHOOL IN:  
INNOVATIVE TECHNOLOGIES FOR MATERIALS,  
SENSORS AND IMAGING.

XXII CYCLE (2006-2009)

**THESIS**

**NUMERICAL-ANALYTICAL METHODS  
FOR PARTICLE ACCELERATORS**

**TUTOR**

Prof. VITTORIO G. VACCARO

**CANDIDATE**

MARCO PANNIELLO



## Summary

<b>Introduction</b> .....	7
<b>Chapter 1: Main Parameters and Adopted Methods</b> .....	13
1.1 Main Parameters.....	13
1.2 The Wire Method.....	20
1.3 The Modal Expansions in a Cylindrical Cavity.....	22
<b>Chapter 2: The Pillbox Cavity</b> .....	31
2.1 Generalities and Fields Expression.....	31
2.2 Matching the Magnetic Field.....	35
2.3 The Excitation Coefficients (PEC).....	38
2.4 The Excitation Coefficients in case of finite losses.....	42
2.5 The Equation System.....	46
2.6 The Longitudinal Coupling Impedance.....	48
2.7 Numerical results.....	55
<b>Chapter 3: The Thick Iris</b> .....	77
3.1 Generality and Fields Expression.....	77
3.2 Matching the Electric Field.....	82

3.3	The Excitation Coefficients (PEC+PMC).....	85
3.4	The Equation System.....	91
3.5	The longitudinal coupling impedance.....	93
3.6	Numerical Results.....	94
<b>Chapter 4: The Coaxial Setup.....</b>		<b>118</b>
4.1	Generalities and Fields Expression.....	118
4.2	Matching the Magnetic Field.....	122
4.3	The Excitation Coefficients (PEC).....	124
4.4	The excitation coefficients (Lossy).....	127
4.5	The Longitudinal Coupling Impedance.....	127
4.6	Numerical results.....	128
<b>Chapter 5 : Comparisons among Results of Various Codes.....</b>		<b>133</b>
5.1	Generalities.....	133
5.2	Analisis of the Pillbox Long. Coupling Impedance.....	135
5.3	Comparison with the Results of Wire Method.....	144
5.4	Comparison of the results with a commercial.....	150
<b>Conclusions.....</b>		<b>153</b>
<b>Appendix A.....</b>		<b>156</b>
<b>Appendix B.....</b>		<b>166</b>

**Appendix C**..... 171

**Appendix D**..... 184

**Bibliography**..... 189



# Introduction

Lately we have assisted to a dramatic increase of the design and realization of high energy and high intensity accelerators. In this contest are the high intensity Linacs for production of ultraviolet and X rays. These activities stimulated several Important Companies (i.e. Mitsubishi) to produce instrumentation specialized for the generation and the acceleration of electron beams of high intensity, where these beams consist in very short bunch trains (up to some tens of nanometers). One of most important features of this instrumentation is to avoid the beam quality perturbation because of the interaction with surrounding medium. This interaction appears because the bunches drag image currents and, consequently, Electromagnetic Energy is stored in the surrounding medium. A deformation of the EM Energy density may produce intense EM Field acting on the primary charges. This phenomenon is represented by the definition of ad hoc parameters: they are the Machine Impedance and the Wake Fields relevant to the frequency domain and time domain respectively. If these parameters exceed some thresholds, we have a deterioration of the beam quality and more in general, limit the maximum beam energy available.

A first approach to this problem is to solve the EM field equations with the appropriate boundary conditions and sources by means of numerical codes. Various type of the above mentioned codes have been developed (ABCI, ROCOCO,

Particle Studio, etc.) which should give the Coupling Impedance (Wake Fields) as function of frequency, for a variety of configuration of the surrounding medium. There are indications that, at least for some configurations and boundary conditions, the results of these codes are not satisfactory. Maybe this is due to the required multi-purpose goal, which sacrifices the reliability to the versatility. In some cases, the results even violate some fundamental physical principles as Energy Conservation. We will analyze this behaviour and we will formulate some hypothesis on the cause of these violation.

The impossibility to submit the portion of the machine to be tested using “in loco” a particle beam, in order to obtain the parameters of interest, forces the researchers to limit their tests and experiments to bench measurements on the Device Under Test (DUT) in a workshop.

In this case, a common approach is to resort to an experimental technique, introduced in 1974 by M.Sands e J.Rees on intuitive basis. This technique consists in replacing the bunch by an impulse riding on a wire, and to perform measurements by means of a Network Analyzer. If the TEM field produced by the electric impulse fairly reproduces the EM field generated by the bunch, the EM behaviour of the DUT induced by the wire, may give good indications on the behaviour of the DUT interacting with the particle beam. This method, which may give sensible indications, is still largely adopted for testing components of particle accelerators. However, even if this method has been largely studied, its results are only partially reliable at least in some range of frequencies, as it will be shown.

This is due to the presence of the wire that may perturb the measurement making uncertain some results.

We intent to resort to analytic/numerical methods to be implemented in homemade codes, conceived “ad hoc”, and therefore more reliable than multipurpose commercial codes. The proposed methods intrinsically limit their applications to the analysis of canonical models of rather simple configurations: cylindrical insertions coupled to cylindrical vacuum tanks such as, cavities, thick irises etc. To this end the method of Mode Matching (MM) has been adopted.

The basic idea of this technique is to represent the EM field in the cavities and in the waveguides by means of a complete set of orthogonal eigenmodes (vectors) of these items, considered as isolated and with homogeneous boundary conditions. In practice, this representation is useful because a limited number of modes are in general sufficient to have a good representation of the field behaviour and therefore of the electromagnetic interaction between the particle beam and the surrounding medium. When applied to finite domains, the Mode Matching Technique makes easy to introduce ohmic losses, in order to emulate real structures.

The structure to analyze is divided in subsets in which it is possible to identify stationary or travelling modes. In the subsets of infinite dimensions, only the travelling waves are taken into account. General rules to subdivide in subsets the device do not exist: one must proceed by attempts.

In order to solve the problem, one has to find the unknown coefficients of the modal expansions. On the borders of adjacent subsets, one has to impose the

continuity conditions of the EM-fields. Thus, a set of functional equations are obtained, equal to the border surfaces. Adopting the Ritz-Galerkin method, one can then project these equations on an orthogonal function set and, therefore, they change into an equal number of matrix/vector equations.

In the first phase the research was oriented on the study of an ideal cylindrical pillbox (PEC-PMC) cavity and one with finite conductivity, both inserted into a cylindrical vacuum chamber. In the ideal case, considerations about energetic balance enforce the real part of the impedance to be strictly zero below the cutoff frequency even if in this range resonances exist.

The second step in the work was to verify the agreement of the results by MM with those obtained by the Stretched Wire Method. The theory developed in connection with this method gives the longitudinal coupling impedance from the scattering parameters produced by the measurements on DUT by means of a Network Analyzer. However, since the MM can model the configuration of the Stretched Wire Method, we have first crosschecked the results of a bench measurement and the one obtained by means of the simulation of the Wire Method by means of MM.

This work, subdivided in five Chapters, can be summarized as follows:

- **Chapter 1:** in this chapter it is introduced the most relevant parameters to analyze the interaction between the beam and the surrounding medium. Furthermore, there is a detailed explanation of the adopted methods.

- **Chapter 2:** here is discussed the Mode Matching Technique applied to a Pillbox Cavity. We will use homogeneous boundary conditions and we will introduce material losses to simulate real devices.
- **Chapter 3:** In this chapter, the MM technique is applied to a Thick Iris. This is a basic study of the reliability of the MM technique with mixed boundary conditions. A convergence study and a comparison with another Mode Matching configuration will be exposed.
- **Chapter 4:** Here is an exhaustive treatment of the mode matching technique applied to Wire Method measurements.
- **Chapter 5:** In this chapter, we will compare the results by our adopted methods with those obtained by commercial codes. Furthermore, we will provide exhaustive treatment about the reliability of the wire method for frequency ranges that include the frequency region below the waveguides cutoff.



# **Chapter 1:**

## **Main Parameters and adopted Methods**

### **1.1 Main parameters**

The way to operate of an accelerator strongly rides on the electromagnetic interaction existing between the bunch of charged particles and the vacuum chamber in which it propagates. The detailed knowledge of this process is necessary to improve the accelerator performances. We can consider the beam as a set of charged particle bunches placed at a correct distance, which should preserve respective space-time positions assigned during the previous acceleration process. Travelling inside the vacuum chamber, the beam induces a secondary electromagnetic field that may influence its dynamics. For a relativistic particle in a perfect and homogeneous structure, the final effect of the secondary field is null. An accelerator can be seen as a device with feedback system in which every longitudinal or transverse beam perturbation can be amplified or attenuated by electromotive forces created by the perturbation itself. The electromagnetic field

induced by the beam is called Wake Field because it remains behind the moving charges.

The study of longitudinal and transverse dynamics needs the knowledge of some fundamental parameters:

- the longitudinal wake potential: it is the voltage variation of a charge, due to the field generated by another charge which precedes it; the longitudinal wake-field is responsible for the energy loss because it is essentially in phase with the particles;
- The transverse wake potential: it takes into account the transverse force applied to the beam due to the transverse wake-fields; its effect is to deflect the beam and, as a consequence, it can generate bunch stretching.

There are other parameters exploited to characterize the interaction beam-accelerator:

The Wake Potentials for charge unit are called *Wake Functions*.

The Fourier Transform of the Wake Potential is called *Coupling Impedance* and it results as function of the frequency.

The two parameters just introduced represent two different description of the same phenomenon, the electromagnetic coupling between beam and accelerator structure.

They depend by structures shape and not by bunch properties. The wake potential, mainly used for linear accelerators, allows a description in time domain, while

Coupling Impedance represents the problem in the frequency domain. Usually, it is employed for circular accelerators, for their intrinsic periodicity.

To better define the concept of wake field, we can consider first a situation of a singular particle that will be use to define a point potential wake function. The final wake field will be the average value on the whole interaction zone for every beam particle. Therefore, let us consider **Fig. 1-1**, with  $q_1$  as a moving charge with fixed velocity parallel to the vacuum chamber axis,  $r_1$  as the vector that indicate the transverse position,  $z_1$  as the vector that indicate the longitudinal position.

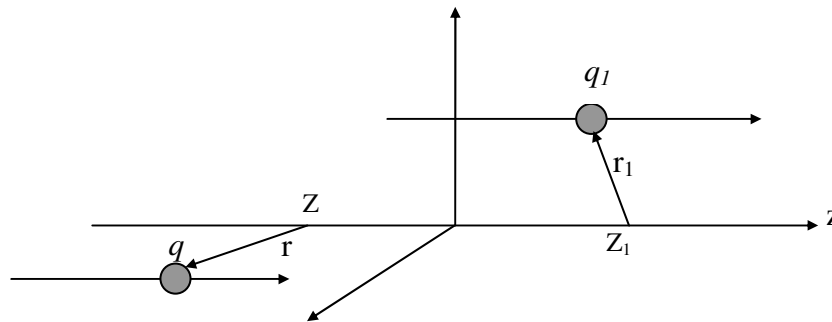


**Fig. 1-1. Reference Frame**

The electromagnetic field produced in the framework by  $q_1$  can be obtained resolving the Maxwell equations with appropriate boundary conditions. This field influences the dynamics of both  $q_1$  and  $q$ .

We can define the energy lost by  $q_1$  as the work that the electromagnetic field does on it [1]:

$$U_{11}(r_1) = - \int_{-\infty}^{\infty} F(r, z, r_1, z_1, t) dz \quad t = \frac{z_1}{v} \quad (1.1)$$

$$U_{21}(r, r_1; \tau) = - \int_{-\infty}^{\infty} F(r, z, r_1, z_1, t) dz \quad t = \frac{z_1}{v} + \tau$$

with  $F$  the Lorentz Force.

We can notice that previous integrals are calculated on an infinite path and it doesn't correspond to a physical condition, but it is to underline that these expressions are an evaluation of the energy gain as good as the wave length is smaller than the considered length.

Besides, we can consider the longitudinal wake function as the energy get by the secondary charge  $q$  for charge unit  $q$  and  $q_1$  [1]:

$$w_z(r, r_1; \tau) = \frac{U_{21}(r, r_1; \tau)}{q_1 q} \quad [\text{V/C}] \quad (1.2)$$

The loss factor as the lost energy by  $q_1$  for unit of squared charge

$$k(r_1) = \frac{U_{11}(r_1)}{q_1^2} \quad [\text{V/C}] \quad (1.3)$$

Finally, we can define the Longitudinal Coupling Impedance as the Fourier Transform of the wake function for a point like charge.

$$Z_{||}(r, r_1; \omega) \equiv \int_{-\infty}^{\infty} w_z(r, r_1; \tau) e^{-j\omega\tau} d\tau \quad (1.4)$$

The wake function can be obtained from longitudinal Impedance through the Fourier Anti-transform. Besides, it counts the typical properties of the Fourier Transform. Another formulation of the Longitudinal Coupling Impedance can be derived by the previous formula considering as a source a beam which has a longitudinal sinusoidal modulation in the particle density. Allowing for the field produced by this beam interacting with the surrounding medium we can derive the Longitudinal Coupling Impedance as function of the wave number  $k$ .

$$Z_{||}(k) = - \int_{-\infty}^{\infty} E_z(r=0, z) e^{j k / \beta z} dz$$

We may consider also wake fields and impedances produced by higher order sources: dipoles, multipoles etc. These sources will lead to the relevant wakefields and impedances. We will limit ourselves to the longitudinal case and, from now on, the longitudinal impedance will be called impedance “tout court” and the sub index

will be dropped. Just to give an example, we give a criterion for longitudinal stability of a coasting beam in a circular accelerator

$$\left| \frac{Z}{n} \right| \leq F \frac{m_0 c^2 \beta^2 \gamma |\eta| (\Delta p / p)^2}{e I_0}$$

Where

$n$  = harmonic number

$e$  = elementary charge

$I_0$  = stored current

$\Delta p$  = momentum spread

$\eta$  = slippage

$m_0$  = particle rest mass

$F$  = form factor (between 1 and 1.6)

Generally, the impedance is a complex function and for this reason can be split in real and imaginary part. The real part results related to beam losses.

As we told before, when the bunch crosses various insertions with variable cross section installed in the vacuum chamber, it excites secondary fields: some of them remain localized around the bunch and others are localized in resonating structures and others propagate in the vacuum chamber.

This assertion can be demonstrated in the ideal case of an infinite length vacuum chamber, representing the longitudinal component of the electric field as a travelling wave through the chamber axis direction with random phase velocity. For

high power devices, wake fields induced by particles can strongly modify the distribution of the accelerating field. Furthermore, when the bunch crosses a cavity, it excites not only the fundamental mode but also the high order modes. They can induce beam energy losses, admittance deterioration (essentially in the bunch area) and instability phenomena with particle losses. Generally, as a consequence of these effects, one can have severe limitations of maximum electric current circulating in the accelerator.

One can reasonably affirm that studies on the wake fields, on coupling impedance as a function of the frequency and, more generally, on the interaction between bunch and surrounding media, are very important to reach high quality beams coming out the accelerators. Therefore, it should be strongly recommended in projecting stage, if it is possible, to look for:

- Developing cavities with as less as possible high order modes (and with very little Q factors) with frequencies not coincident with the fundamental mode higher harmonics, with the purpose of reducing the coupling between beam and high order modes and therefore to minimize the energy losses;
- Testing devices devoted to the attenuation of high order modes excited by the beam to avoid them to subtract energy stored in the cavity.

In some cases, with highly collimated high energy beams, as the Free Electron Laser ones, this goal is very hard to reach.

## 1.2 The wire method

This technique was proposed in 1974 by M. Sands and J. Rees which, on intuitive considerations, with the purpose to measure the energy lost by an electron bunch riding through a particle accelerator component to test, as a resonant cavity. This method, that allows to get measurements sufficiently meaningful without need to use the particles beam but simply with the normal equipments for bench measurements, it is still broadly used in the study of particle accelerator components. The simulation of the bunch passage through the device under test (DUT) is realized inserting inside the structure a metallic wire along the beam axis, in which flows a current impulse having a spatial shape similar to the bunch [2]. This configuration allows to gain the scattering parameters of the considered structure as feed by two coaxial waveguides, and therefore also the longitudinal coupling impedance.

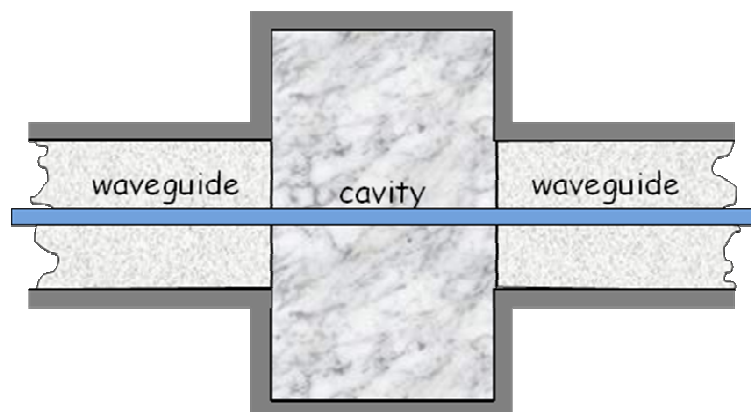


Fig. 1-2. Representation of a circular cross section pillbox and the wire stretched along beam axis.

The basic idea consists of consider to be possible, with the purpose of the energy losses evaluation by a particle bunch caused by the non-uniformity in a vacuum chamber, the substitution of the current impulse produced by the beam, with a current impulse having the same temporal behaviour, flowing through a wire stretched along the beam axis. One can see that the electric charge associated to a particle beam crossing through a generic vacuum chamber produces inside of it electromagnetic field, which produces on the walls of the structure a charge distribution and induced currents. Stretching a metallic wire along the cavity axis, and neglecting the coupling effect with the inside radial line, it makes the cavity similar to a coaxial transmission line. It is worth of note that the introduced perturbation totally modifies the boundary conditions of the system. In fact, the section of the fundamental structure obtained will have not the simply connection property. As known, this has as a consequence the possibility to have TEM modes and all frequencies propagating modes as a solution of the Maxwell equations. Nevertheless, carrying a current impulse having the same temporal behaviour of the one related to the beam on the conductor, it has been shown that, the TEM field produced by this impulse exactly reproduces the field produced by the beam if initial energy is equal to that of the bunch, unless in the immediate proximity of the wire. The intuition suggests that independently by the wire presence, the field generated initially by the current impulse is the same of the one produced by the beam, provided that the wire dimensions do not perturb the electromagnetic field

existing without the wire. After this, the first charges and current induced on structure walls can be held equal in the two cases. This means that in a very first moment the cavity doesn't acknowledge the boundary condition variation. All affirmed till now, based exclusively on intuitive considerations, lead to believe that if the bunch duration results to be small in comparison to the time of relaxation of the cavity with the wire, then the energy loss by the impulse that circulates on the conductor, and lost as electromagnetic energy, it will be next to that lost by the particles beam emulated. Therefore, the electromagnetic behaviour of the cavity, with the wire inserted, is strongly indicative of the attenuation suffered from the High Order Modes and at the same time allows to understand the coupling between cavity and beam, thus to appraise the cavity loss factor in function of the frequency [2].

### **1.3 The modal expansions in a cylindrical cavity**

The basic idea of the proposed analytical approach is to subdivide the system in subsets (cavities and the waveguides) characterized by homogeneous boundary conditions and to expand the field as a superposition of the relevant eigenmodes.

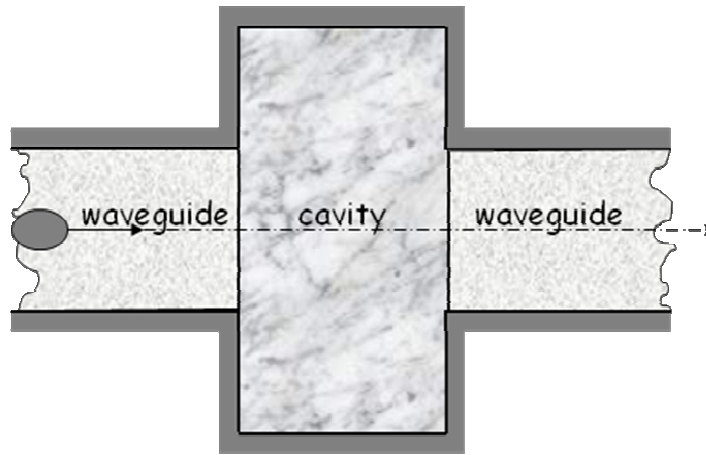


**Fig. 1-3. Representation of a circular cross section pillbox subdivided in subsets.**

The solution is found by matching the expansions solutions on the ports that separate the subsets. This can be easily done for the tangential component of magnetic field, while for the Electric Field is not possible because its tangential component on ports is zero by definition. The expansion has non-uniform convergence on these boundaries. However, it will be shown that it is possible to overcome this inconvenience.

The complete set of eigenmodes consists in divergenceless modes plus irrotational modes. Taking into account the circular symmetry of the boundaries and of the excitations in cavity, the field can be expressed in terms of a complete set of basic functions in a cylindrical frame  $(r, z)$ , in the following way [ 3]:

$$\vec{E} = \sum_n V_n \vec{e}_n + \sum_n F_n \vec{f}_n \quad (1.5)$$

$$\vec{H} = \sum_n I_n \vec{h}_n + \sum_n G_n \vec{g}_n$$

where the above modes satisfy the following equations

$$\nabla \times \vec{e}_n = k_n \vec{h}_n \Rightarrow \nabla \cdot \vec{h}_n = 0; \quad \nabla \times \vec{h}_n = k_n \vec{e}_n \Rightarrow \nabla \cdot \vec{e}_n = 0 \quad (1.6)$$

$$\vec{f}_n = \nabla \phi_n \Rightarrow \nabla \times \vec{f}_n = 0; \quad \vec{g}_n = \nabla \phi_n \Rightarrow \nabla \times \vec{g}_n = 0$$

The boundary conditions are homogeneous for the tangential Electric Field on the surface  $S_1$  and for the tangential Magnetic Field on the surface  $S_2$ , where  $S_1 \cup S_2$  is the whole surface.

Furthermore, as usual, the modes are orthonormal, so that is:

$$\int_V \vec{e}_n(r) \cdot \vec{e}_m^*(r) dV = \int_V \vec{h}_n(r) \cdot \vec{h}_m^*(r) dV = \delta_{nm} \quad (1.7)$$

$$\int_V \vec{f}_n(r) \cdot \vec{f}_m^*(r) dV = \int_V \vec{g}_n(r) \cdot \vec{g}_m^*(r) dV = \delta_{nm}$$

$$\left\{ \begin{array}{l} Z_0 I_m = \frac{jk \int_{S_1} (\vec{E} \times \vec{h}_m^*) \cdot \hat{n} dS + Z_0 k_m \int_{S_2} (\vec{H} \times \vec{e}_m^*) \cdot \hat{n} dS}{k^2 - k_m^2} \\ V_m = \frac{k_m \int_{S_1} (\vec{E} \times \vec{h}_m^*) \cdot \hat{n} dS - jZ_0 k \int_{S_2} (\vec{H} \times \vec{e}_m^*) \cdot \hat{n} dS}{k^2 - k_m^2} \end{array} \right. \quad (1.8)$$

The problem of the non-uniform convergence is solved [3] resorting to the modal excitation coefficients (the current  $I_{ps}$  or the tension  $V_{ps}$ ) are drawn considering the coupling of the cavity with the guides. Using the Maxwell equations and exploiting modal orthonormality, after some passages one can reach the followings relationships between the equivalent sources and the excitation coefficients

$$\zeta_0 I_{ps} = \frac{jk}{k^2 - k_p^2 - k_s^2} \int_S \hat{n} \times \vec{E} \cdot \vec{H}_{ps}^* dS \quad (1.9)$$

$$V_{ps} = -\frac{j\sqrt{k_p^2 + k_s^2}}{k} \zeta_0 I_{ps}$$

where  $\zeta_0$  is the impedance of the medium that fill the cavity and  $\hat{n}$  is the unit vector outgoing from surface cavity. In the propagation region, the propagation constant is:

$$k_{ps}^2 = k_p^2 + k_s^2 = \left(\frac{c_p}{a}\right)^2 + \left(\frac{\pi s}{2L}\right)^2 \quad (1.10)$$

**it is worth to notice that the expressed tangential field in eq.(1.9) won't be the same expressed by eq.(1.5) because the not uniform convergence of the series on cavity surface.** The integral in eq.(1.5), as we can see afterwards, can be calculated only on the coupling surfaces with the guides and starting from its modes. The procedure has certainly some critical points on boundary edges in which, the field would be infinite. But this is not a problem, if we consider integral parameters that mediate on some local difficulties. The coefficients in the  $I_{ps}$  expansions and those correspondents of the guides are unknown and they must be drawn by the conditions of continuity guide-cavity, as we will show in next Chapters.



# Chapter 2:

## The Pillbox cavity

### 2.1 Generalities and Fields Expression

In this chapter, we will deal with the pillbox cavity case. We want to calculate the Longitudinal Coupling Impedance using the Mode Matching technique as already successfully done for the iris. This technique can easily analyze the coupling between the cylindrical cavity and the waveguides characterized by circular symmetry that represent the vacuum chamber as shown in **Fig.2-1**. Let us consider a charged particle riding the positive  $z$  direction, along the symmetry axis of a Perfect Electric Conductor vacuum chamber. We assume the particle moving with constant velocity, even though the vacuum chamber discontinuities would imply little velocity changes. Like in iris case, this approximation does not affect our calculus. Similarly, as it was done for the iris, we assume that the forcing primary field is produced by the spatial spectrum of the previously mentioned point like particle  $q$ , riding on the axis at velocity  $v = \beta c$ .

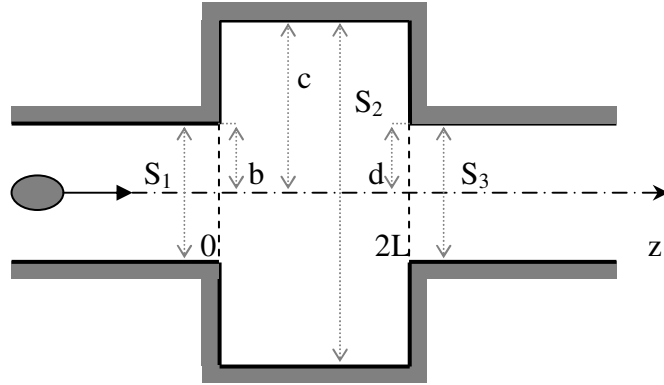


**Fig. 2-1. Scheme of a Pillbox cavity:  $b = d \equiv$  waveguides radius;  $c \equiv$  cavity radius;  $2L \equiv$  cavity length.**

It is worth of note that we have TM modes, with radial and longitudinal component of Electric Field and azimuthal component of Magnetic Field, as follows:

$$\begin{aligned}
 E_z^0(r,z) &= \frac{jq\zeta_0\kappa}{2\pi\gamma|\beta|} \left[ K_0(\kappa r) - \frac{I_0(\kappa r)}{I_0(\kappa g)} K_0(\kappa g) \right] \tilde{H}(g-r) \exp(-jkz/\beta) \text{sng}(k/\beta) \\
 E_r^0(r,z) &= \frac{q\zeta_0\kappa}{2\pi|\beta|} \left[ K_1(\kappa r) + \frac{I_1(\kappa r)}{I_0(\kappa g)} K_0(\kappa g) \right] \tilde{H}(g-r) \exp(-jkz/\beta) \\
 H_\phi^0(r,z) &= \frac{q\kappa}{2\pi} \left[ K_1(\kappa r) + \frac{I_1(\kappa r)}{I_0(\kappa g)} K_0(\kappa g) \right] \tilde{H}(g-r) \exp(-jkz/\beta) \text{sng}(\beta)
 \end{aligned} \tag{2.1}$$

where  $\mathbf{g} = \mathbf{b}$  (in the pipe);  $\mathbf{g} = \mathbf{c}$  (in the cavity) ,  $\kappa = k/\beta\gamma$  ,  $\mathbf{q}$  is the particle charge

(In the following formulas we adopted  $q=1$  for simplicity), and  $\tilde{H}(g-r)$  is the Heaviside function.

As expressed in detail in **Appendix B**, resonant modes in a cylindrical structure of generic radius  $\mathbf{g}$  are represented by the formula

$$\Phi_{1q}^g(k_q r) = \frac{J_1(k_q r)}{g\sqrt{\pi}J_1(\alpha_q)} \quad (2.2)$$

where  $k_q = \alpha_q/g$   $\alpha_q$  is the  $q^{\text{th}}$  zero of the equation  $J_0(\alpha) = 0$ .

The EM Traveling Modes inside a waveguide of radius  $\mathbf{g}$  are

$$\Phi_{0q}^g(k_q r) = \frac{J_0(k_q r)}{g\sqrt{\pi}J_1(\alpha_q)} \quad (2.3)$$

For a PEC cylindrical cavity of radius  $\mathbf{c}$  and length  $\mathbf{2L}$  the normalized eigenmodes are [13]

$$\begin{aligned} \vec{e}_{ps}(r, z) &= e_{ps}(r, z)\hat{r} + e_{ps}^z(r, z)\hat{z} = \\ &= \frac{1}{k_{ps}} \sqrt{\frac{\epsilon_s}{2L}} \left[ -k_s \sin(k_s z) \Phi_{1p}^c(k_p r) \hat{r} + k_p \cos(k_s z) \Phi_{0p}^c(k_p r) \hat{z} \right] \end{aligned} \quad (2.4)$$

$$\vec{h}_{ps}(r, z) = h_{ps}(r, z)\hat{\phi} = \sqrt{\frac{\epsilon_s}{2L}} \cos(k_s z) \Phi_p^c(k_p r) \hat{\phi}$$

where  $\epsilon_s$  is the Neumann symbol ( $\epsilon_s=1$  if  $s=1$ ,  $\epsilon_s=2$  else ) and  $k_s = \frac{\pi s}{2L}$ .

At difference with the previous case, for the cavity we will resort to eigenmodes of all PEC surfaces. This implies a change in the function that describes the longitudinal behavior. Furthermore, we will not need to take into account the divergenceless modes. The explicit expression of the fields is given as an expansion of the eigenmodes weighted with the expansion coefficients  $I_{ps}$  and  $V_t$  in the cavities and in the waveguides respectively:

$$\begin{cases} E_{1z}(r, z) = j \sum_t V_{1t}^- \frac{k_t Y_t^b}{k} \Phi_{0t}^b(k_t r) \exp(jz \sqrt{k^2 - k_t^2}) \\ E_{1r}(r, z) = \sum_t V_{1t}^- \Phi_{1t}^b(k_t r) \exp(jz \sqrt{k^2 - k_t^2}) \\ H_{1\phi}(r, z) = - \sum_t V_{1t}^- \frac{Y_t^b}{Z_0} \Phi_{1t}^b(k_t r) \exp(jz \sqrt{k^2 - k_t^2}) \end{cases} \quad z < 0 \quad (2.5)$$

$$\begin{cases} E_z^c(r, z) = -jZ_0 \sum_{p,s} \frac{k_p}{k} \sqrt{\frac{\epsilon_s}{2L}} \cos(k_s z) \Phi_{0p}^c(k_p r) I_{ps} \\ E_r^c(r, z) = -Z_0 \sum_{p,s} \sqrt{\frac{\epsilon_s}{2L}} k_s \sin(k_s z) \Phi_{1p}^c(k_p r) I_{ps} \\ H_\phi^c(r, z) = \sum_{p,s} \sqrt{\frac{\epsilon_s}{2L}} \cos(k_s z) \Phi_{1p}^c(k_p r) I_{ps} \end{cases} \quad 0 < z < 2L \quad (2.6)$$

$$\begin{cases} E_{2z}(r, z) = -j \sum_t V_{2t}^+ \frac{k_t Y_t^b}{k} \Phi_{0t}^b(k_t r) \exp[-j(z-2L)\sqrt{k^2 - k_t^2}] \\ E_{2r}(r, z) = \sum_t V_{2t}^+ \Phi_{1t}^b(k_t r) \exp[-j(z-2L)\sqrt{k^2 - k_t^2}] \\ H_{2\phi}(r, z) = \sum_t V_{2t}^+ \frac{Y_t^b}{Z_0} \Phi_{1t}^b(k_t r) \exp[-j(z-2L)\sqrt{k^2 - k_t^2}] \end{cases} \quad 2L < z \quad (2.7)$$

where

$$Y_t^b = \frac{k}{\sqrt{k^2 - (\alpha_t/b)^2}} = \frac{1}{Z_t^b}$$

( $b$  is the waveguide radius and  $t$  is the index of the  $t^{\text{th}}$  zero). The total field inside all regions is given by the superposition of the primary fields in **eq.(2.1)** and the fields just defined. This superposition will be the expression used in the next paragraph, for the Field Continuity.

## 2.2 Matching the magnetic field

We tackle the problem in the same way as done for the iris. Namely assuming on the surfaces and on the ports the primary fields and impose that the modes must cancel this primary fields. We may only consider the continuity of the magnetic field tangential component on the two ports connecting the waveguides and the

cavity, as already done for the Electric Field in the iris case. On the surfaces 1,2 the total magnetic field continuity is written as:

$$\begin{cases} H_{\varphi}^0(r,0^-) + H_{\varphi}(r,0^-) = [H_{\varphi}^0(r,0^+) + H_{\varphi}(r,0^+)]\tilde{H}(b-r) & 0 \leq r \leq b \\ H_{\varphi}^0(r,2L^+) + H_{\varphi}(r,2L^+) = [H_{\varphi}^0(r,2L^-) + H_{\varphi}(r,2L^-)]\tilde{H}(b-r) & 0 \leq r \leq b \end{cases} \quad (2.8)$$

where we have taken into account the primary field indicated by superscript “0”, and  $\tilde{H}(b-r)$  is the Heaviside step function needed to limit the integral path to the ports instead of the total interface surfaces. We continue following the same procedure as done for the iris case, by adopting the Ritz Galerkin method, projecting **eq.(2.8)** on the waveguide eigenfunctions  $\Phi_{1r}^b(k,r)$  and obtaining the following system:

$$\begin{cases} A_{1t} - Y_0 Y^b V_{1t}^- = \sum_p M_{pt} I_{1p} \\ A_{2t} + Y_0 Y^b V_{2t}^+ = \sum_p M_{pt} I_{2p} \end{cases} \quad (2.9)$$

where the vectors  $A_{1t}$  and  $A_{2t}$  are defined as

$$A_{1t} = \int_{S_1} H_{\varphi}^0(r, 0^-) \Phi_{1t}^b(k_t r) dS - \int_{S_2} [H_{\varphi}^0(r, 0^+) \Phi_{1t}^b(k_t r)] \tilde{H}(b-r) dS \quad (2.10)$$

$$A_{2t} = A_{1t} e^{\frac{-jk2L}{\beta}}$$

and the matrix  $M_{pt}$  is defined as

$$M_{pt} = 2\pi \int_0^b \Phi_{1p}^c(k_p r) \Phi_{1t}^b(k_t r) r dr \quad (2.11)$$

and

$$I_{1p} = \sum_s \sqrt{\frac{\epsilon_s}{2L}} I_{ps}$$

$$I_{2p} = \sum_s (-1)^s \sqrt{\frac{\epsilon_s}{2L}} I_{ps} \quad (2.12)$$

are functions of the excitation coefficients  $I_{ps}$ .

The explicit expressions of the vectors  $A_i$  and the matrix  $M_{pt}$  are given in **Appendix C**.

The system expression using matrices and vectors is represented in the following equation

$$\begin{cases} \underline{A}_1 - Y_0 \underline{Y}^b \underline{V}_1^- = \underline{M}^T \underline{I}_1 \\ \underline{A}_2 + Y_0 \underline{Y}^b \underline{V}_2^+ = \underline{M}^T \underline{I}_2 \end{cases} \quad (2.13)$$

## 2.3 The excitation coefficients (PEC)

The procedure adopted here is analogous to the one adopted for the iris again. Because of the new boundary conditions, the only difference is that we will resort to the excitation coefficients  $I_{ps}$  instead of  $V_{ps}$ . Therefore, the expression of  $I_{ps}$  is:

$$I_{ps} = \frac{jkY_0}{k^2 - k_p^2 - k_s^2} \int_S \hat{n} \times \vec{E} \cdot \vec{h}_{ps}^* dS \quad (2.14)$$

where  $S$  defines the ideal cylindrical cavity surface,  $\vec{E}$  is the total electric field,  $\hat{n}$  is the outgoing unity vector orthogonal to this surface and  $h_{ps}$  is given by **eq.(2.4)**.

On the lateral surface of this cylinder, for a lossless material,  $\hat{n} \times \vec{E}$  is null. Let us define  $S_1$  and  $S_2$  as the surfaces of the two bases. On these surfaces, only the radial components of the total Electric Field have to be taken into account.

Therefore, one can write the **eq.(2.14)** as

$$\begin{aligned}
 I_{ps} &= \frac{jkY_0}{k^2 - k_p^2 - k_s^2} \left[ - \int_{S_1} \hat{z} \times \vec{E}(r, 0^+) \cdot \vec{h}_{ps}^*(r, 0) dS + \int_{S_2} \hat{z} \times \vec{E}(r, 2L^-) \cdot \vec{h}_{ps}^*(r, 2L) dS \right] = \\
 &= \frac{jkY_0}{k^2 - k_p^2 - k_s^2} \left[ - \int_{S_1} E_r^c(r, 0^+) \cdot h_{ps}^*(r, 0) dS + \int_{S_2} E_r^c(r, 2L^-) \cdot h_{ps}^*(r, 2L) dS \right]
 \end{aligned} \tag{2.15}$$

where  $\hat{z}$  is the unit vector having the z axis direction.

We impose the boundary conditions of the tangential Electric Field on the surfaces  $S_1$  and  $S_2$ . Even if the radial component of the modes vanishes on these surfaces (see eq.(2.6) ), however they must behave a non-uniform convergence to values different from zero such as to satisfy the following conditions:

$$\begin{aligned}
 E_r^c(r, z = 0^+) + E_r^0(r, z = 0^+) &= \left[ E_r^0(r, z = 0^-) + \sum_t V_{1t}^- \Phi_{1t}^b(k_t r) \right] \tilde{H}(b - r) \\
 E_r^c(r, z = 2L^-) + E_r^0(r, z = 2L^-) &= \left[ E_r^0(r, z = 2L^+) + \sum_t V_{2t} \Phi_{1t}^b(k_t r) \right] \tilde{H}(b - r)
 \end{aligned} \tag{2.16}$$

This equation for the tangential components can be interpreted that the Electric Field of the resonant modes plus the impressed Electric Field inside the cavity:

- For  $b < r < c$  must be zero because of the perfect conducting walls on the corona.

- Must be continuous and equal to the sum of the Electric Field of the traveling modes plus the impressed Electric Field inside the waveguides.

Taking into account the definition of the matrix element  $M_{pt}$  given by **eq.(2.11)**, one may get the formula:

$$I_{ps} = \frac{jkY_0}{(k^2 - k_{ps}^2)} \sqrt{\frac{\epsilon_s}{2L}} \left[ (-1)^s \cdot \left( -N_{2p} + \sum_t M_{pt} V_{2t}^+ \right) - \left( -N_{1p} + \sum_t M_{pt} V_{1t}^- \right) \right] \quad (2.17)$$

where the known vectors  $N_{1p}$  and  $N_{2p}$ , the extended expression of which is given in **Appendix C**, are given by the following formula:

$$N_{1p} = -2\pi \int_0^c \left[ E_r^0(r, z=0^-) \cdot \tilde{H}(b-r) - E_r^0(r, z=0^+) \right] \cdot \Phi_p^c(k_p r) r dr \quad (2.18)$$

$$N_{2p} = N_{1p} e^{\frac{-jk2L}{\beta}}$$

By inserting the just written equation in the expression of  $I_{1p}$  and  $I_{2p}$  given by **eq.(2.12)**, we get:

$$\begin{aligned}
 I_{1p} &= \frac{jkY_0}{2L} \left\{ \left[ \sum_s \frac{\epsilon_s (-1)^s}{k^2 - k_p^2 - k_s^2} \right] \left( -N_{2p} + \sum_t M_{pt} V_{2t}^+ \right) - \left[ \sum_s \frac{\epsilon_s}{k^2 - k_p^2 - k_s^2} \right] \left( -N_{1p} + \sum_t M_{pt} V_{1t}^- \right) \right\} \\
 I_{2p} &= \frac{jkY_0}{2L} \left\{ \left[ \sum_s \frac{\epsilon_s}{k^2 - k_p^2 - k_s^2} \right] \left( -N_{2p} + \sum_t M_{pt} V_{2t}^+ \right) - \left[ \sum_s \frac{\epsilon_s (-1)^s}{k^2 - k_p^2 - k_s^2} \right] \left( -N_{1p} + \sum_t M_{pt} V_{1t}^- \right) \right\}
 \end{aligned} \tag{2.19}$$

A key feature of these expressions is that the two sums with the s-index can be put in a closed form. This is a general property and it is related to the modal expansion of Green Function. In addition to the undoubted advantage of the analytical sum, one has the further advantage that the matrices are reduced of one dimension. The electromagnetic problems will also benefit of this behavior: all the longitudinal electromagnetic modes are taken into account and therefore only a few transverse modes are sufficient to describe the phenomenon.

For the sum of the series in square brackets, we adopt the same procedure as done for the iris, so

$$\begin{aligned}
 I_{1p} &= jY_0 Y_p^c \left[ \csc(2LkZ_p^c) \cdot \left( \sum_t M_{pt} V_{2t}^+ - N_{2p} \right) - \cot(2LkZ_p^c) \cdot \left( \sum_t M_{pt} V_{1t}^- - N_{1p} \right) \right] \\
 I_{2p} &= jY_0 Y_p^c \left[ \cot(2LkZ_p^c) \cdot \left( \sum_t M_{pt} V_{2t}^+ - N_{2p} \right) - \csc(2LkZ_p^c) \cdot \left( \sum_t M_{pt} V_{1t}^- - N_{1p} \right) \right]
 \end{aligned} \tag{2.20}$$

where  $Z_p^c = \frac{\sqrt{k^2 - (\alpha_p/c)^2}}{k} = \frac{1}{Y_p^c}$  ( $\mathbf{c}$  is the cavity cross section radius).

Expressing the above formula in terms of matrices and vectors we get:

$$\begin{aligned} \underline{I}_1 &= jY_0 \underline{Y}^c \left[ \csc(2kL\underline{Z}^c) \cdot (\underline{M} \underline{V}_2^+ - \underline{N}_2) - \cot(2kL\underline{Z}^c) \cdot (\underline{M} \underline{V}_1^- - \underline{N}_1) \right] \\ \underline{I}_2 &= jY_0 \underline{Y}^c \left[ \cot(2kL\underline{Z}^c) \cdot (\underline{M} \underline{V}_2^+ - \underline{N}_2) - \csc(2kL\underline{Z}^c) \cdot (\underline{M} \underline{V}_1^- - \underline{N}_1) \right] \end{aligned} \quad (2.21)$$

## 2.4 The Excitation Coefficients in case of finite losses

So far, we have discussed of a PEC device. Therefore, we spoke about a structure characterized by the following properties:

- Electric field is perpendicular to the walls.
- The current in the walls is a surface current.
- No energy dissipation in the walls.
- Below cutoff the field amplitude becomes infinite at resonance frequencies.

When we consider a lossy device, the above properties will change because of the finite conductivity. There will be energy losses in the walls that limit the Fields amplitude at the resonance frequencies. It will be still very large, but not infinite. Furthermore, the current in the walls becomes a volume current with penetration dept depending on the material. The most important change for our evaluations is that the Electric field has a tangential component at the wall. This component is

very little and depends on the penetration depth, but we need to add it to **eq.(2.14)** as a term under integral.

The finite conductivity is represented by the surface impedance

$$Z_s = \frac{1+j}{\sigma \delta} \quad (2.22)$$

where  $\sigma$  and  $\delta$  represent the material conductivity and the penetration depth respectively [3, 4].

The Surface Impedance has the meaning that, on the metallic surfaces, there is a relationship between the tangential component of the Electric Field and the Magnetic Field, given by:

$$\vec{E}_l = Z_s \hat{n} \times \vec{H} \quad (2.23)$$

where the subscript  $l$  indicates losses. This term has to be added to the **eq.(2.14)** and then the excitation coefficients formula becomes:

$$\begin{aligned}
 I_{ps} &= \frac{jkY_0}{k^2 - k_p^2 - k_s^2} \left[ \int_{S_1+S_2} (\vec{E}_{tot} \times \vec{h}_{ps}) \cdot \hat{n} ds + \int_S (\hat{n} \times \vec{E}_l) \cdot \vec{h}_{ps} ds \right] = \\
 &= \frac{jkY_0}{k^2 - k_p^2 - k_s^2} \left[ \int_{S_1+S_2} (\vec{E}_{tot} \times \vec{h}_{ps}) \cdot \hat{n} ds \right] - \frac{jkY_0 Z_s}{k^2 - k_p^2 - k_s^2} \int_S \vec{H} \cdot \vec{h}_{ps} ds = \quad (2.24) \\
 &= \frac{jkY_0}{k^2 - k_p^2 - k_s^2} \left[ \int_{S_1+S_2} (\vec{E}_{tot} \times \vec{h}_{ps}) \cdot \hat{n} ds \right] - \frac{jkY_0 Z_s}{k^2 - k_p^2 - k_s^2} \int_S \sum_{vw} I_{vw} \vec{h}_{vw} \cdot \vec{h}_{ps} ds
 \end{aligned}$$

We remark that the excitation coefficients  $I_{ps}$  are significantly different from zero only at frequencies such that

$$k = \sqrt{k_p^2 + k_s^2}$$

Therefore, in the above equation we may neglect in the sum all the excitation coefficients but  $I_{ps}$ . So that, we may approximate the expression given by **eq.(2.24)**

as

$$\begin{aligned}
 I_{ps} &= \frac{jkY_0}{k^2 - k_p^2 - k_s^2} \int_{S_1+S_2} (\vec{E}_{tot} \times \vec{h}_{ps}^*) \cdot \hat{n} dS - \frac{jkY_0 Z_s}{k^2 - k_p^2 - k_s^2} I_{ps} \int_S \vec{h}_{ps} \cdot \vec{h}_{ps}^* dS = \\
 &= \frac{jkY_0}{(k^2 - k_{ps}^2)} \int_{S_1+S_2} (\vec{E}_{tot} \times \vec{h}_{ps}^*) \cdot \hat{n} dS - \frac{jkY_0 Z_s}{k^2 - k_{ps}^2} I_{ps} \frac{\epsilon_s}{2L} \int_S [\cos(k_s z) \Phi_p^c(k_p r)]^2 dS \quad (2.25)
 \end{aligned}$$

By means of some algebra described in the **Appendix C**, we finally obtain the following formula:

$$I_{ps} = \frac{jkY_0}{(k^2 - k_{ps}^2) + jkY_0Z_s \left( \frac{2}{c} + \frac{\epsilon_s}{L} \right)} \int_{S_1+S_2} (\vec{E}_{tot} \times \vec{h}_{ps}^*) \cdot \hat{n} dS \quad (2.26)$$

Before substituting the just written formula in **eq.(2.12)** to obtain the excitation coefficients, we need to resort to a new definition of modal impedance as:

$$Z_p^c = \frac{\sqrt{k^2 - k_p^2 + \Delta}}{k}$$

And define the new quantities

$$\delta_p = \frac{jk^2Y_0Z_s}{2L^2 [(k^2 - k_p^2) + \Delta] [(k^2 - k_p^2) + \Delta - jkY_0Z_s/L]} \quad (2.27)$$

$$\Delta = jkY_0Z_s \left( \frac{2}{c} + \frac{2}{L} \right)$$

As demonstrated in **Appendix C**, the excitation currents for a lossy Pillbox are:

$$\begin{aligned}
 \underline{I}_1 &= jY_0 \left\{ \left[ \underline{\delta} + \underline{Y}^c \csc(2kL\underline{Z}^c) \right] \cdot (\underline{M}\underline{V}_2^+ - \underline{N}_2) - \left[ \underline{\delta} + \underline{Y}^c \cot(2kL\underline{Z}^c) \right] \cdot (\underline{M}\underline{V}_1^- - \underline{N}_1) \right\} \\
 \underline{I}_2 &= jY_0 \left\{ \left[ \underline{\delta} + \underline{Y}^c \cot(2kL\underline{Z}^c) \right] \cdot (\underline{M}\underline{V}_2^+ - \underline{N}_2) - \left[ \underline{\delta} + \underline{Y}^c \csc(2kL\underline{Z}^c) \right] \cdot (\underline{M}\underline{V}_1^- - \underline{N}_1) \right\}
 \end{aligned}
 \tag{2.28}$$

## 2.5 The Equation System

The excitation currents expressed in **eq.(2.21)** and in **eq.(2.28)** allow us to reach the ultimate expression of the **eq.(2.13)** system in either loss free and lossy cases. We will report either formulas, even if it is possible to shift from lossy to loss free case simply equating to zero the parameters defined in **eq.(2.27)**.

For a loss free pillbox, equating **eq.(2.13)** with **eq.(2.21)** we get the following system:

$$\begin{cases}
 \underline{A}_1 - Y_0 \underline{Y}^b \underline{V}_1^- = jY_0 \underline{M}^T \underline{Y}^c \left[ \csc(2kL\underline{Z}^c) \cdot (\underline{M}\underline{V}_2^+ - \underline{N}_2) - \cot(2kL\underline{Z}^c) \cdot (\underline{M}\underline{V}_1^- - \underline{N}_1) \right] \\
 \underline{A}_2 + Y_0 \underline{Y}^b \underline{V}_2^+ = jY_0 \underline{M}^T \underline{Y}^c \left[ \cot(2kL\underline{Z}^c) \cdot (\underline{M}\underline{V}_2^+ - \underline{N}_2) - \csc(2kL\underline{Z}^c) \cdot (\underline{M}\underline{V}_1^- - \underline{N}_1) \right]
 \end{cases}
 \tag{2.29}$$

By means of some algebra it is possible to uncouple the unknowns and, therefore, to simplify the solution. By adding and subtracting the two expressions, we obtain:

$$\begin{aligned}
 & \left[ \underline{I} - j\underline{Z}^b \underline{M}^T \underline{Y}^c \cot(kL\underline{Z}^c) \underline{M} \right] (\underline{V}_1^- - \underline{V}_2^+) = \\
 & = Z_0 \underline{Z}^b (\underline{A}_1 + \underline{A}_2) - j\underline{Z}^b \underline{M}^T \underline{Y}^c \cot(kL\underline{Z}^c) (\underline{N}_1 - \underline{N}_2)
 \end{aligned} \tag{2.30}$$

$$\begin{aligned}
 & \left[ \underline{I} - j\underline{Z}^b \underline{M}^T \underline{Y}^c \tan(kL\underline{Z}^c) \underline{M} \right] (\underline{V}_1^- + \underline{V}_2^+) = \\
 & = Z_0 \underline{Z}^b (\underline{A}_1 - \underline{A}_2) + j\underline{Z}^b \underline{M}^T \underline{Y}^c \tan(kL\underline{Z}^c) (\underline{N}_1 + \underline{N}_2)
 \end{aligned} \tag{2.31}$$

where  $\underline{I}$  is the identity matrix. Here we resorted to the following trigonometric expressions:

$$\tan(x/2) = \csc(x) - \cot(x) \quad \text{and} \quad \cot(x/2) = \csc(x) + \cot(x) \tag{2.32}$$

For a lossy pillbox, equating **eq.(2.13)** with **eq.(2.28)** as already done for the loss free pillbox, we get the following system:

$$\left\{ \begin{aligned}
 & \underline{A}_1 - Y_0 \underline{Y}^b \underline{V}_1^- = \\
 & = jY_0 \underline{M}^T \left\{ \left[ \underline{\delta} + \underline{Y}^c \csc(2kL\underline{Z}^c) \right] \cdot (\underline{M} \underline{V}_2^+ - \underline{N}_2) - \left[ \underline{\delta} + \underline{Y}^c \cot(2kL\underline{Z}^c) \right] \cdot (\underline{M} \underline{V}_1^- - \underline{N}_1) \right\} \\
 & \underline{A}_2 + Y_0 \underline{Y}^b \underline{V}_2^+ = \\
 & = jY_0 \underline{M}^T \left\{ \left[ \underline{\delta} + \underline{Y}^c \cot(2kL\underline{Z}^c) \right] \cdot (\underline{M} \underline{V}_2^+ - \underline{N}_2) - \left[ \underline{\delta} + \underline{Y}^c \csc(2kL\underline{Z}^c) \right] \cdot (\underline{M} \underline{V}_1^- - \underline{N}_1) \right\}
 \end{aligned} \right. \tag{2.33}$$

By adding and subtracting the two expressions and applying the trigonometric expressions shown in **eq.(2.32)**, we obtain:

$$\begin{aligned} & \left\{ \underline{I} - j\underline{Z}^b \underline{M}^T \left[ 2\underline{\delta} + \underline{Y}^c \cot(kL\underline{Z}^c) \right] \underline{M} \right\} (\underline{V}_1^- - \underline{V}_2^+) = \\ & \underline{Z}_0 \underline{Z}^b (\underline{A}_1 + \underline{A}_2) - j\underline{Z}^b \underline{M}^T \left[ 2\underline{\delta} + \underline{Y}^c \cot(kL\underline{Z}^c) \right] (\underline{N}_1 - \underline{N}_2) \end{aligned} \quad (2.34)$$

$$\begin{aligned} & \left[ \underline{I} - j\underline{Z}^b \underline{M}^T \underline{Y}^c \tan(kL\underline{Z}^c) \underline{M} \right] (\underline{V}_1^- + \underline{V}_2^+) = \\ & = \underline{Z}_0 \underline{Z}^b (\underline{A}_1 - \underline{A}_2) + j\underline{Z}^b \underline{M}^T \underline{Y}^c \tan(kL\underline{Z}^c) (\underline{N}_1 + \underline{N}_2) \end{aligned} \quad (2.35)$$

A commonly used computer tool, Mathworks Matlab, easily solves the just obtained equations. Actually, it is necessary to truncate the infinite matrices before trying to solve the equations. In **section 2.7** we will show a good method to truncate the matrices without lose results goodness.

## 2.6 The Longitudinal Coupling Impedance

We determine the Coupling impedance separating the integral in components related to the cavity regions where, to be consistent with the previous assumptions, we take the charge  $q=1$ .

$$Z(k) = - \int_{-\infty}^0 E_{1z}(r=0, z) e^{j k / \beta z} dz - \int_0^{2L} E_z^c(r=0, z) e^{j k / \beta z} dz - \int_{2L}^{+\infty} E_{2z}(r=0, z) e^{j k / \beta z} dz \quad (2.36)$$

the longitudinal component of the Electric field for the three regions is given in **eq.(2.1)** and summarized as follows.

$$\begin{aligned} E_{1z}(r, z) &= j \sum_t V_{1t}^- \frac{k_t Y_t^b}{k} \Phi_{0t}^b(k_t r) \exp(j z \sqrt{k^2 - k_t^2}) & z < 0 \\ E_z^c(r, z) &= -j Z_0 \sum_{p,s} \frac{k_p}{k} \sqrt{\frac{\epsilon_s}{2L}} \cos(k_s z) \Phi_{0p}^c(k_p r) I_{ps} & 0 < z < 2L \\ E_{2z}(r, z) &= -j \sum_t V_{2t}^+ \frac{k_t Y_t^b}{k} \Phi_{0t}^b(k_t r) \exp[-j(z - 2L) \sqrt{k^2 - k_t^2}] & 2L < z \end{aligned} \quad (2.37)$$

For the  $z < 0$  integral, substituting the Electric field for  $r = 0$  and deprived of the factors not relevant for integration, we obtain an expression like the following

$$\int_{-\infty}^0 \exp\left(j \sqrt{k^2 - k_t^2} z + j \frac{k}{\beta} z\right) dz \quad (2.38)$$

which is the same of the integral

$$\int e^{\alpha x} dx = \frac{1}{\alpha} e^{\alpha x}$$

Resorting to the above formula to resolve the integral in **eq.(2.38)** we obtain

$$-j \frac{\sqrt{k^2 - k_t^2} - k/\beta}{k^2 - k_t^2 - \left(\frac{k}{\beta}\right)^2}$$

that can be written in a more elegant expression (using  $\kappa = k/\beta\gamma$ )

$$j \frac{\sqrt{k^2 - k_t^2} - k/\beta}{\kappa^2 + k_t^2} \quad (2.39)$$

Returning to the general expression of the integral, we notice that

$$\Phi_{0q}^\rho(k_q r) \Big|_{r=0} = \frac{J_0(k_q r) \Big|_{r=0}}{\rho \sqrt{\pi} J_1(\alpha_q)} = \frac{1}{\rho \sqrt{\pi} J_1(\alpha_q)}$$

Therefore, substituting everything in the first integral of **eq.(2.36)** we have

$$\boxed{- \int_{-\infty}^0 E_{1z}(r=0, z) e^{j k/\beta z} dz = \frac{1}{kb\sqrt{\pi}} \sum_t V_{1t}^- \frac{k_t Y_t^b \left( \sqrt{k^2 - k_t^2} - k/\beta \right)}{J_1(\alpha_t) (\kappa^2 + k_t^2)}} \quad (2.40)$$

For what concerns the integral of Longitudinal Impedance related to the case  $0 < z < 2L$ , the Electric field along the  $z$  axis is given in **eq.(2.37)**. Recalling the explicit expression of  $I_{ps}$

$$I_{ps} = \frac{jkY_0}{k^2 - k_{ps}^2} \sqrt{\frac{\epsilon_s}{2L}} \left[ N_{1p} - \sum_t M_{pt} V_{1t}^- - (-1)^s \left( N_{2p} - \sum_t M_{pt} V_{2t}^+ \right) \right]$$

we obtain the expression of the integrand

$$- \sum_{ps} \frac{\epsilon_s k_p \cos(k_s z)}{2L(k^2 - k_{ps}^2)} \Phi_{0p}^c(r) \left[ N_{1p} - \sum_t M_{pt} V_{1t}^- - (-1)^s \left( N_{2p} - \sum_t M_{pt} V_{2t}^+ \right) \right] \quad (2.41)$$

For  $r = 0$  and without elements not relevant to the integral solution, we obtain the following integral and the relative solution

$$\int_0^{2L} \cos(k_s z) \exp\left(\frac{jkz}{\beta}\right) dz = \left[ \frac{-j \frac{k}{\beta} \left( -1 + (-1)^s \exp\left(\frac{2jkL}{\beta}\right) \right)}{\left(\frac{k}{\beta}\right)^2 - k_s^2} \right] \quad (2.42)$$

Therefore, the integral of the Longitudinal Coupling Impedance we are looking for, will be

$$\int_0^{2L} E_z^c(r=0, z) \exp\left(\frac{jkz}{\beta}\right) dz = -\sum_{ps} \frac{\varepsilon_s k_p [\tilde{A}_p - (-1)^s \tilde{B}_p]}{2L(k^2 - k_{ps}^2) c \sqrt{\pi} J_1(\alpha_p)} \left[ \frac{-j \frac{k}{\beta} \left(-1 + (-1)^s e^{\frac{2jkL}{\beta}}\right)}{\left(\frac{k}{\beta}\right)^2 - k_s^2} \right] \quad (2.43)$$

where

$$\begin{aligned} \tilde{A}_p &= N_{1p} - \sum_t M_{pt} V_{1t}^- \\ \tilde{B}_p &= N_{2p} - \sum_t M_{pt} V_{2t}^+ \end{aligned}$$

The sums on  $s$  can be analytically calculated as already seen for iris, with a similar result. In fact, from the integral result we gain four sums on  $s$  to solve, derived by the follows:

$$\sum_s \frac{\varepsilon_s}{(k^2 - k_{ps}^2) \left[ \left(\frac{k}{\beta}\right)^2 - k_s^2 \right]}$$

$$\sum_s \frac{\varepsilon_s (-1)^s}{(k^2 - k_{ps}^2) \left[ \left(\frac{k}{\beta}\right)^2 - k_s^2 \right]}$$

Solving the above sums we reach this result

$$\begin{aligned}
 & \sum_p \frac{-k_p \beta}{c\sqrt{\pi}J_1(\alpha_p)} \left\{ \tilde{A}_p \cdot \frac{jk \left[ \csc(2L\sqrt{k^2 - k_p^2}) e^{\frac{2jkL}{\beta}} - \cot(2L\sqrt{k^2 - k_p^2}) \right] + \beta\sqrt{k^2 - k_p^2}}{\sqrt{k^2 - k_p^2} [k^2(-1 + \beta^2) - \beta^2 k_p^2]} + \right. \\
 & \left. - \tilde{B}_p \cdot \frac{jk \left[ \cot(2L\sqrt{k^2 - k_p^2}) e^{\frac{2jkL}{\beta}} - \csc(2L\sqrt{k^2 - k_p^2}) \right] + e^{\frac{2jkL}{\beta}} \beta\sqrt{k^2 - k_p^2}}{\sqrt{k^2 - k_p^2} [k^2(-1 + \beta^2) - \beta^2 k_p^2]} \right\}
 \end{aligned} \tag{2.44}$$

After some algebra we obtain the final result for the second integral of eq.(2.36)

$$\begin{aligned}
 & - \int_0^{2L} E_z^c(r=0, z) \exp\left(j \frac{k}{\beta} z\right) dz = \\
 & \frac{1}{c\sqrt{\pi}} \sum_p k_p \frac{\left[ \sum_t M_{pt} \left( V_{2t}^+ e^{\frac{2jLk}{\beta}} - V_{1t}^- \right) \right]}{(\kappa^2 + k_p^2) J_1(\alpha_p)} + \\
 & + \frac{j}{c\sqrt{\pi}\beta} \sum_p k_p \frac{\left[ \csc(2L\sqrt{k^2 - k_p^2}) \left( \tilde{A}_p e^{\frac{2jkL}{\beta}} + \tilde{B}_p \right) - \cot(2L\sqrt{k^2 - k_p^2}) \left( \tilde{A}_p + \tilde{B}_p e^{\frac{2jkL}{\beta}} \right) \right]}{Z_p^c (\kappa^2 + k_p^2) J_1(\alpha_p)}
 \end{aligned} \tag{2.45}$$

For the  $z > 0$  integral, substituting the Electric field for  $r = 0$  and without elements not relevant to the integral solution, we obtain an expression like the following

$$\int_{2L}^{\infty} \exp\left[j\frac{k}{\beta}z - j(z-2L)\sqrt{k^2 - k_t^2}\right] dz \quad (2.46)$$

The above integral can be written as already done for the integral of the first region

$$\exp\left(j2L\sqrt{k^2 - k_t^2}\right) \int_{2L}^{\infty} \exp\left[-jz\left(\sqrt{k^2 - k_t^2} - \frac{k}{\beta}\right)\right] dz \quad (2.47)$$

which has the same solution, with different signs.

Solving the integral and using  $\kappa = k/\beta\gamma$  we obtain this result

$$j \frac{\sqrt{k^2 - k_t^2} + k/\beta}{\kappa^2 + k_t^2} \exp\left(j2L\frac{k}{\beta}\right) \quad (2.48)$$

Therefore, recalling the expression of  $\Phi_{0q}^{\rho}(k_q r)\big|_{r=0}$  and substituting everything in

the third integral of **eq.(2.36)**

$$\boxed{-\int_{2L}^{\infty} E_{2z}(r=0, z) e^{jk/\beta z} dz = \frac{-1}{kb\sqrt{\pi}} \sum_t V_{2t}^- \frac{k_t Y_t^b\left(\sqrt{k^2 - k_t^2} + k/\beta\right)}{J_1(\alpha_t)(\kappa^2 + k_t^2)} \exp\left(j2L\frac{k}{\beta}\right)} \quad (2.49)$$

The Longitudinal Coupling Impedance of the Pillbox is given by the sum of the three integrals **eq.(2.29)**, **eq.(2.34)**, **eq.(2.38)**.

## 2.7 Numerical results

The two Equation Systems (**eq.2.30-2.31** and **eq.2.34-2.35**) involves infinite equations and infinite unknowns. To allow the system inversion it is necessary to truncate the infinite matrices without hack the results validity. As already seen for the iris, through the Relative Convergence phenomenon, it is possible to reach a different result for different matrix truncation.

Following the scheme reported on Lee and Mittra book [6] we imposed a relation between the number of modes of different zones in order to respect the Meixner condition [7].

The choice of the ratios  $N1/N2$  and  $N3/N2$  (where  $N_i$  indicate the number of modes for the  $i^{\text{th}}$  region) has a considerable effect on the result goodness as seen for the iris.

$$\frac{N_2}{N_1} = \frac{b}{c} = w_{12} \quad (2.50)$$

In our specific case, we chosen

$$\begin{cases} N_1 = \frac{N/w_{12}}{1+1/w_{12}+1/w_{23}} \\ N_2 = \frac{N}{1+1/w_{12}+1/w_{23}} \\ N_3 = \frac{N/w_{23}}{1+1/w_{12}+1/w_{23}} \end{cases} \quad (2.51)$$

where  $N = N_1 + N_2 + N_3$  and  $w_{23} = w_{12}$  (because  $b = d$ ), then  $N_1 = N_3$ . After truncation and inversion of the linear equations, we solved the problem. It will be represented the Longitudinal Coupling Impedance, as a fundamental parameter for accelerators project, subdivided in real and imaginary parts and for different values of number of modes, geometrical parameters and particle speed. The number of points is chosen as a simulation constant,  $n = 500$ , and the same is done for the waveguide radius ( $b = 12$  mm). The number of modes is fixed ( $N = 200$ ), but in some cases this number may be changed, when it is needed to increase it to reach the convergence, as already discussed for iris case.

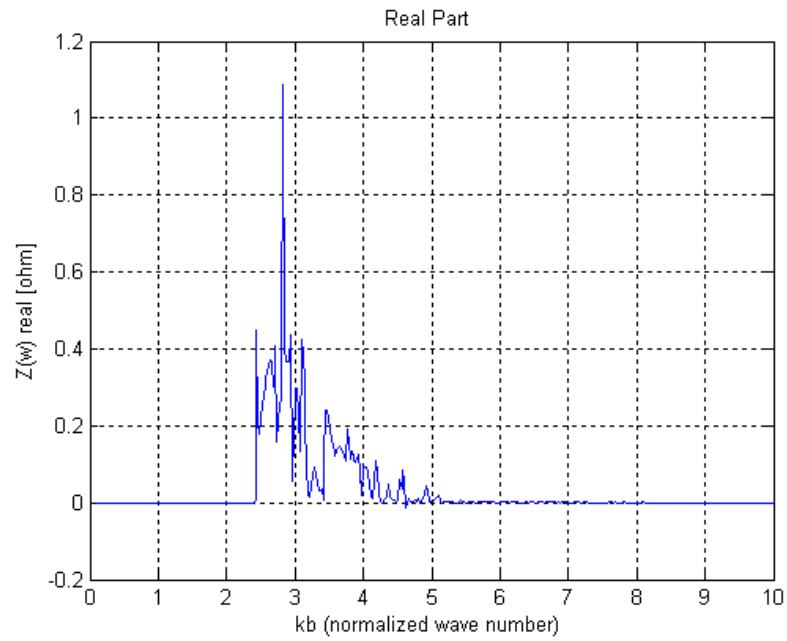


Fig. 2-2. Longitudinal Coupling Impedance, real part:  $\beta\gamma = 1$ ,  $c/b = 4$ ,  $L/b = 4$ .

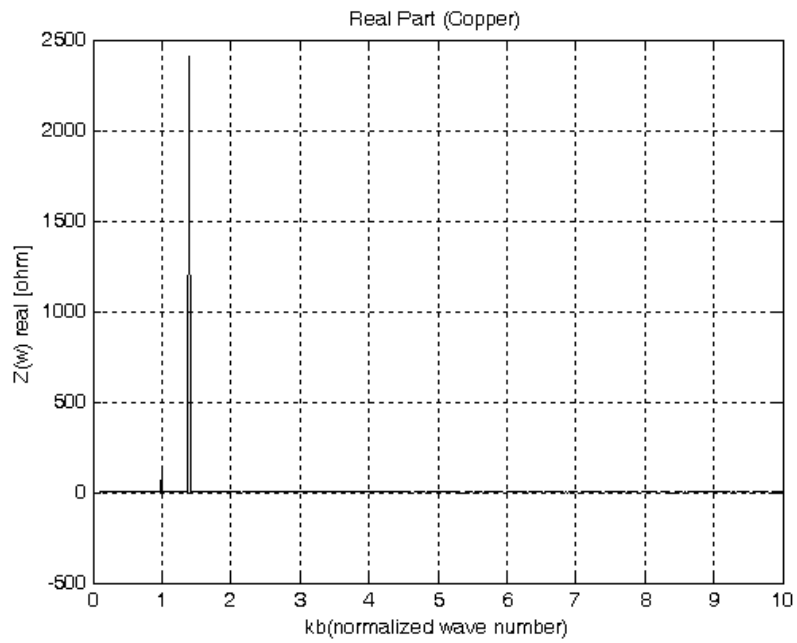


Fig. 2-3. Longitudinal Coupling Impedance with losses, real part:  $\beta\gamma = 1$ ,  $c/b = 4$ ,  $L/b = 4$ ,  $\rho=1/(5.98 \cdot 10^7)$ .

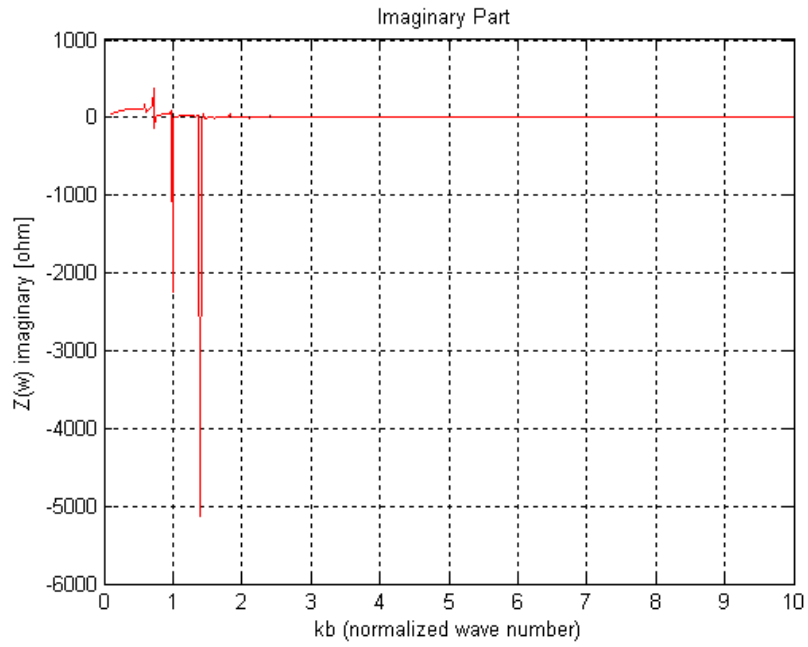


Fig. 2-4. Longitudinal Coupling Impedance, imaginary part:  $\beta\gamma = 1$ ,  $c/b = 4$ ,  $L/b = 4$ .

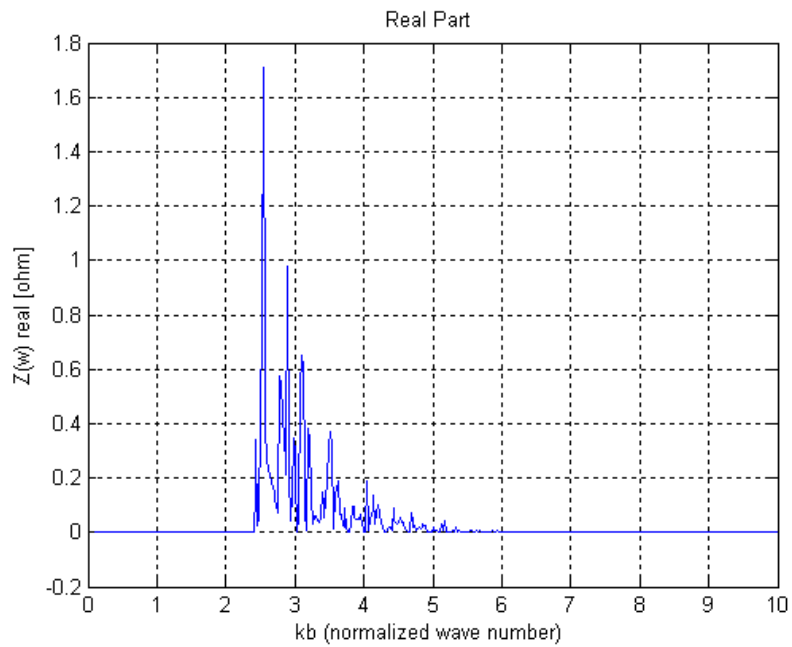


Fig. 2-5. Longitudinal Coupling Impedance, real part:  $\beta\gamma = 1$ ,  $c/b = 6$ ,  $L/b = 4$ .

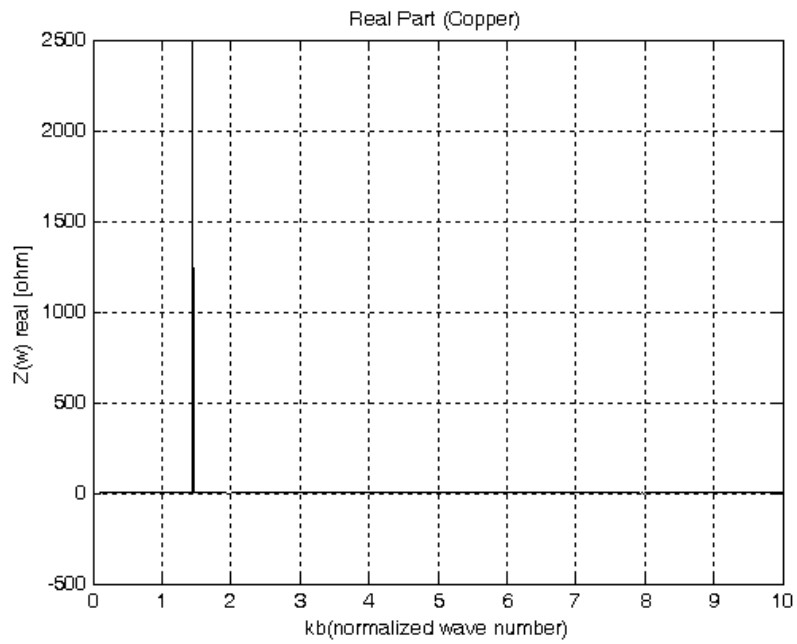


Fig. 2-6. Longitudinal Coupling Impedance with losses, real part:  $\beta\gamma = 1$ ,  $c/b = 6$ ,  $L/b = 4$ ,  $\rho = 1/(5.98 \cdot 10^7)$ .

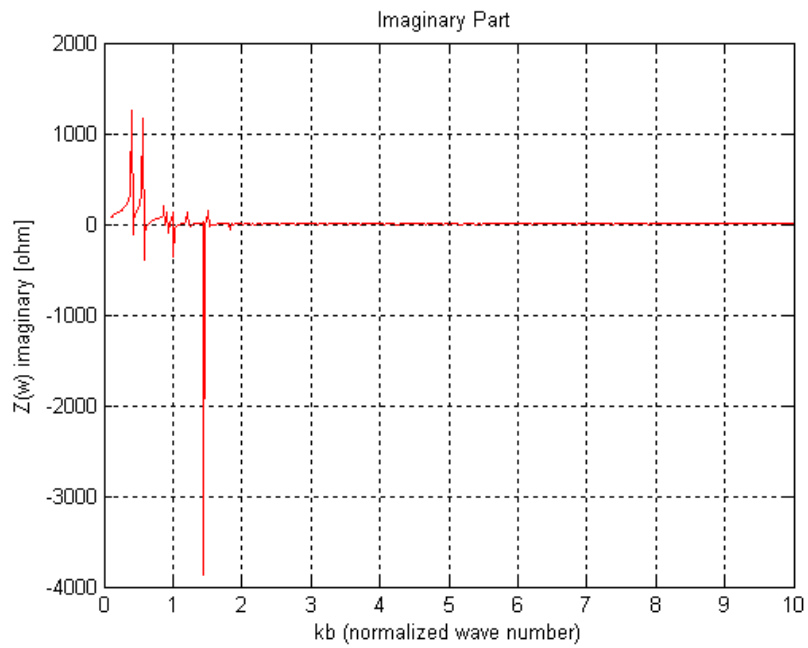


Fig. 2-7. Longitudinal Coupling Impedance, imaginary part:  $\beta\gamma = 1$ ,  $c/b = 6$ ,  $L/b = 4$ .

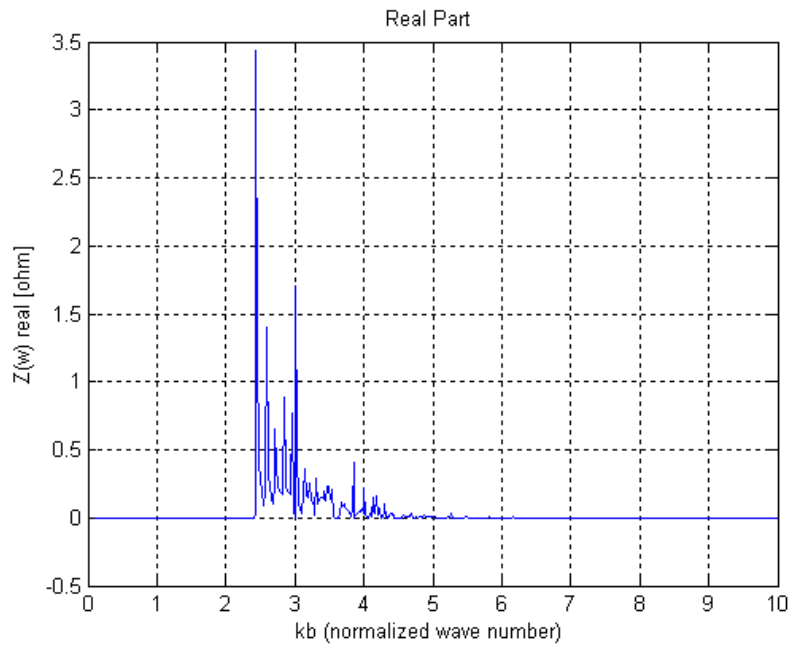


Fig. 2-8. Longitudinal Coupling Impedance, real part:  $\beta\gamma = 1$ ,  $c/b = 8$ ,  $L/b = 4$ .

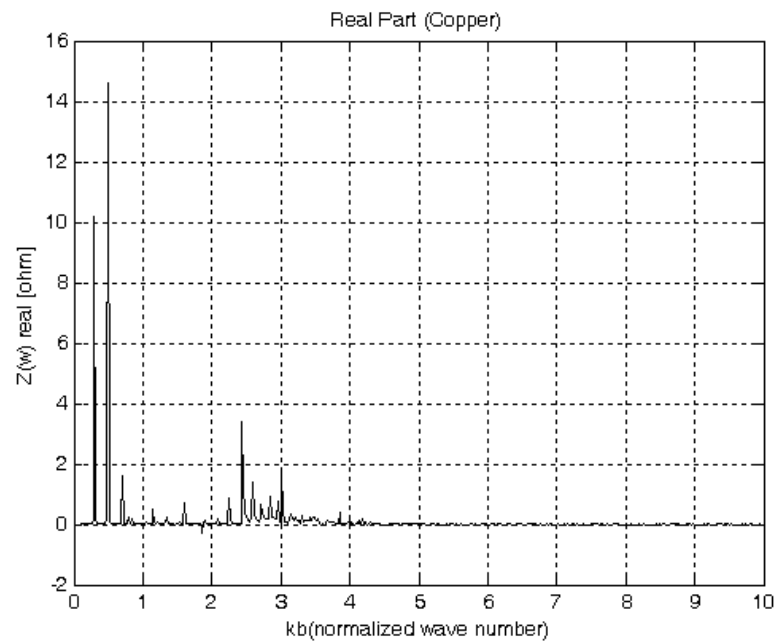


Fig. 2-9. Longitudinal Coupling Impedance with losses, real part:  $\beta\gamma = 1$ ,  $c/b = 8$ ,  $L/b = 4$ ,  $\rho=1/(5.98 \cdot 10^7)$ .

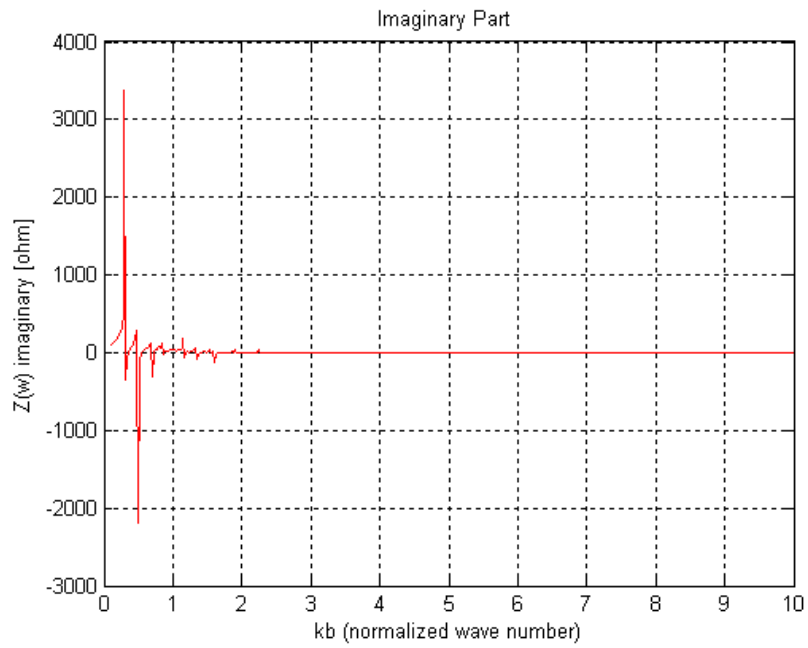


Fig. 2-10. Longitudinal Coupling Impedance, imaginary part:  $\beta\gamma = 1$ ,  $c/b = 8$ ,  $L/b = 4$ .

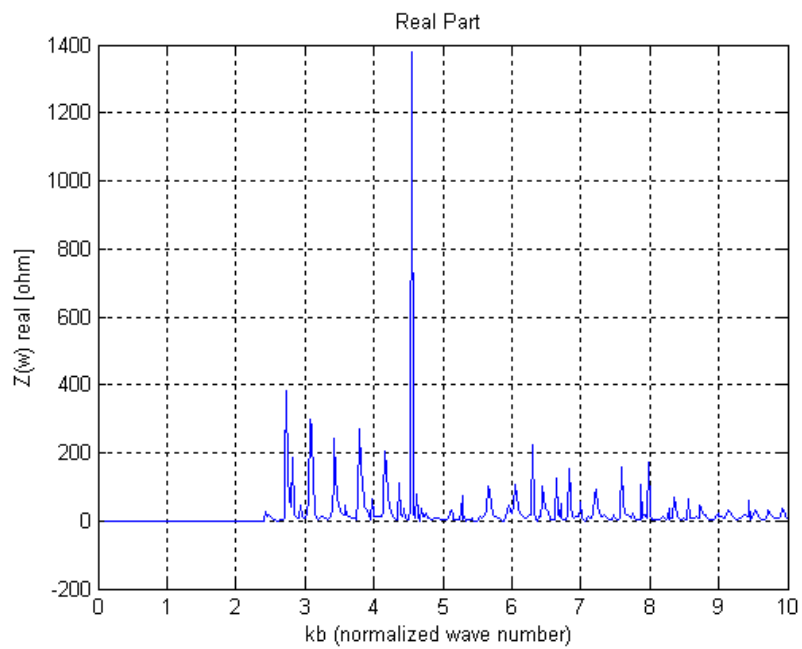


Fig. 2-11. Longitudinal Coupling Impedance, real part:  $\beta\gamma = 10$ ,  $c/b = 4$ ,  $L/b = 4$ .

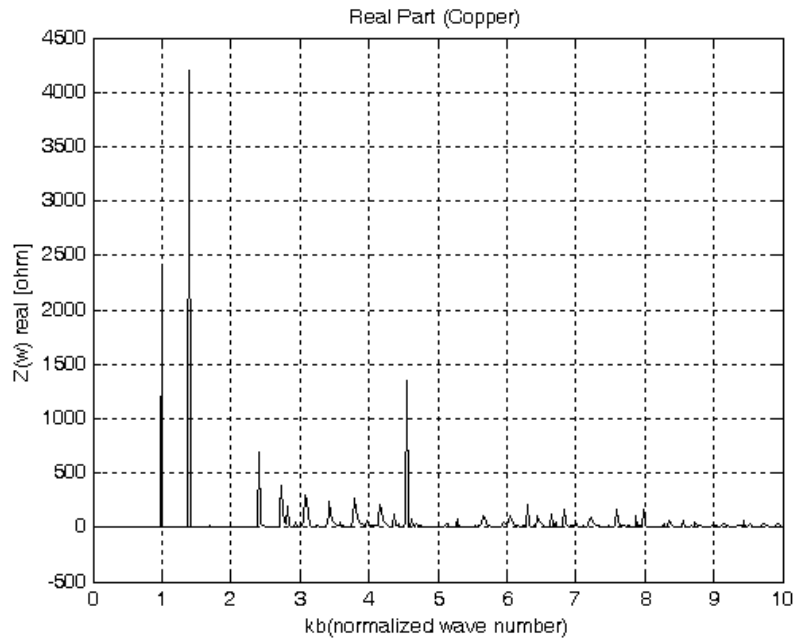


Fig. 2-12. Longitudinal Coupling Impedance with losses, real part:  $\beta\gamma = 10$ ,  $c/b = 4$ ,  $L/b = 4$ ,  $\rho=1/(5.98 \cdot 10^7)$ .

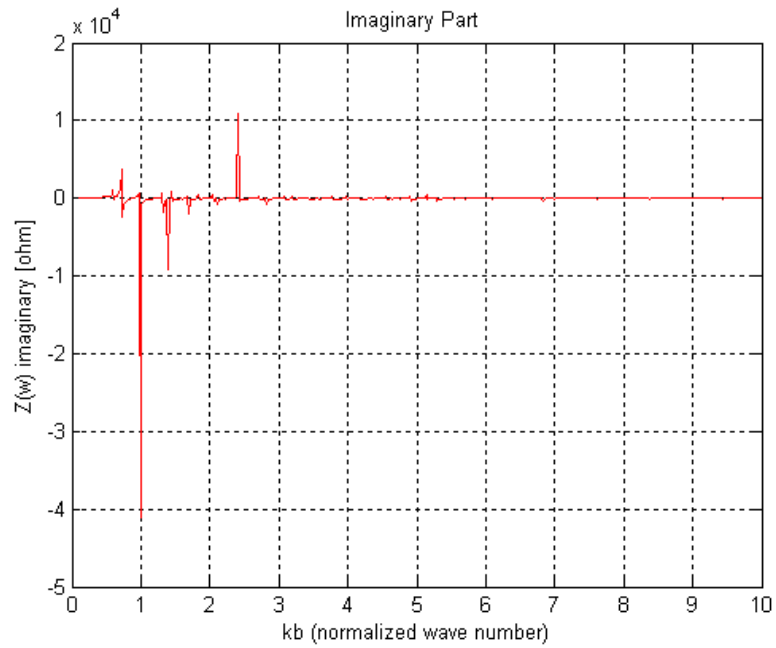


Fig. 2-13. Longitudinal Coupling Impedance, imaginary part:  $\beta\gamma = 10$ ,  $c/b = 4$ ,  $L/b = 4$ .

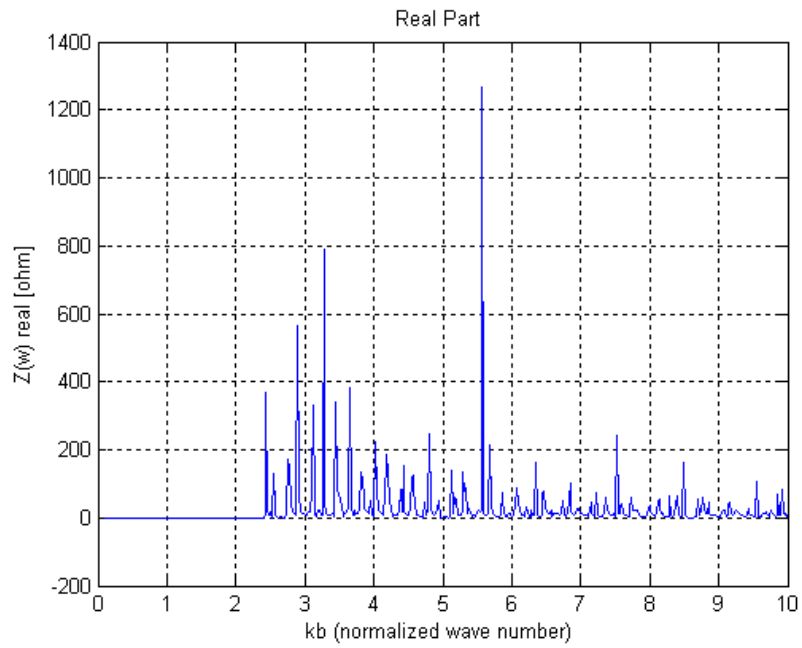


Fig. 2-14. Longitudinal Coupling Impedance, real part:  $\beta\gamma = 10$ ,  $c/b = 6$ ,  $L/b = 4$ .

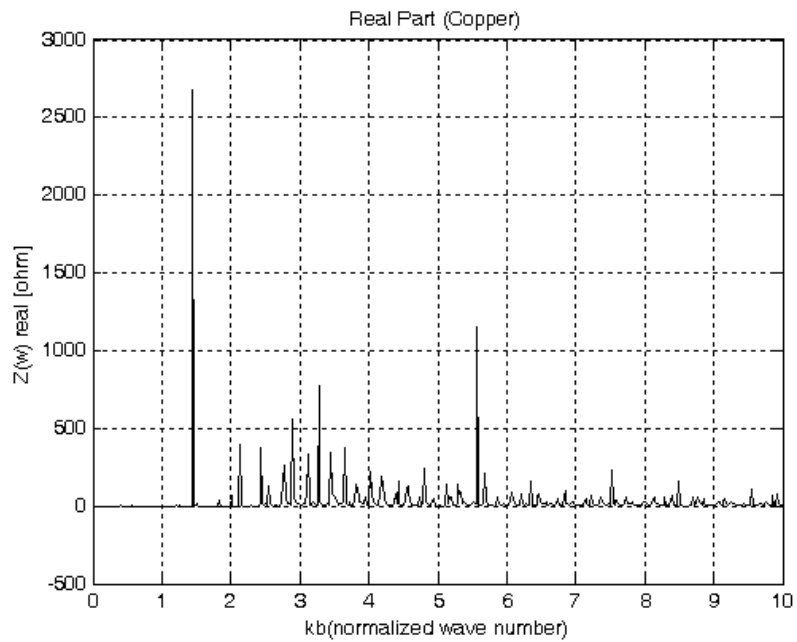


Fig. 2-15. Longitudinal Coupling Impedance with losses, real part:  $\beta\gamma = 10$ ,  $c/b = 6$ ,  $L/b = 4$ ,  $\rho = 1/(5.98 \cdot 10^7)$ .

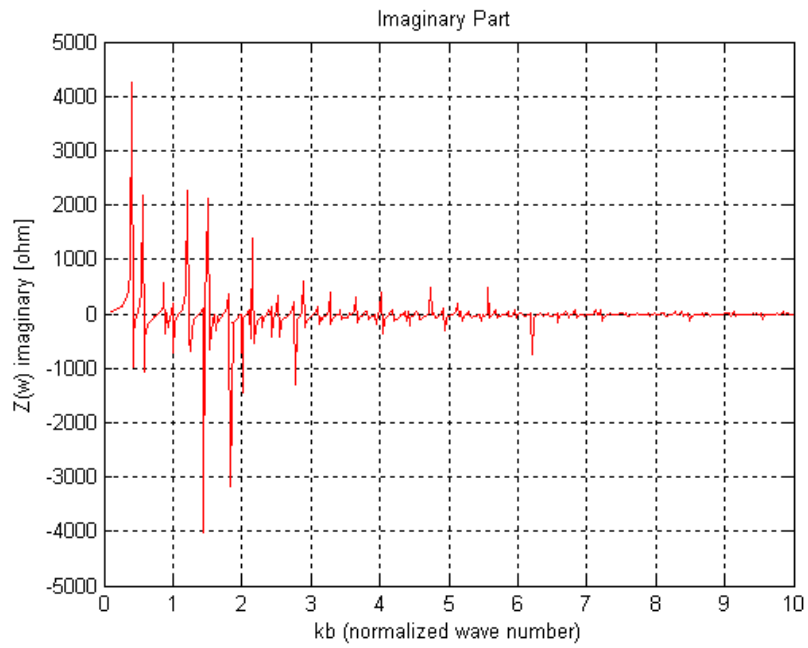


Fig. 2-16. Longitudinal Coupling Impedance, imaginary part:  $\beta\gamma = 10$ ,  $c/b = 6$ ,  $L/b = 4$ .

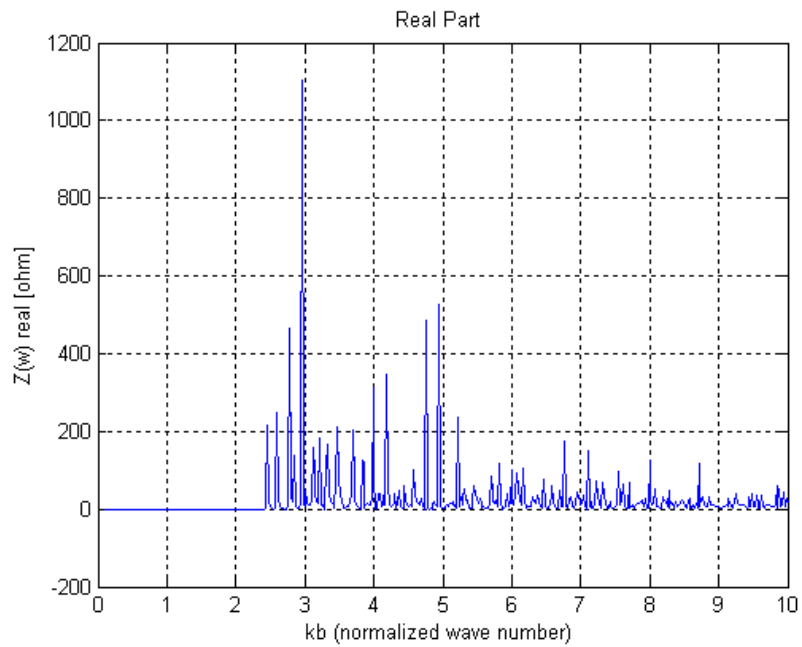


Fig. 2-17. Longitudinal Coupling Impedance, real part:  $\beta\gamma = 10$ ,  $c/b = 8$ ,  $L/b = 4$ .

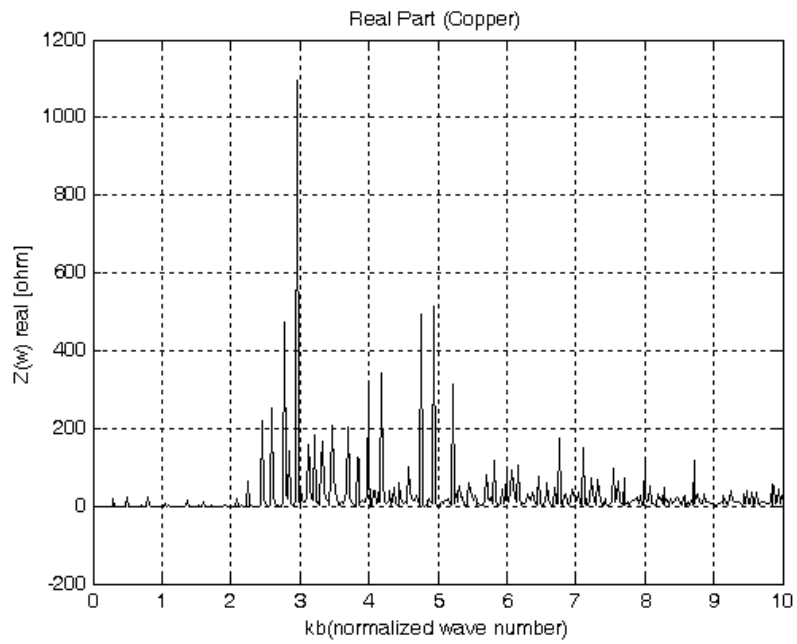


Fig. 2-18. Longitudinal Coupling Impedance with losses, real part:  $\beta\gamma = 10$ ,  $c/b = 8$ ,  $L/b = 4$ ,  $\rho=1/(5.98 \cdot 10^7)$ .

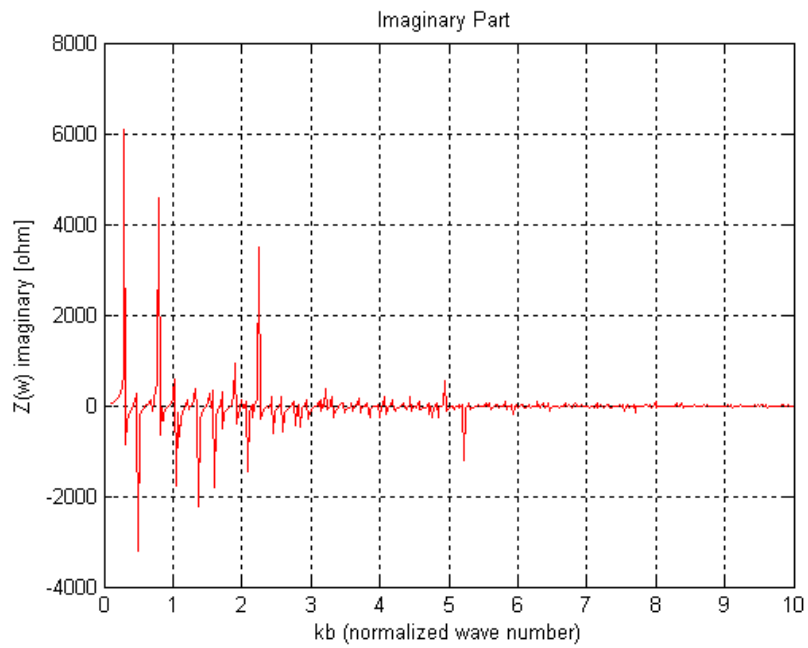


Fig. 2-19. Longitudinal Coupling Impedance, imaginary part:  $\beta\gamma = 10$ ,  $c/b = 8$ ,  $L/b = 4$ .

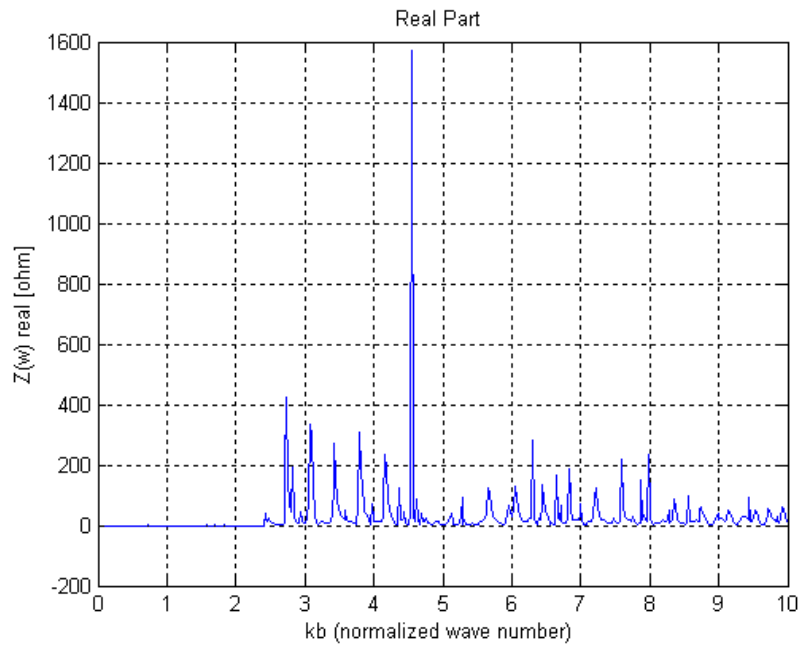


Fig. 2-20. Longitudinal Coupling Impedance, real part:  $\beta\gamma = 100$ ,  $c/b = 4$ ,  $L/b = 4$ .

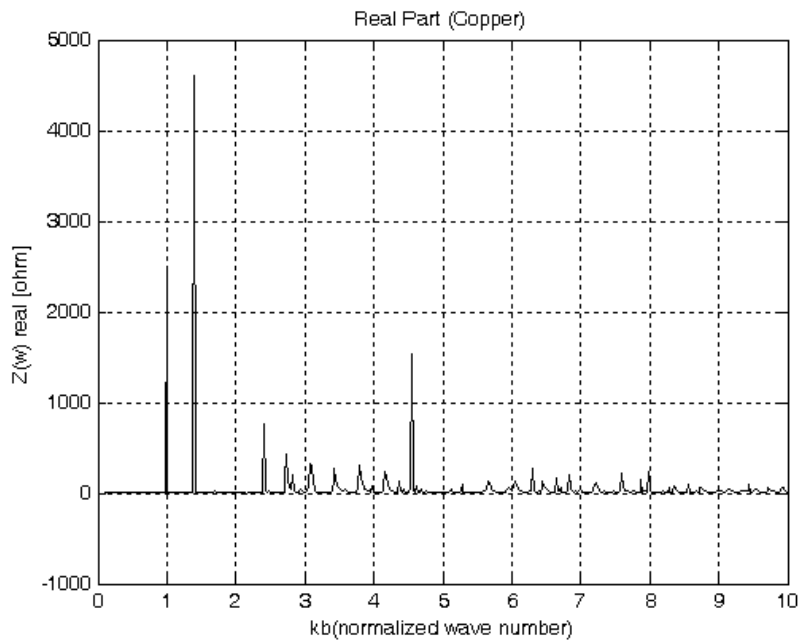


Fig. 2-21. Longitudinal Coupling Impedance with losses, real part:  $\beta\gamma = 100$ ,  $c/b = 4$ ,  $L/b = 4$ ,  $\rho=1/(5.98 \cdot 10^7)$ .

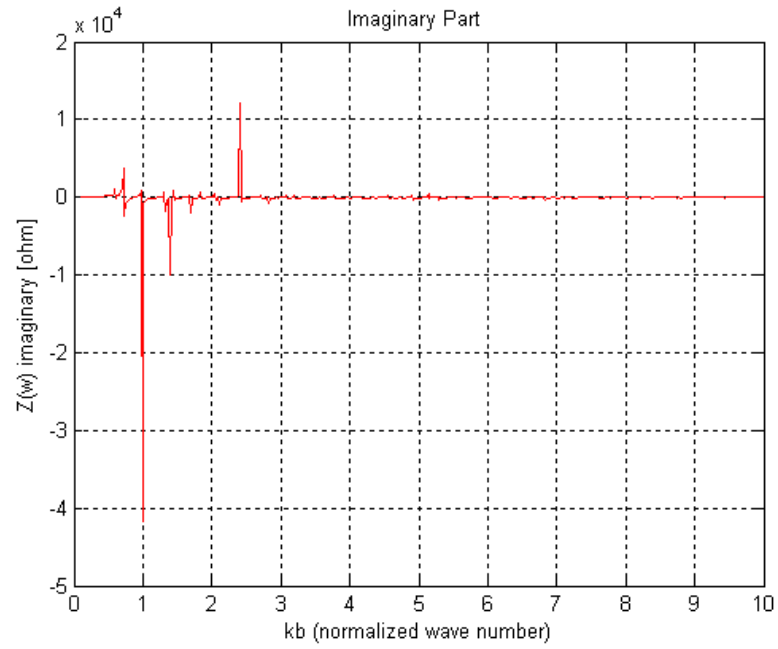


Fig. 2-22. Longitudinal Coupling Impedance, imaginary part:  $\beta\gamma = 100$ ,  $c/b = 4$ ,  $L/b = 4$ .

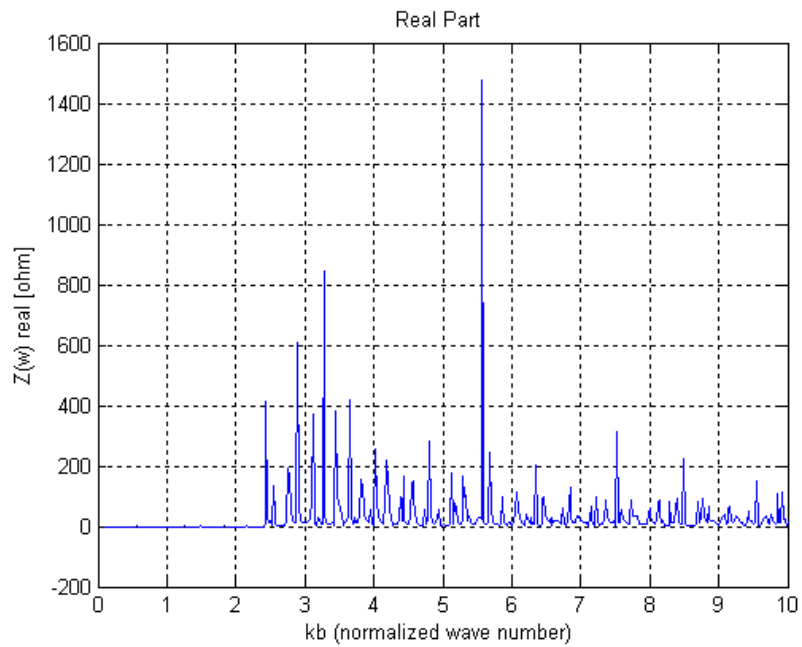


Fig. 2-23. Longitudinal Coupling Impedance, real part:  $\beta\gamma = 100$ ,  $c/b = 6$ ,  $L/b = 4$ .

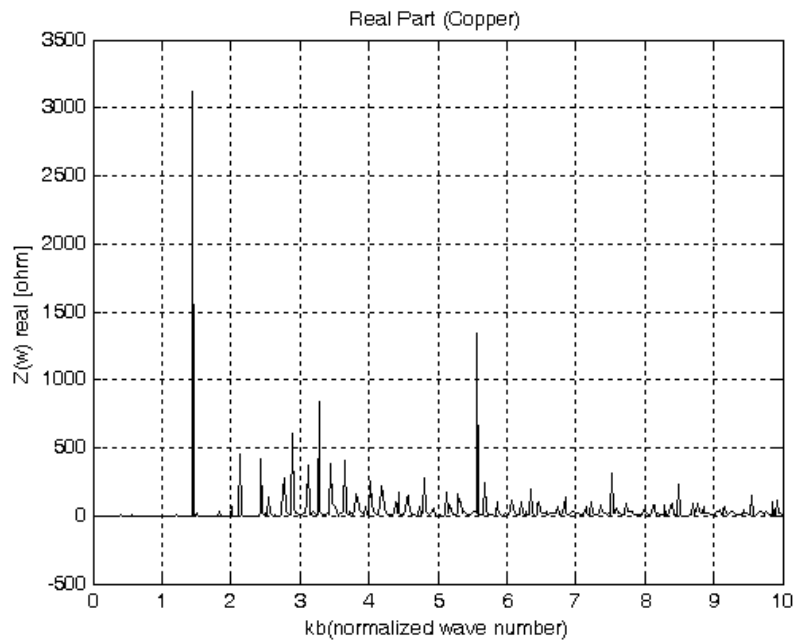


Fig. 2-24. Longitudinal Coupling Impedance with losses, real part:  $\beta\gamma = 100$ ,  $c/b = 6$ ,  $L/b = 4$ ,  $\rho=1/(5.98 \cdot 10^7)$ .

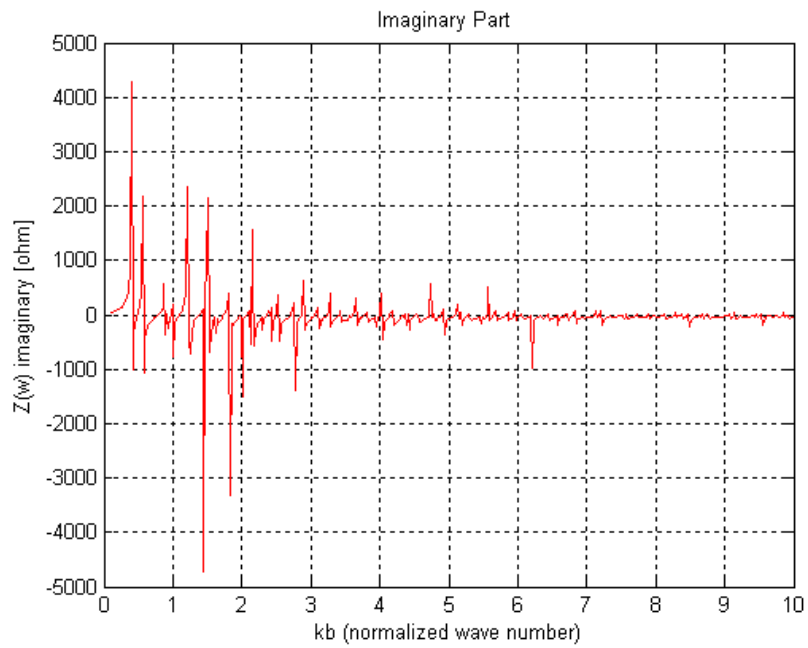


Fig. 2-25. Longitudinal Coupling Impedance, imaginary part:  $\beta\gamma = 100$ ,  $c/b = 6$ ,  $L/b = 4$ .

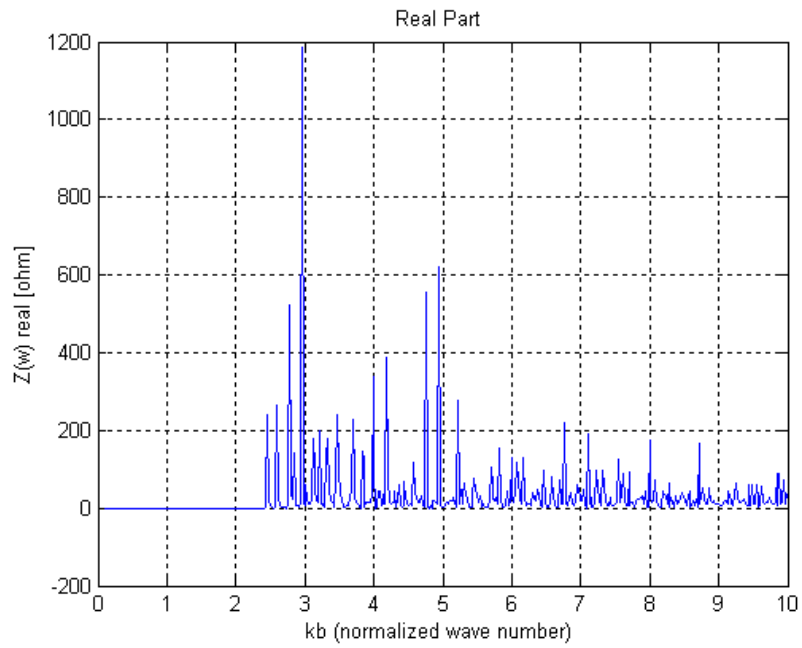


Fig. 2-26. Longitudinal Coupling Impedance, real part:  $\beta\gamma = 100$ ,  $c/b = 8$ ,  $L/b = 4$ .

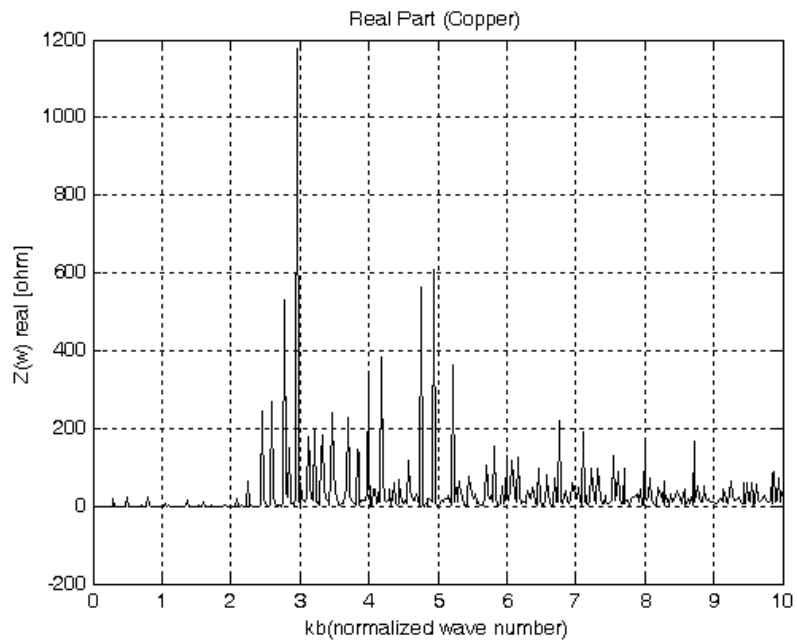


Fig. 2-27. Longitudinal Coupling Impedance with losses, real part:  $\beta\gamma = 100$ ,  $c/b = 8$ ,  $L/b = 4$ ,  $\rho = 1/(5.98 \cdot 10^7)$ .

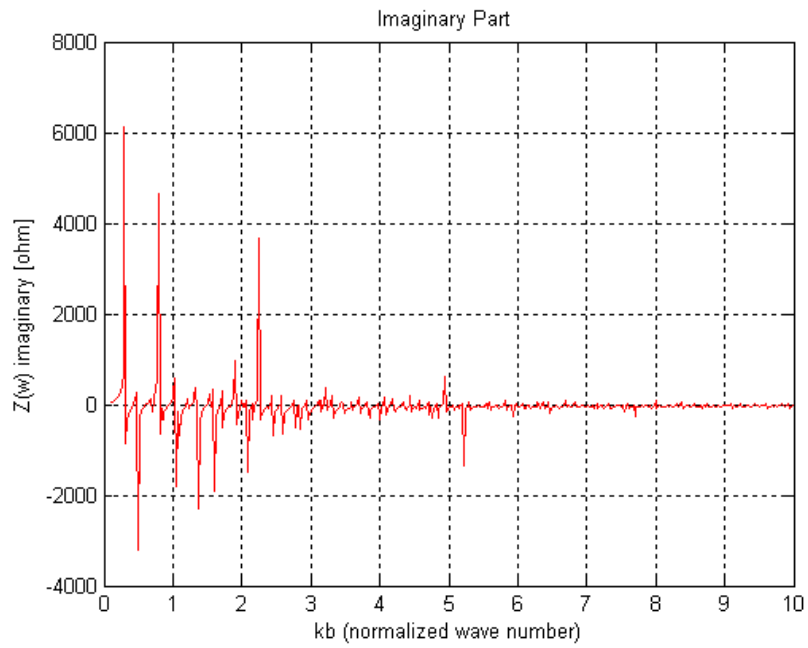


Fig. 2-28. Longitudinal Coupling Impedance, imaginary part:  $\beta\gamma = 100$ ,  $c/b = 8$ ,  $L/b = 4$ .

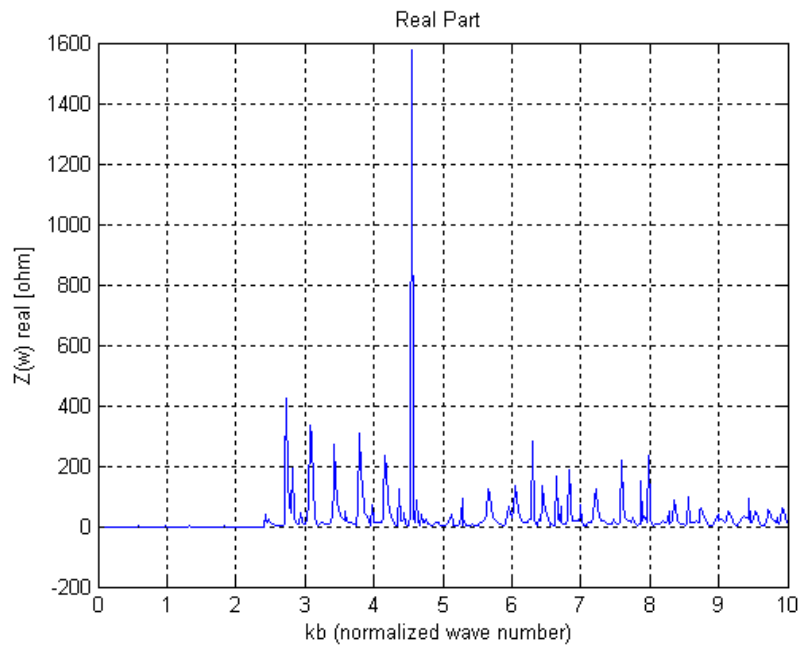


Fig. 2-29. Longitudinal Coupling Impedance, real part:  $\beta\gamma = \infty$ ,  $c/b = 4$ ,  $L/b = 4$ .

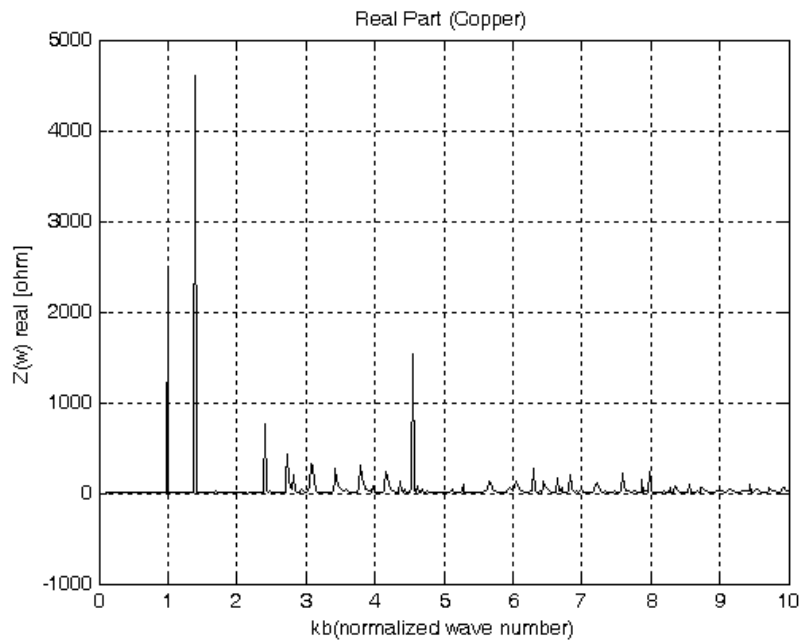


Fig. 2-30. Longitudinal Coupling Impedance with losses, real part:  $\beta\gamma = \infty$ ,  $c/b = 4$ ,  $L/b = 4$ ,  $\rho=1/(5.98 \cdot 10^7)$ .

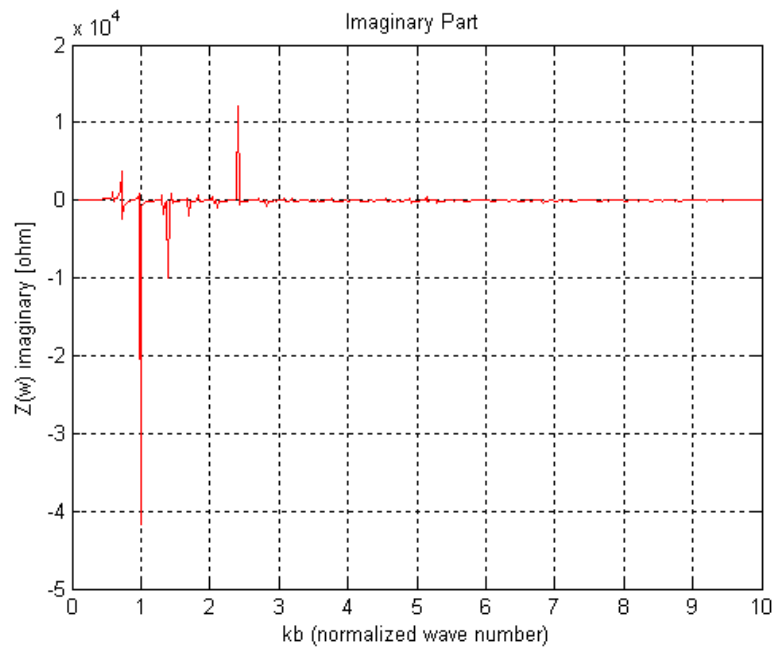


Fig. 2-31. Longitudinal Coupling Impedance, imaginary part:  $\beta\gamma = \infty$ ,  $c/b = 4$ ,  $L/b = 4$ .

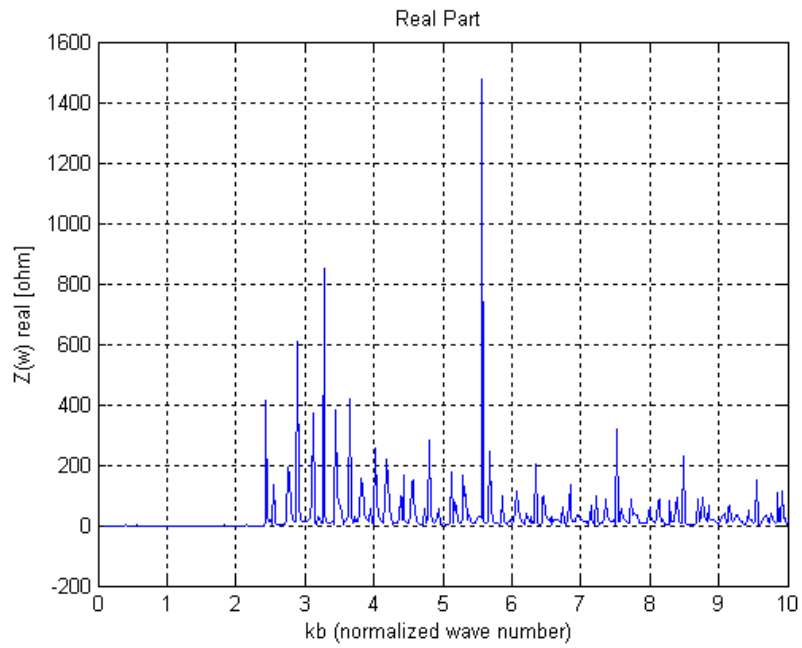


Fig. 2-32. Longitudinal Coupling Impedance, real part:  $\beta\gamma = \infty$ ,  $c/b = 6$ ,  $L/b = 4$ .

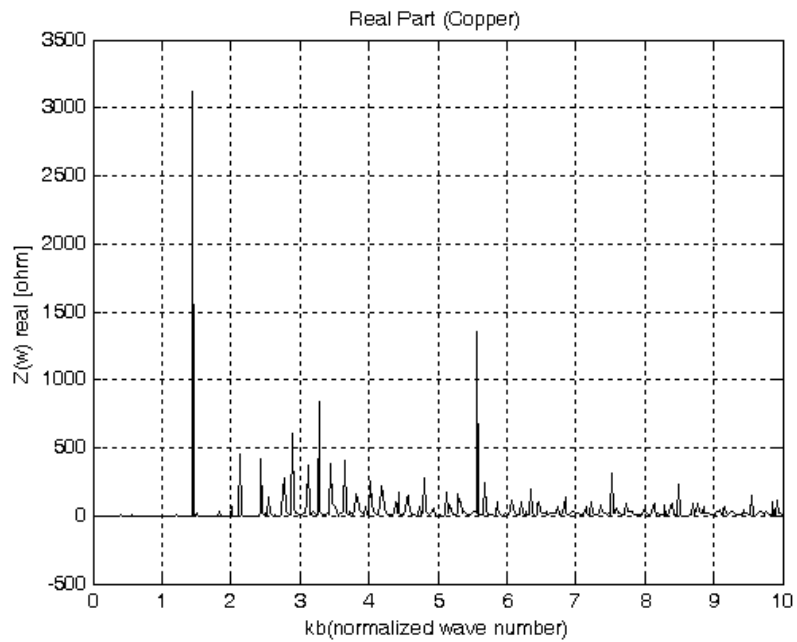


Fig. 2-33. Longitudinal Coupling Impedance with losses, real part:  $\beta\gamma = \infty$ ,  $c/b = 4$ ,  $L/b = 6$ ,  $\rho=1/(5.98 \cdot 10^7)$ .

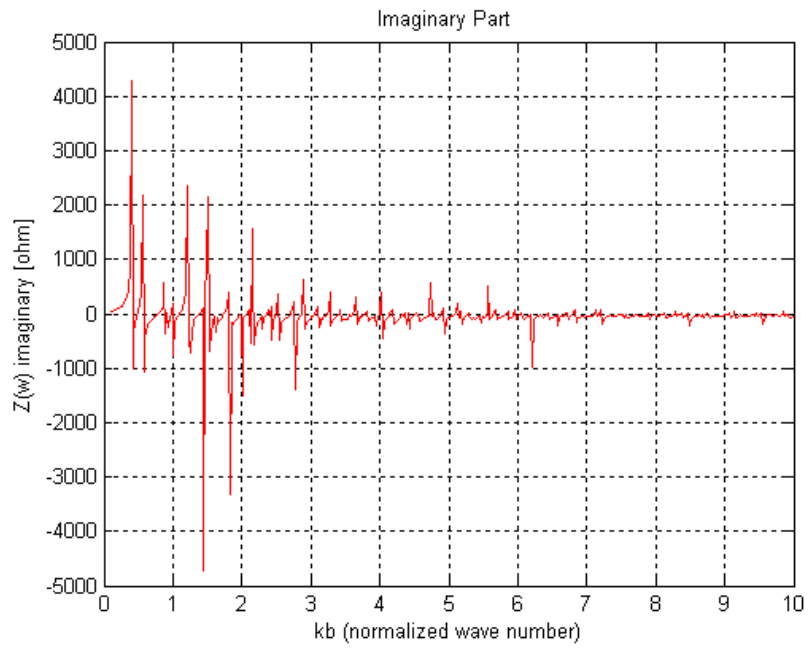


Fig. 2-34. Longitudinal Coupling Impedance, imaginary part:  $\beta\gamma = \infty$ ,  $c/b = 6$ ,  $L/b = 4$ .

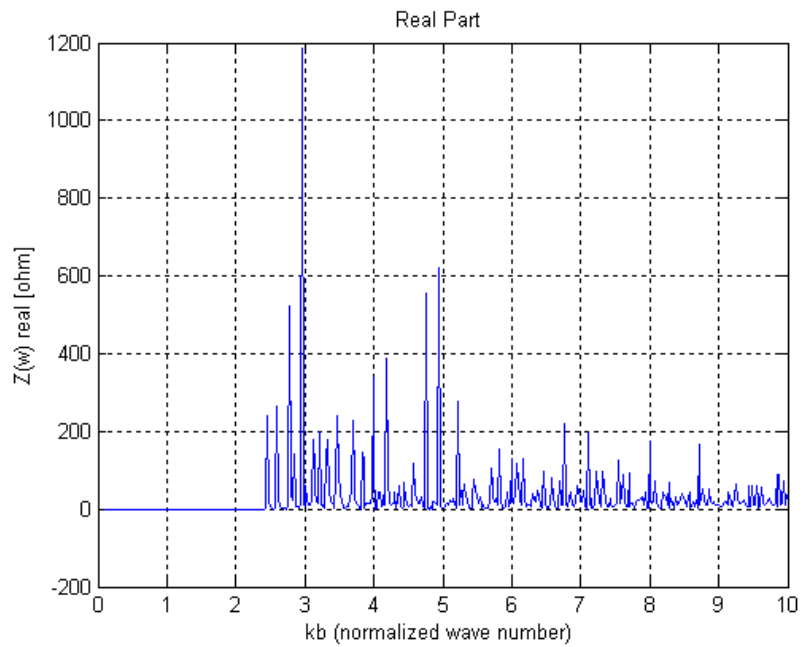
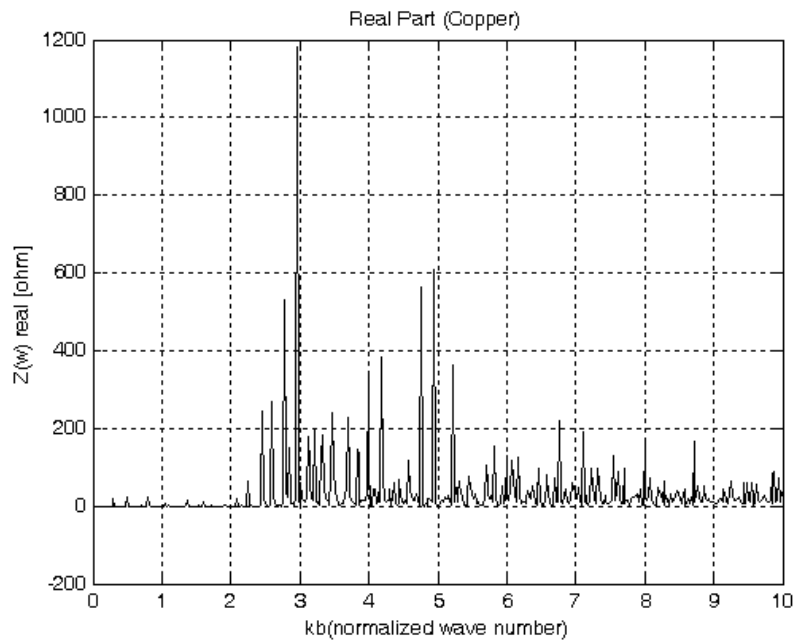
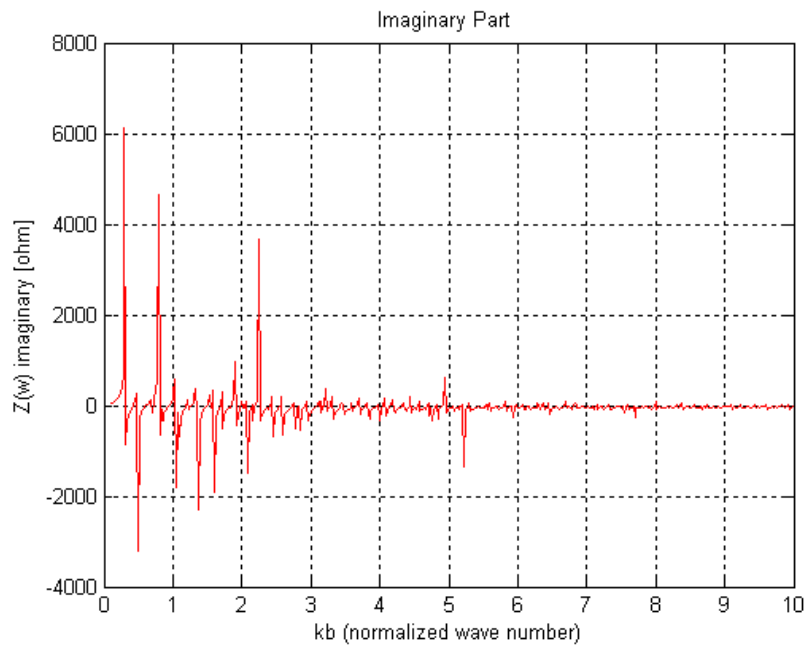


Fig. 2-35. Longitudinal Coupling Impedance, real part:  $\beta\gamma = \infty$ ,  $c/b = 8$ ,  $L/b = 4$ .



**Fig. 2-36. Longitudinal Coupling Impedance with losses, real part:  $\beta\gamma = \infty$ ,  $c/b = 4$ ,  $L/b = 8$ ,  $\rho=1/(5.98 \cdot 10^7)$ .**



**Fig. 2-37. Longitudinal Coupling Impedance, imaginary part:  $\beta\gamma = \infty$ ,  $c/b = 8$ ,  $L/b = 4$ .**

When the values of the real part of the Coupling Impedance are as low as  $10^{-13}$ - $10^{-14}$  Ohm, it is useless to increase the number of modes: the results are quite erratic. This is a consequence that we are approaching to the accuracy given for the zeros of the Bessel Functions [8]. This inconvenience, which happens at very low energies, affects only the real part of the Coupling Impedance and not the imaginary part.

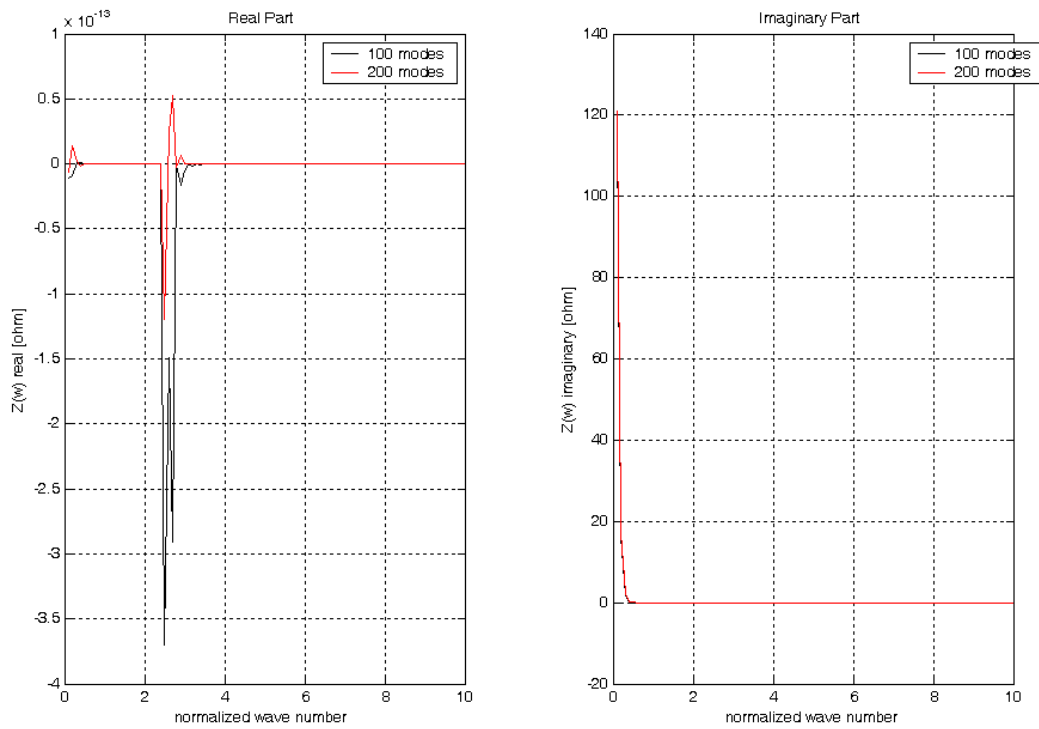


**Fig. 2-38. Convergence test for Mode Matching Technique, Coupling Impedance. ( $\beta\gamma=0.1$ ,  $c/b=2$ ,  $L/b=4$ ).**



# Chapter 3:

## The Thick Iris

### 3.1 Generality and Fields Expression

Here we want to analyze the interaction between a beam and a thick iris inserted in a cylindrical vacuum chamber both of circular cross section.

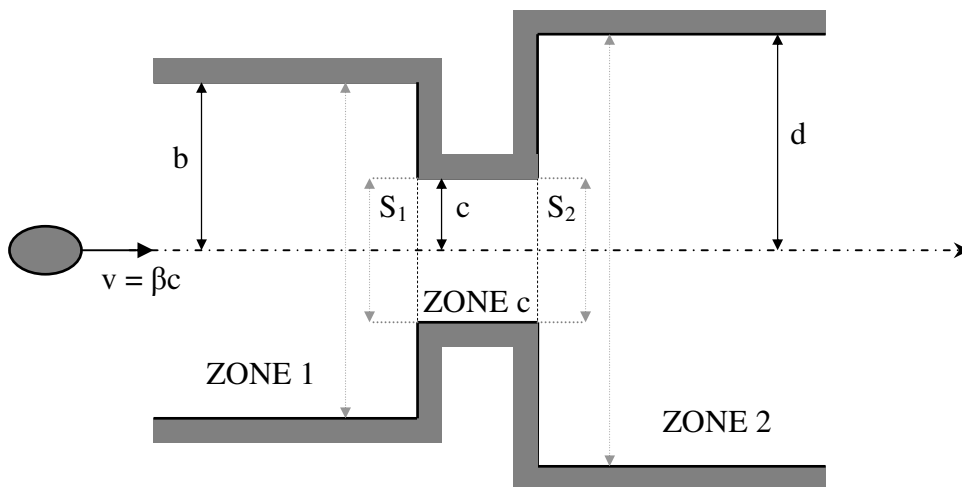


Fig. 3-1. Schematic representation of a generic Thick Iris.

We assume the forcing primary field as produced by the spatial spectrum of a point like particle  $\mathbf{q}$  riding on the axis with a velocity  $\beta\mathbf{c}$ . Therefore, the primary fields are TM type and their explicit expression are given below

$$\begin{aligned}
E_z^0(r,z) &= \frac{jqZ_0\kappa}{2\pi\gamma|\beta|} \left[ K_0(\kappa r) - \frac{I_0(\kappa r)}{I_0(\kappa g)} K_0(\kappa g) \right] \exp(-jkz/\beta) \operatorname{sng}(k/\beta) \\
E_r^0(r,z) &= \frac{qZ_0\kappa}{2\pi|\beta|} \left[ K_1(\kappa r) + \frac{I_1(\kappa r)}{I_0(\kappa g)} K_0(\kappa g) \right] \exp(-jkz/\beta) \\
H_\varphi^0(r,z) &= \frac{q\kappa}{2\pi} \left[ K_1(\kappa r) + \frac{I_1(\kappa r)}{I_0(\kappa g)} K_0(\kappa g) \right] \exp(-jkz/\beta) \operatorname{sng}(\beta)
\end{aligned} \tag{3.1}$$

where  $\mathbf{g} = \mathbf{b}$  (in the waveguide);  $\mathbf{g} = \mathbf{c}$  (in the iris) ,  $\kappa = k/\beta\gamma$  ,  $\mathbf{K}_m$  and  $\mathbf{I}_m$  are modified Bessel Function, (In the following formulas we adopted  $q=1$  for simplicity). In **Appendix A** is given a detailed exposition.

This configuration is split in two semi-infinite pipes, separated by a cylindrical region of the same radius as the iris and of same length. The pipes are considered as waveguides and the cylindrical region as a pillbox cavity. The basic idea of the analytical approach is to represent the EM Fields in the cavity and in the waveguides by means of eigenmodes of these structures as considered isolated and with perfect (magnetic or electric) walls. It is well known that these modes form a complete set by means of which we can represent any EM Field configurations. Then, in order to find the expansion coefficients, we must impose the continuity of the electric and the magnetic fields on the borders separating adjacent structures.

The boundary conditions on the iris are:

- Perfect magnetic conductor on the bases
- Perfect electric conductor on the lateral surface

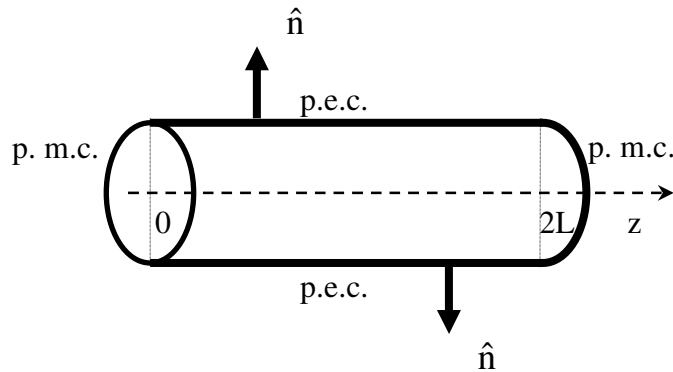


**Fig. 3-2. Scheme of the boundary conditions.**

The primary fields are of TM type. The cylindrical symmetry does not introduce any longitudinal Magnetic Field. Therefore, the scattered field will be of TM type too.

One can tackle the problem in two different ways:

1. Assume the primary source and impose the boundary conditions on the surface and the continuity on the ports [4]
2. Assume on the surfaces and on the port the primary fields and impose that the modes must cancel these primary fields.

We will adopt the second approach. It is clear that the primary field alone does not satisfy all the boundary conditions: for instance, the tangent electric primary field on the corona is not vanishing. Therefore, the modes must restore this condition on this surface.

The EM Travelling Modes inside a generic cylindrical structure of radius  $g$  can be represented by the following normalized eigenmodes:

$$\Phi_{0q}^g(k_q r) = \frac{J_0(k_q r)}{g\sqrt{\pi}J_1(\alpha_q)} \quad (3.2)$$

$$\Phi_{1q}^g(k_q r) = \frac{J_1(k_q r)}{g\sqrt{\pi}J_1(\alpha_q)} \quad (3.3)$$

where  $k_q = \alpha_q/g$  and  $\alpha_q$  is the  $q^{\text{th}}$  zero of the equation  $J_0(\alpha) = 0$ . More details about these expressions are written in **Appendix B**.

For a cylindrical cavity of radius  $\mathbf{c}$  and length  $2\mathbf{L}$  the formula of the normalized eigenmodes is written [4] as

$$\begin{aligned} \vec{e}_{ps}(r, z) &= e_{ps}(r, z)\hat{r} + e_{ps}^z(r, z)\hat{z} = \\ &= \frac{1}{k_{ps}} \sqrt{\frac{\epsilon_s}{2L}} \left[ -k_s \cos(k_s z) \Phi_{1p}^c(k_p r)\hat{r} + k_p \sin(k_s z) \Phi_{0p}^c(k_p r)\hat{z} \right] \end{aligned} \quad (3.4)$$

$$\vec{h}_{ps}(r, z) = h_{ps}(r, z)\hat{\phi} = \sqrt{\frac{\epsilon_s}{2L}} \sin(k_s z) \Phi_p^c(k_p r)\hat{\phi}$$

where  $\epsilon_s$  is the Neumann symbol ( $\epsilon_s = 1$  if  $s=1$ ,  $\epsilon_s = 2$  else ) and  $k_s = \frac{\pi s z}{2L}$ .

The fields inside the three zones in which we divided the device are represented as follows

$$\begin{cases} E_{1z}(r, z) = j \sum_t V_{1t}^- \frac{k_t Y_t^b}{k} \Phi_{0t}^b(k_t r) e^{jz\sqrt{k^2 - k_t^2}} \\ E_{1r}(r, z) = \sum_t V_{1t}^- \Phi_1^b(k_t r) e^{jz\sqrt{k^2 - k_t^2}} \\ H_{1\phi}(r, z) = - \sum_t V_{1t}^- \frac{Y_t^b}{Z_0} \Phi_{1t}^b(k_t r) e^{jz\sqrt{k^2 - k_t^2}} \end{cases} \quad (3.5)$$

$$\begin{cases} E_z^c(r, z) = - \sum_{p,s} \frac{V_{ps} k_p + F_{ps} k_s}{\sqrt{k_p^2 + k_s^2}} \sqrt{\frac{\epsilon_s}{2L}} \sin(k_s z) \Phi_{0p}^c(k_p r) \\ E_r^c(r, z) = \sum_{p,s} \frac{V_{ps} k_s + F_{ps} k_p}{\sqrt{k_p^2 + k_s^2}} \sqrt{\frac{\epsilon_s}{2L}} \cos(k_s z) \Phi_{1p}^c(k_p r) \\ H_\phi^c(r, z) = - \sum_{p,s} I_{ps} \sqrt{\frac{\epsilon_s}{2L}} \sin(k_s z) \Phi_{1p}^c(k_p r) \end{cases} \quad (3.6)$$

$$\begin{cases} E_{2z}(r, z) = -j \sum_t V_{2t}^+ \frac{k_t Y_t^b}{k} \Phi_0^b(k_t r) e^{-j(z-2L)\sqrt{k^2 - k_t^2}} \\ E_{2r}(r, z) = \sum_t V_{2t}^+ \Phi_1^b(k_t r) e^{-j(z-2L)\sqrt{k^2 - k_t^2}} \\ H_{2\phi}(r, z) = \sum_t V_{2t}^+ \frac{Y_t^b}{Z_0} \Phi_{1t}^b(k_t r) e^{-j(z-2L)\sqrt{k^2 - k_t^2}} \end{cases} \quad (3.7)$$

where  $I_{ps} = -\frac{Z_0 k_{ps}}{j\alpha\mu} V_{ps} = j \frac{k_{ps}}{k} V_{ps}$  ;  $k_{ps} = \sqrt{k_p^2 + k_s^2}$  ;  $\epsilon_s$  is the Neumann symbol

( $\epsilon_s = 1$  if  $s=1$ ,  $\epsilon_s = 2$  else );  $Y_t^b = \frac{k}{\sqrt{k^2 - (\alpha_t/b)^2}} = \frac{1}{Z_t^b}$  ( $\mathbf{b}$  is the pipe cross section

radius);  $V_{ps}$  and  $F_{ps}$  are the excitation coefficients of the divergenceless and irrotational resonant modes respectively.

The total field inside every region is given by the superposition of the primary fields in **eq.(3.1)** and the fields just defined. This superposition will be the expression used in the next paragraph, for the Field Continuity verification.

### 3.2 Matching the electric field

Now we will define the Electric field continuity at the interfaces between the three subsets in which we divided the device, taking into account the irrotational modes too:

$$\begin{cases} E_r^0(r,0^-) + E_{1r}(r,0^-) = [E_r^0(r,0^+) + E_r^c(r,0^+)]\tilde{H}(c-r) & z=0 \\ E_r^0(r,2L^+) + E_{2r}(r,2L^+) = [E_r^0(r,2L^-) + E_r^c(r,2L^-)]\tilde{H}(c-r) & z=2L \end{cases} \quad (3.8)$$

where the primary field are indicated by the superscript “0”, and  $\tilde{H}(c-r)$  is the Heaviside step function that represents the neglecting of the fields in correspondence to the coronas.

From **eq.(3.8)** and using the expressions of the Transverse Magnetic Modes, we get the explicit expression of the continuity at the interfaces:

$$\begin{cases}
\frac{Z_0 \kappa}{2\pi|\beta|} \left[ K_1(\kappa r) + \frac{I_1(\kappa r)}{I_0(\kappa b)} K_0(\kappa b) \right] + \sum_t V_{1t}^- \Phi_{1t}^b(k, r) = \\
= \left\{ \frac{Z_0 \kappa}{2\pi|\beta|} \left[ K_1(\kappa r) + \frac{I_1(\kappa r)}{I_0(\kappa c)} K_0(\kappa c) \right] + \sum_p \left[ \Phi_{1p}^c(k, r) \sum_s \frac{V_{ps} k_s + F_{ps} k_p}{\sqrt{k_p^2 + k_s^2}} \sqrt{\frac{\epsilon_s}{2L}} \right] \right\} \tilde{H}(c-r) \\
\frac{Z_0 \kappa}{2\pi|\beta|} \left[ K_1(\kappa r) + \frac{I_1(\kappa r)}{I_0(\kappa b)} K_0(\kappa b) \right] e^{-\frac{jk2L}{\beta}} + \sum_t V_{2t}^+ \Phi_{1t}^b(k, r) = \\
= \left\{ \frac{Z_0 \kappa}{2\pi|\beta|} \left[ K_1(\kappa r) + \frac{I_1(\kappa r)}{I_0(\kappa c)} K_0(\kappa c) \right] e^{-\frac{jk2L}{\beta}} + \sum_p \left[ \Phi_{1p}^c(k, r) \sum_s \frac{V_{ps} k_s + F_{ps} k_p}{\sqrt{k_p^2 + k_s^2}} \sqrt{\frac{\epsilon_s}{2L}} (-1)^s \right] \right\} \tilde{H}(c-r)
\end{cases} \quad (3.9)$$

where  $b$  and  $c$  are the waveguide and cavity radii respectively; indices 1,2 indicate the left and the right interface between subsets.

By adopting the Ritz Galerkin method, we project **eq.(3.9)** on the eigenfunctions  $\Phi_{1t}^b(k, r)$  and we obtain the following system:

$$\begin{cases}
A_{1t} + V_{1t}^- = \sum_p M_{pt} V_{1p} \\
A_{2t} + V_{2t}^+ = \sum_p M_{pt} V_{2p}
\end{cases} \quad (3.10)$$

where the vectors  $\mathbf{A}_{1t}$  and  $\mathbf{A}_{2t}$  are related to the primary fields and are defined as

$$A_{1t} = \int_S E_r^0(r, 0^-) \Phi_{1t}^b(k_t, r) dS - \left[ \int_S E_r^0(r, 0^+) \Phi_{1t}^b(k_t, r) dS \right] \tilde{H}(c-r)$$

$$A_{2t} = A_{1t} e^{\frac{-jk2L}{\beta}} \quad (3.11)$$

where  $S$  indicates the interfaces surface and the matrix  $M_{pt}$  is defined as

$$M_{pt} = 2\pi \int_0^c \Phi_{1p}^c(k_p, r) \Phi_{1t}^b(k_t, r) r dr \quad (3.12)$$

and their explicit expression is given in **Appendix C**.

It is worth of note that it is needed to get the sums  $V_{1p}$  e  $V_{2p}$  defined as:

$$V_{1p} = \sum_s \sqrt{\frac{\epsilon_s}{2L}} \frac{V_{ps} k_s + F_{ps} k_p}{\sqrt{k_p^2 + k_s^2}}$$

$$V_{2p} = \sum_s (-1)^s \sqrt{\frac{\epsilon_s}{2L}} \frac{V_{ps} k_s + F_{ps} k_p}{\sqrt{k_p^2 + k_s^2}} \quad (3.13)$$

The just given definition will introduce a simplification because one index has been “saturated”.

### 3.3 The excitation coefficients (PEC+PMC)

The mode excitation coefficients  $V_{ps}$  and  $F_{ps}$  defined in the above paragraph, are determined taking into account the coupling between cavity and waveguides. Using Maxwell Equations and the modal orthonormality, after some algebra it is possible to reach the formulas we are looking for. Operating in such way, it is implicit to impose the continuity of the tangential Magnetic Fields on the interfaces between cavities and waveguides. This means that we build a non-zero Field in correspondence of the cavity ports, using Field distributions that result zero on the same ports (cavity modes). This operation is done because the sum converge not uniformly, so the limit of the sum calculated in a point that lies on the perfect magnetic conductor surface cannot be changed to the sum in a point whose limit tends to the surface of the conductor. In fact, the first limit is zero, whereas the second tends to the assigned Magnetic Field. This procedure has a critical point in correspondence of the edges angles where the field should tend to infinite. However, this effect is not a real problem because the parameters we are calculating are of global type, so they means on these critical points.

Summarizing what written above, the continuity of the Electric Field cannot be expressed “tout court” using the eigenfunction expansions because they satisfy the homogeneous boundary conditions. However, this inconvenient can be circumvented resorting to the excitation coefficients  $V_{ps}$  as function of the Magnetic Field distribution on the ports [3] as:

$$V_{ps} = -\frac{jkZ_0}{k^2 - k_p^2 - k_s^2} \int_S (\vec{H} \times \vec{e}_{ps}^*) \cdot \hat{n} dS \quad (3.14)$$

where  $\hat{n}$  is the outgoing unity vector orthogonal to the cavity surface  $S$  and  $\vec{e}_{ps}$  is given by **eq.(3.4)**.

We will have a non-zero Electric Field tangent component only on the two ports  $S_1$  and  $S_2$ . Therefore, one can write the **eq.(3.14)** as:

$$\begin{aligned} V_{ps} &= \frac{jkZ_0}{k^2 - k_p^2 - k_s^2} \left[ -\int_{S_1} \hat{z} \times \vec{H} \cdot \vec{e}_{ps}^*(r,0) dS + \int_{S_2} \hat{z} \times \vec{H} \cdot \vec{e}_{ps}^*(r,2L) dS \right] = \\ &= \frac{jkZ_0}{k^2 - k_p^2 - k_s^2} \left[ -\int_{S_1} H_\varphi^c(r,0^+) e_{ps}^*(r,0) dS + \int_{S_2} H_\varphi^c(r,2L^-) e_{ps}^*(r,2L) dS \right] \end{aligned} \quad (3.15)$$

where  $\hat{z}$  indicate the positive direction of  $\mathbf{z}$  axis from left to right and  $\vec{H}$  represents the total Magnetic Field at the interface surfaces. We impose the boundary conditions of the tangential Electric Field on the surfaces  $S_1$  and  $S_2$ . Even if the radial component of the modes vanishes on these surfaces (see **eq.(3.8)**), however they must behave a non-uniform convergence to values different from zero such as to satisfy the following conditions:

$$\begin{aligned}
 H_\varphi^0(r, z = 0^-) + \sum_t \frac{V_{1t}^-}{Z_0 Z_t^b} \Phi_{1t}^b(k_t r) &= [H_\varphi^c(r, z = 0^+) + H_\varphi^0(r, z = 0^+)] \tilde{H}(c - r) \\
 H_\varphi^0(r, z = 2L^+) + \sum_t \frac{V_{2t}}{Z_0 Z_t^b} \Phi_{1t}^b(k_t r) &= [H_\varphi^c(r, z = 2L^-) + H_\varphi^0(r, z = 2L^-)] \tilde{H}(c - r)
 \end{aligned}
 \tag{3.16}$$

Expanding the integral and taking into account the definition of the matrix element

$M_{pt}$  one may get the formula:

$$V_{ps} = -\frac{j2\pi k Z_0 k_s}{(k^2 - k_p^2 - k_s^2) k_{ps}} \sqrt{\frac{\epsilon_s}{2L}} \left[ \left( N_{1p} - \sum_t M_{pt} \frac{V_{1t}^-}{Z_0 Z_t^b} \right) - (-1)^s \left( N_{2p} + \sum_t M_{pt} \frac{V_{2t}^+}{Z_0 Z_t^b} \right) \right]
 \tag{3.17}$$

where

$$N_{1p} = -2\pi \int_0^c [H_\varphi^c(r, z = 0^-) - H_\varphi^c(r, z = 0^+)] \cdot \Phi_p^c(k_p r) r dr
 \tag{3.18}$$

$$N_{2p} = N_{1p} e^{\frac{-jk2L}{\beta}}$$

and its explicit expression is given in **Appendix C**.

For what concerns the irrotational modes we have [4]

$$F_{ps} = -\frac{j\beta\sqrt{\pi}}{k} \left[ \int_S (\vec{f}_{ps} \times \vec{H}) \cdot \hat{n} dS \right] \quad (3.19)$$

where  $\hat{n}$  is the outgoing versor orthogonal to the cavity surface  $S$  and  $\vec{f}_{ps}$  is given by

$$\begin{aligned} \vec{f}_{ps}(r,z) &= \nabla \left[ \sqrt{\frac{\epsilon_s}{2L}} \frac{\cos(k_s z) J_0(k_p r)}{c\sqrt{\pi} k_{ps} J_1(\alpha_p)} \right] = \\ &= \frac{1}{k_{ps}} \sqrt{\frac{\epsilon_s}{2L}} \left[ \frac{k_p \cos(k_s z) J_1(k_p r) \hat{r} - k_s \sin(k_s z) J_0(k_p r) \hat{z}}{c\sqrt{\pi} J_1(\alpha_p)} \right] \end{aligned} \quad (3.20)$$

We will have a non-zero Electric Field tangent component only on the two ports  $S_1$  and  $S_2$ . Therefore, one can write

$$F_{ps} = -\frac{j\beta\sqrt{\pi}}{k} \left[ \int_{S_1} (\vec{f}_{ps}(r,0) \times \vec{H}) \cdot \hat{n} dS + \int_{S_2} (\vec{f}_{ps}(r,2L) \times \vec{H}) \cdot \hat{n} dS \right] \quad (3.21)$$

where  $\vec{H}$  represents the total field at the interface surfaces.

Expanding  $\vec{f}_{ps}$  we obtain after some algebra

$$F_{ps} = -\frac{j2\pi Z_0 k_p}{k k_{ps}} \sqrt{\frac{\epsilon_s}{2L}} \left[ \int_0^c (\vec{H}_{1\varphi} - (-1)^s \vec{H}_{2\varphi}) \Phi_{1p}^c(k_p r) r dr \right] \quad (3.22)$$

Taking into account the definition of  $V_{1p}$  and  $V_{2p}$  as given by **eq.(3.13)**, we get:

$$\begin{aligned}
 V_{1p} &= -\frac{j}{kL} (k^2 - k_p^2) \sum_s \frac{\epsilon_s}{(k^2 - k_{ps}^2)} \left[ \left( Z_0 N_{1p} - \sum_t M_{pt} \frac{V_{1t}^-}{Z_t^b} \right) - (-1)^s \left( Z_0 N_{2p} + \sum_t M_{pt} \frac{V_{2t}^+}{Z_t^b} \right) \right] \\
 V_{2p} &= -\frac{j}{kL} (k^2 - k_p^2) \sum_s \frac{\epsilon_s}{(k^2 - k_{ps}^2)} \left[ (-1)^s \left( Z_0 N_{1p} - \sum_t M_{pt} \frac{V_{1t}^-}{Z_t^b} \right) - \left( Z_0 N_{2p} + \sum_t M_{pt} \frac{V_{2t}^+}{Z_t^b} \right) \right]
 \end{aligned}
 \tag{3.23}$$

A key feature of this expression is the two sums with the s-index can be put in a closed form. This is a general property and is related with the modal expansion of Green Function. Resorting to **eq.(1.421.4)** of reference [5] one can compact the sums over “s” as:

$$\frac{1}{2L} \sum_s \frac{\epsilon_s}{(k^2 - k_{ps}^2)} = \frac{\cot(2L\sqrt{k^2 - k_p^2})}{\sqrt{k^2 - k_p^2}}
 \tag{3.24}$$

$$\frac{1}{2L} \sum_s \frac{(-1)^s \epsilon_s}{(k^2 - k_{ps}^2)} = \frac{\csc(2L\sqrt{k^2 - k_p^2})}{\sqrt{k^2 - k_p^2}}$$

In addition to the undoubted advantage of the analytical sum, one has the further advantage that the matrices are reduced of one dimension. The electromagnetic

problems will also benefit of this behaviour: all the longitudinal electromagnetic modes are taking into account and therefore only a few transverse modes are sufficient to describe the phenomenon.

From the above algebra, we obtain then the simplified form:

$$\begin{aligned}
 V_{1p} &= -jZ_p^c \left[ \cot(2LkZ_p^c) \left( Z_0 N_{1p} - \sum_t M_{pt} \frac{V_{1t}^-}{Z_t^b} \right) - \csc(2LkZ_p^c) \left( Z_0 N_{2p} + \sum_t M_{pt} \frac{V_{2t}^+}{Z_t^b} \right) \right] \\
 V_{2p} &= -jZ_p^c \left[ \csc(2LkZ_p^c) \left( Z_0 N_{1p} - \sum_t M_{pt} \frac{V_{1t}^-}{Z_t^b} \right) - \cot(2LkZ_p^c) \left( Z_0 N_{2p} + \sum_t M_{pt} \frac{V_{2t}^+}{Z_t^b} \right) \right]
 \end{aligned}
 \tag{3.25}$$

where  $Z_p^c = \frac{\sqrt{k^2 - (\alpha_p/c)^2}}{k} = \frac{1}{Y_p^c}$  ( $\mathbf{c}$  is the iris cross section radius).

Expressing the above formula in terms of matrices and vectors, we get:

$$\begin{aligned}
 \underline{V}_1 &= j\underline{Z}^c \left[ \csc(2kL\underline{Z}^c) \cdot (Z_0 \underline{N}_2 + \underline{M} \underline{Y}^b \underline{V}_2^+) - \cot(2kL\underline{Z}^c) \cdot (Z_0 \underline{N}_1 - \underline{M} \underline{Y}^b \underline{V}_1^-) \right] \\
 \underline{V}_2 &= j\underline{Z}^c \left[ \cot(2kL\underline{Z}^c) \cdot (Z_0 \underline{N}_2 + \underline{M} \underline{Y}^b \underline{V}_2^+) - \csc(2kL\underline{Z}^c) \cdot (Z_0 \underline{N}_1 - \underline{M} \underline{Y}^b \underline{V}_1^-) \right]
 \end{aligned}
 \tag{3.26}$$

where  $\underline{Z}^c$  and  $\underline{Y}^b$  are diagonal matrices.

### 3.4 The Equation System

By equating eq. (3.10) with eq. (3.26), we get the following infinite system in infinite unknowns:

$$\begin{cases} \underline{A}_1 + \underline{V}_1^- = j\underline{M}^T \underline{Z}^c \left[ \csc(2kL\underline{Z}^c) \cdot (\underline{Z}_0 \underline{N}_2 + \underline{M} \underline{Y}^b \underline{V}_2^+) - \cot(2kL\underline{Z}^c) \cdot (\underline{Z}_0 \underline{N}_1 - \underline{M} \underline{Y}^b \underline{V}_1^-) \right] \\ \underline{A}_2 + \underline{V}_2^+ = j\underline{M}^T \underline{Z}^c \left[ \cot(2kL\underline{Z}^c) \cdot (\underline{Z}_0 \underline{N}_2 + \underline{M} \underline{Y}^b \underline{V}_2^+) - \csc(2kL\underline{Z}^c) \cdot (\underline{Z}_0 \underline{N}_1 - \underline{M} \underline{Y}^b \underline{V}_1^-) \right] \end{cases} \quad (3.27)$$

By means of some algebra it is possible to uncouple the unknowns and, therefore, to simplify the solution. By adding and subtracting the two expressions, we obtain:

$$\begin{aligned} \left[ \underline{I} - j\underline{M}^T \underline{Z}^c \cot(kL\underline{Z}^c) \underline{M} \underline{Y}^b \right] (\underline{V}_1^- + \underline{V}_2^+) &= \\ = -(\underline{A}_1 + \underline{A}_2) - j\underline{Z}_0 \underline{M}^T \underline{Z}^c \cot(kL\underline{Z}^c) (\underline{N}_1 - \underline{N}_2) & \end{aligned} \quad (3.28)$$

$$\begin{aligned} \left[ \underline{I} + j\underline{M}^T \underline{Z}^c \tan(kL\underline{Z}^c) \underline{M} \underline{Y}^b \right] (\underline{V}_1^- + \underline{V}_2^+) &= \\ = (\underline{A}_2 - \underline{A}_1) + j\underline{Z}_0 \underline{M}^T \underline{Z}^c \tan(kL\underline{Z}^c) (\underline{N}_1 + \underline{N}_2) & \end{aligned} \quad (3.29)$$

Where we resorted to the following trigonometric expressions:

$$\tan(x/2) = \csc(x) - \cot(x) \quad \text{and} \quad \cot(x/2) = \csc(x) + \cot(x)$$

As a conclusion one can see that the equations are uncoupled since in the first one appears only the unknown  $(\underline{V}_1^- + \underline{V}_2^+)$  and in the second one only  $(\underline{V}_1^- - \underline{V}_2^+)$ .

Therefore, they can be solved by the inversion of a simpler matrix.

Other authors in a similar way solve the problem for this case resorting to a wave representation inside the iris (**Travelling Wave Mode Matching**):

$$\begin{cases} E_{2z}(r, z) = j \frac{1}{\beta\sqrt{\pi}} \sum_p \frac{k_p}{\sqrt{k^2 - k_p^2}} \Phi_{0p}^c(k_p r) \left[ -V_{2p}^+ e^{-j\sqrt{k^2 - k_p^2}z} + V_{2p}^- e^{j\sqrt{k^2 - k_p^2}(z-2L)} \right] \\ E_{2r}(r, z) = \frac{1}{\beta\sqrt{\pi}} \sum_p \Phi_{1p}^c(k_p r) \left[ V_{2p}^+ e^{-j\sqrt{k^2 - k_p^2}z} + V_{2p}^- e^{j\sqrt{k^2 - k_p^2}(z-2L)} \right] \\ H_{2\phi}(r, z) = -\frac{1}{Z_0\beta\sqrt{\pi}} \sum_p \frac{k}{\sqrt{k^2 - k_p^2}} \Phi_{1p}^c(k_p r) \left[ V_{2p}^+ e^{-j\sqrt{k^2 - k_p^2}z} - V_{2p}^- e^{j\sqrt{k^2 - k_p^2}(z-2L)} \right] \end{cases} \quad (3.30)$$

where  $k_p = \alpha_p / c$  and  $\alpha_p$  are the zeros of the Bessel function  $J_0(x)$  and  $\Phi_0^c(k_p r)$  and  $\Phi_1^c(k_p r)$  are the modal functions. However, their results are restricted to the lossless case, but it is not the only limitation.

One can see that, being equivalent to each other, the mode-matching technique needs only half modes in respect to the number of modes needed by travelling wave

mode matching. This means that our technique needs less computational power to reach the result than the classical travelling wave mode matching.

However, this advantage is not enough to justify the increased mathematic difficulties introduced by this method, due to not uniformly convergent series. As will be shown, the mixed mode matching technique allows reaching better results than the other method.

### 3.5 The longitudinal coupling impedance

When a structure as the iris is studied in an accelerator project, it is important to evaluate its interaction with the particle beam. In time domain, a global parameter that defines this interaction is the wake potential, already defined. Its analogous in the frequency domain is the longitudinal coupling impedance, easily obtained from the potential using the Fourier Transform. Here we will start from the more general definition of the Impedance already given in previous paragraphs, to reach a particular expression fitted to the iris structure, as:

$$Z(k) = -\frac{1}{q} \int_{-\infty}^0 E_{1z}(r=0, z) e^{jk/\beta z} dz - \frac{1}{q} \int_0^{2L} E_{2z}(r=0, z) e^{jk/\beta z} dz + \frac{1}{q} \int_{2L}^{+\infty} E_{3z}(r=0, z) e^{jk/\beta z} dz. \quad (3.31)$$

The procedure adopted is the same as the one of the previous Chapter, and we get the numerical results listed in the next Section.

### 3.6 Numerical Results

The two Equation Systems (eq.3.28-3.29) involves infinite equations and infinite unknowns. To allow the system inversion it is necessary to truncate the infinite matrices without hack the results validity. Doing some simulations on the device is possible to see a different result for different matrix truncation. It is the Relative Convergence phenomenon [6].

At this, a finite number of modes for each waveguide and cavity must be considered. The choice of the ratios  $N_1/N_2$  and  $N_3/N_2$  (where  $N_i$  indicate the number of modes for the  $i^{\text{th}}$  region) has a considerable effect on the result goodness. Following the scheme reported on Lee and Mittra book [6] we imposed the written below relations between the numbers of modes of different zones in order to respect the Meixner condition [7].

$$\frac{N_2}{N_1} = \frac{c}{b} = w_{12} \quad (3.32)$$

In our specific case, we chosen

$$\begin{cases} N_1 = \frac{N/w_{12}}{1+1/w_{12}+1/w_{23}} \\ N_2 = \frac{N}{1+1/w_{12}+1/w_{23}} \\ N_3 = \frac{N/w_{23}}{1+1/w_{12}+1/w_{23}} \end{cases} \quad (3.33)$$

where  $N = N_1 + N_2 + N_3$  and  $w_{23} = w_{12}$  (because  $b = d$ ), then  $N_1 = N_3$ . After truncation and inversion of the linear equations, we solved the problem. It will be shown the goodness of the mode-matching analysis to manage the particle passing through a thick iris problem. It will be represented the Longitudinal Coupling Impedance, as a fundamental parameter for accelerators project, subdivided in real and imaginary parts and for different values of number of modes, geometrical parameters and particle velocity.

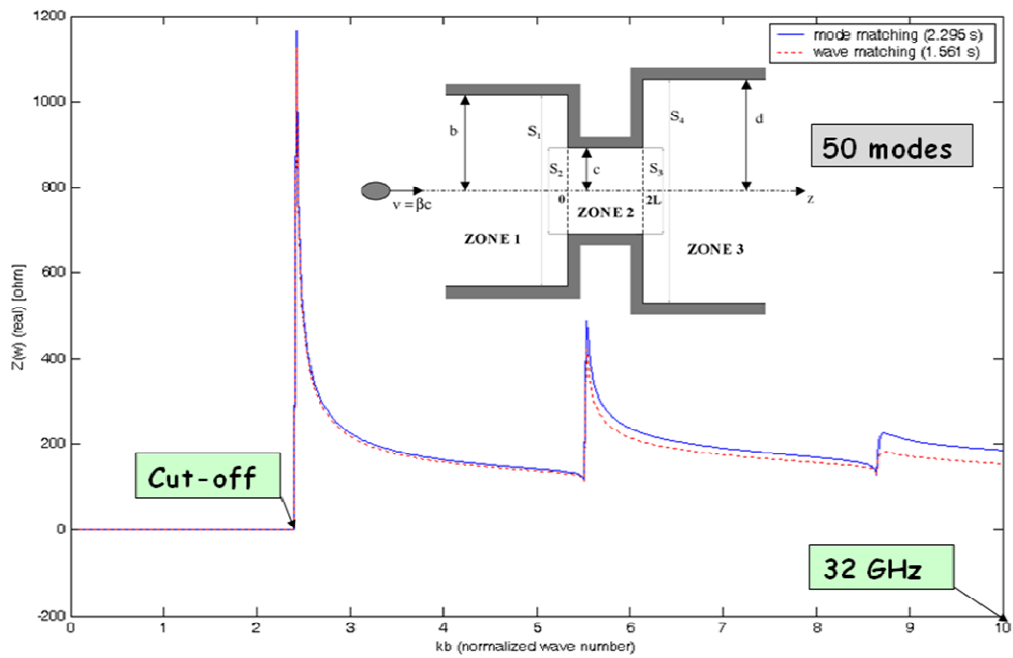


Fig. 3-3. Comparison between mixed mode matching and travelling wave mode matching applied on the same device: Real part of Coupling Impedance ( $\beta\gamma=10$ ,  $c/b=0.2$ ,  $L/b=0.25$ )

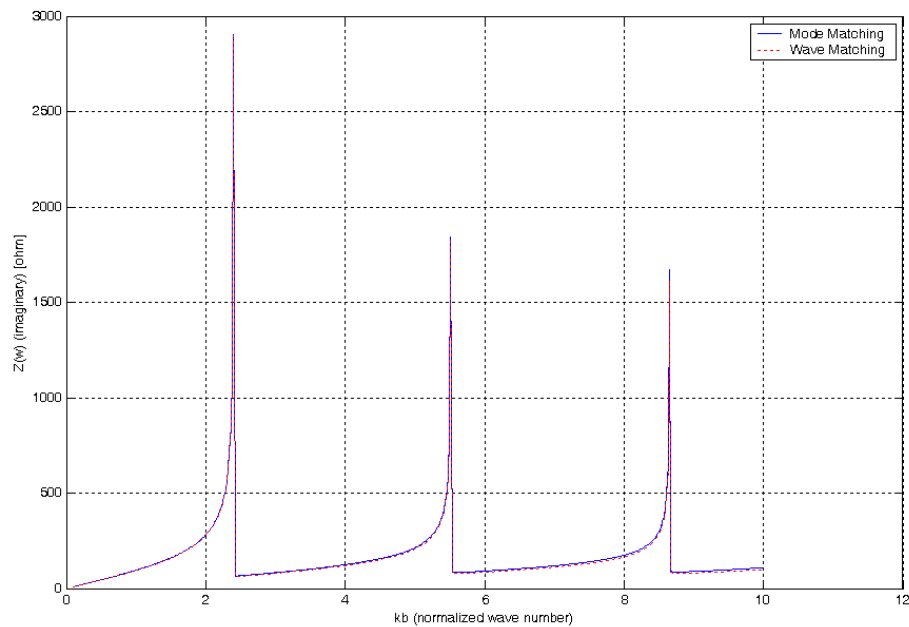


Fig. 3-4. Comparison between mixed mode matching and travelling wave mode matching applied on the same device: Imaginary part of Coupling Impedance. ( $\beta\gamma=10$ ,  $c/b=0.2$ ,  $L/b=0.25$ )

In **Fig.3-3** is shown the comparison between the method adopted here and the travelling wave mode matching (usually called mode matching in literature), applied to the same structure. It is worth of note that the normalization of wave number to the guide radius implies that the cutoff frequency will always fall on the same value of the normalized wave number. This value ( $kb = 2.4$ ) corresponds to the first zero of the Bessel Function  $J_0(x)=0$ . One should not be surprised by the vanishing of the real part of the Impedance for all the frequencies below the cutoff. A different behaviour would conflict with the energy conservation principle. Allowing for the energy released by the beam into the room delimited by the discontinuity of the iris, this energy “must be entirely given back” again to the beam itself. Since we are below the cutoff, no energy is indeed allowed to freely flow inside the pipes. Therefore, the real part of Coupling Impedance must be zero because the beam did not lose any energy. By converse, the imaginary part is certainly different from zero since there is a balanced exchange of energy between the beam and the room inside the discontinuity, as shown in **Fig.3-4**. We expect that this will not happen when the walls of the iris have a finite conductivity, since a certain amount of the energy exchanged will be dissipated on the walls. We expect that in this case at some frequencies (related to the device resonances) it will appear a non-vanishing real part in the Coupling Impedance. Above cutoff, the real part the coupling may be different from zero: a certain amount of the energy, released by the beam into the room delimited by the discontinuity of the iris, may flow into the

beam pipes. Since the phase velocity of its EM field is larger than the particle velocity, the mean power exchange between the beam and the field is zero: in sum, this energy is irreversibly lost and a non-zero real part appears in the Coupling impedance, even in the case of lossless walls.

While at low frequency the results of the two methods are almost superposable, the discrepancy between these results becomes macroscopic at high frequency, where it attains almost 10%. In order to understand which method is more convenient, we performed a convergence test for the mixed mode matching case. The results of this procedure are represented in **Fig.3-5**. In **Fig.3-3** is also reported the time needed by the computer to reach the result and it is clear that in this case the travelling wave mode matching method faster than Mixed mode matching method. It is only a coincidence, because usually the M.M. is intrinsically faster and, as more little is  $\beta\gamma$  as more evident is the difference in time.

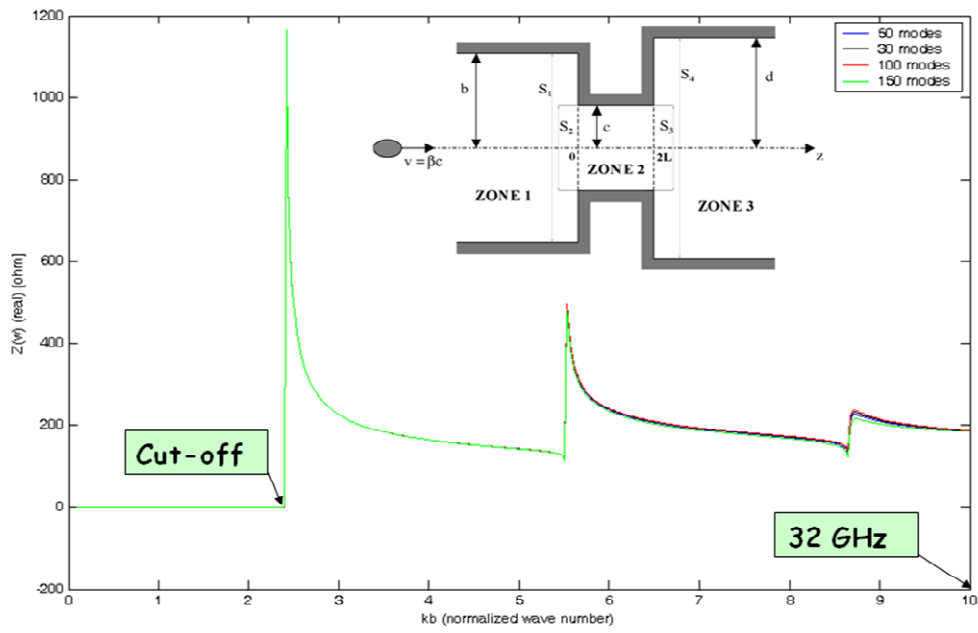


Fig. 3-5. Four Convergence test for Mixed mode matching Technique, Imaginary Part of Coupling Impedance. ( $\beta\gamma=10$ ,  $c/b=0.2$ ,  $L/b=0.25$ ).

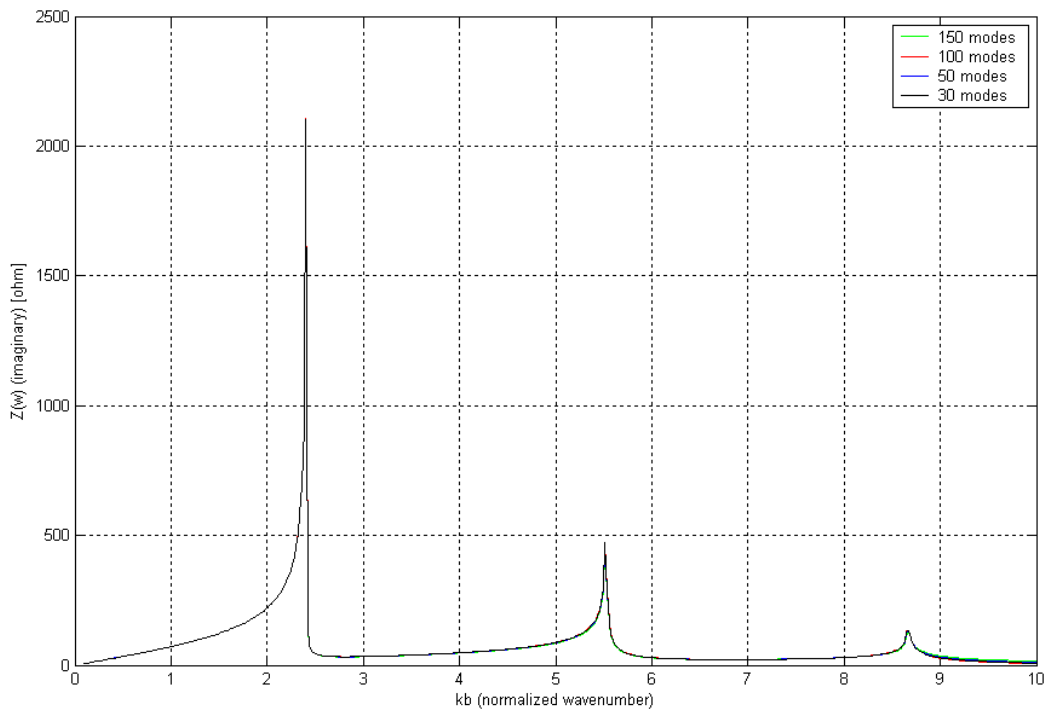
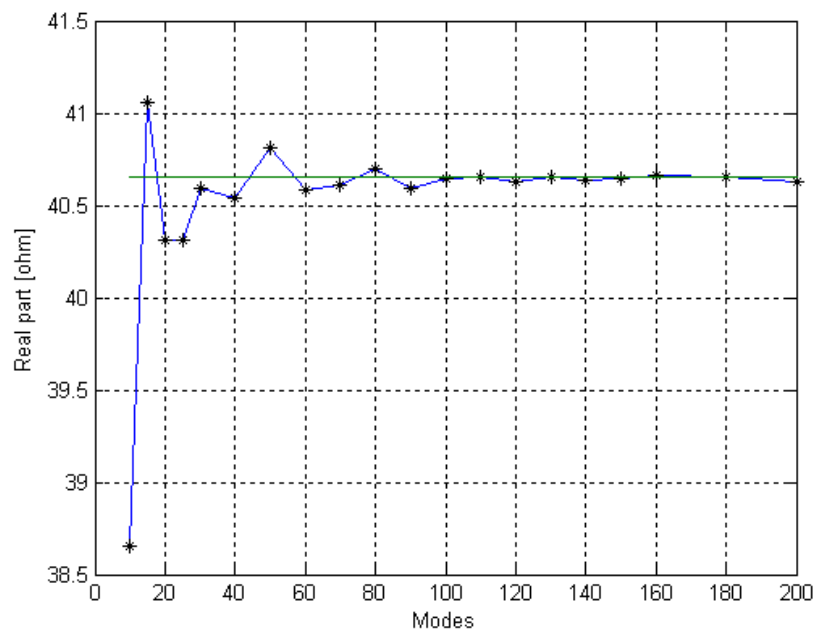


Fig. 3-6. Convergence test for Mixed mode matching Technique, Imaginary Part of Coupling Impedance. ( $\beta\gamma=10$ ,  $c/b=0.2$ ,  $L/b=0.25$ ).

This method exhibits a fast convergence in the estimation of the longitudinal coupling impedance. Few modes are required to obtain an error lower than percent and then an accurate value of the impedance. In **Fig.3-5** and **Fig.3-6** is shown the convergence study on the real part of the Coupling Impedance. If 100 modes are used, one can be find an error lower than 1%.



**fig. 3-7. Convergence of the real part of the Longitudinal Impedance. ( $kb=3$ ).**

In the figures below, we want to show how much the Longitudinal Coupling Impedance is useful to understand the interaction between the particle and the iris for some particle speed values and varying some iris parameters. Every simulation

is done using 100 modes and taking 500 points for every graphic. The only constant parameter is the waveguide radius  $b=30$  mm.

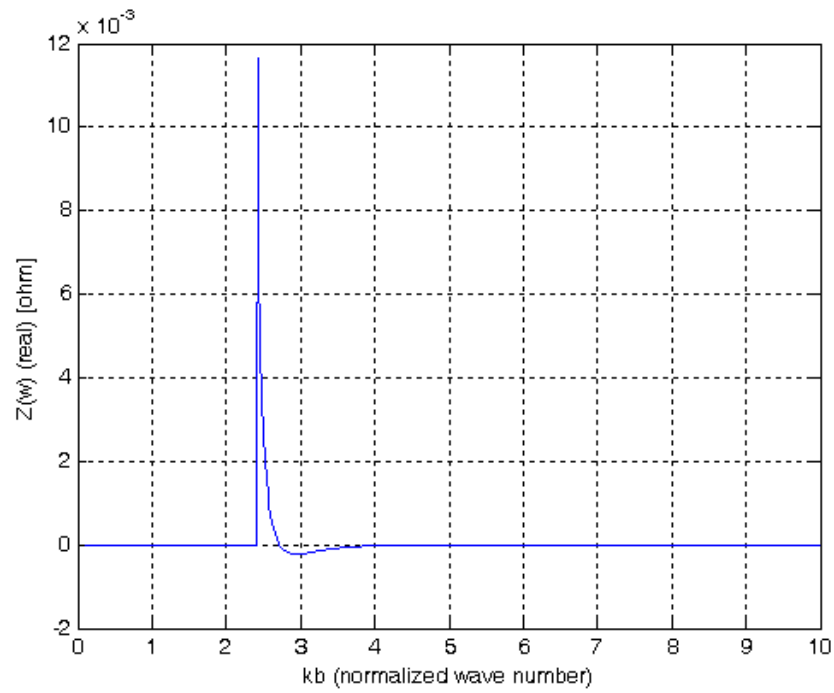


Fig. 3-8. Longitudinal Coupling Impedance, real part:  $\beta\gamma = 0.1$ ,  $c/b = 0.2$ ,  $L/b = 0.25$ .

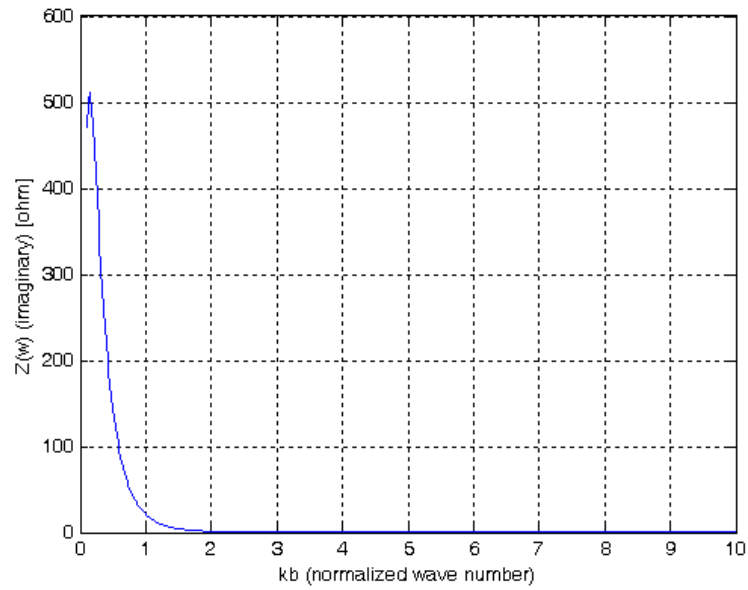


Fig. 3-9. Longitudinal Coupling Impedance, imaginary part:  $\beta\gamma = 0.1$ ,  $c/b = 0.2$ ,  $L/b = 0.25$ .

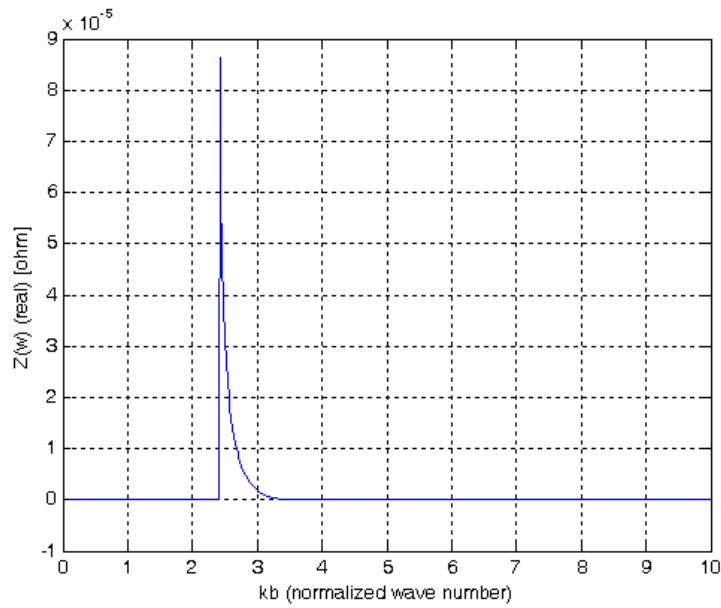


Fig. 3-10. Longitudinal Coupling Impedance, real part:  $\beta\gamma = 0.1$ ,  $c/b = 0.4$ ,  $L/b = 0.25$ .

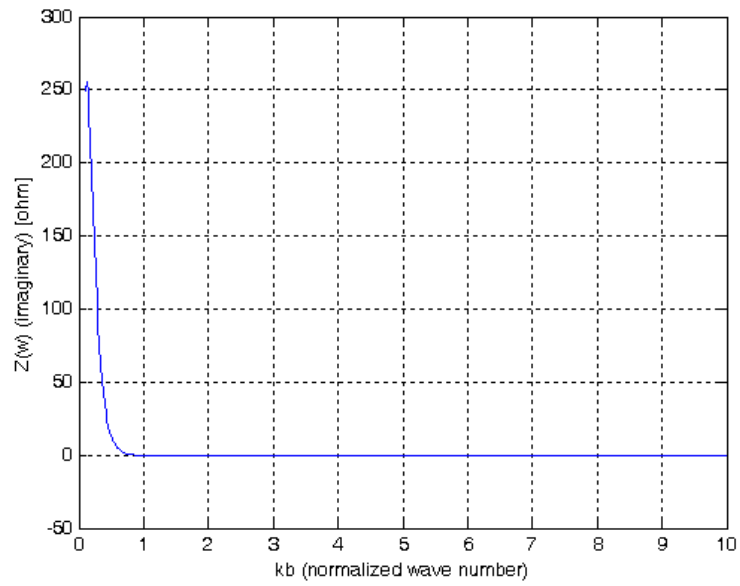


Fig. 3-11. Longitudinal Coupling Impedance, imaginary part:  $\beta\gamma = 0.1$ ,  $c/b = 0.4$ ,  $L/b = 0.25$ .

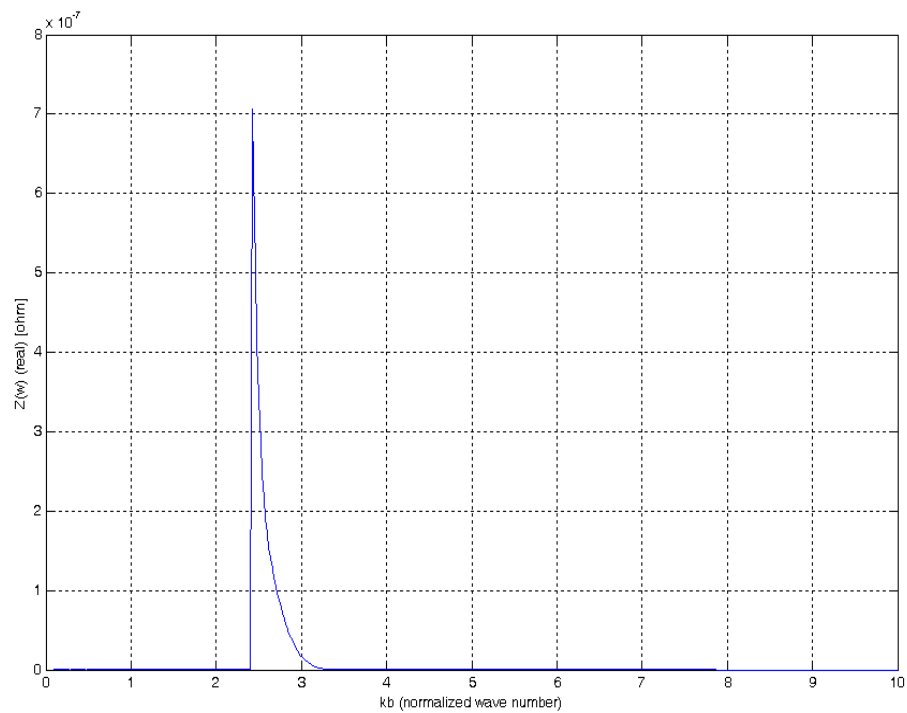


Fig. 3-12. Longitudinal Coupling Impedance, real part:  $\beta\gamma = 0.1$ ,  $c/b = 0.6$ ,  $L/b = 0.25$ .

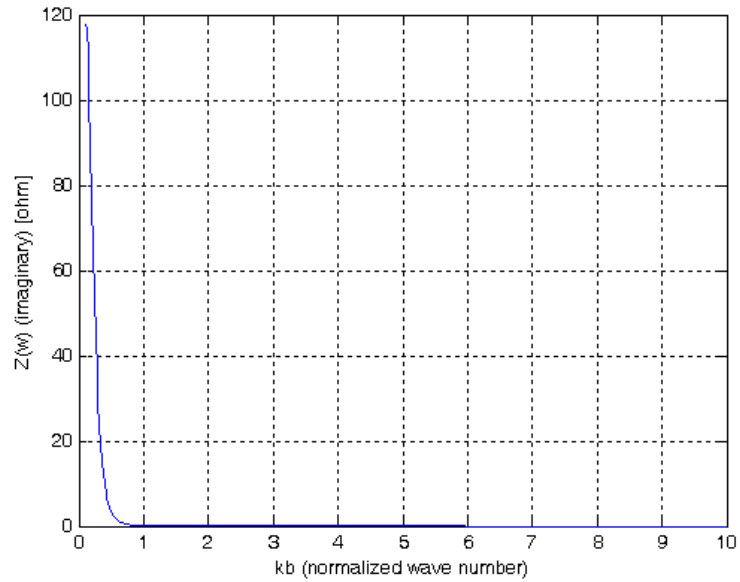


Fig. 3-13. Longitudinal Coupling Impedance, imaginary part:  $\beta\gamma = 0.1$ ,  $c/b = 0.6$ ,  $L/b = 0.25$ .

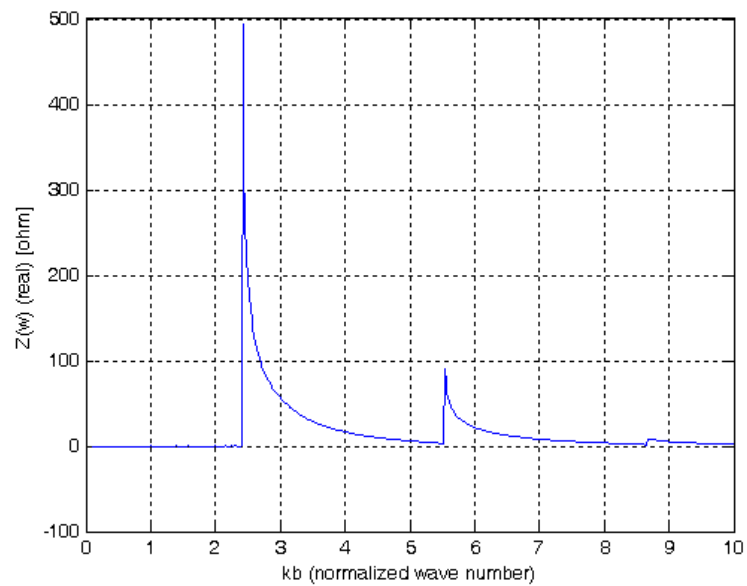


Fig. 3-14. Longitudinal Coupling Impedance, real part:  $\beta\gamma = 1$ ,  $c/b = 0.2$ ,  $L/b = 0.25$ .

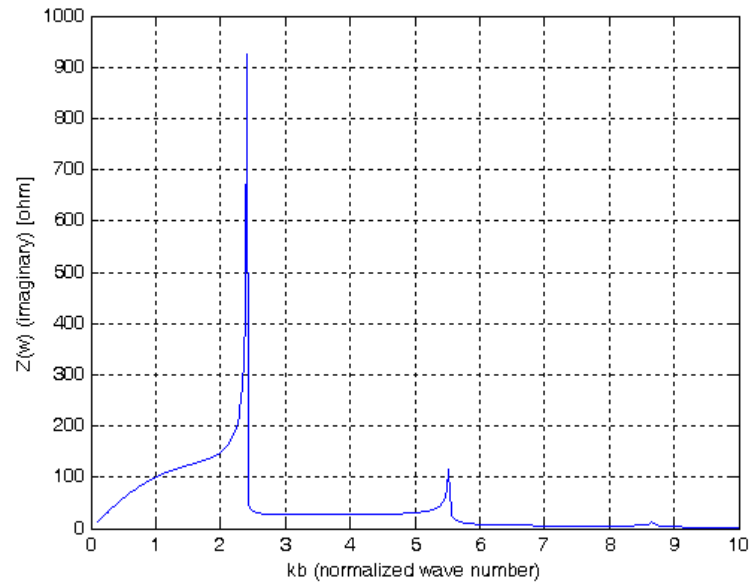


Fig. 3-15. Longitudinal Coupling Impedance, imaginary part:  $\beta\gamma = 1$ ,  $c/b = 0.2$ ,  $L/b = 0.25$ .

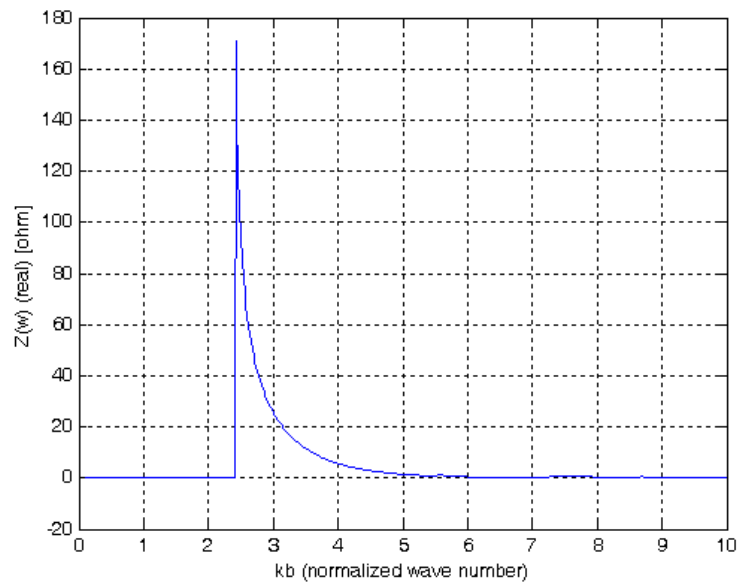


Fig. 3-16. Longitudinal Coupling Impedance, real part:  $\beta\gamma = 1$ ,  $c/b = 0.4$ ,  $L/b = 0.25$ .

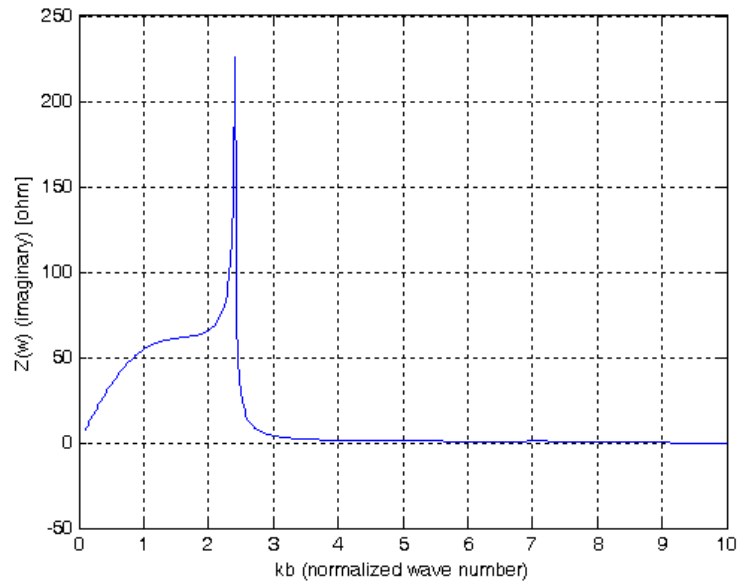


Fig. 3-17. Longitudinal Coupling Impedance, imaginary part:  $\beta\gamma = 1$ ,  $c/b = 0.4$ ,  $L/b = 0.25$ .

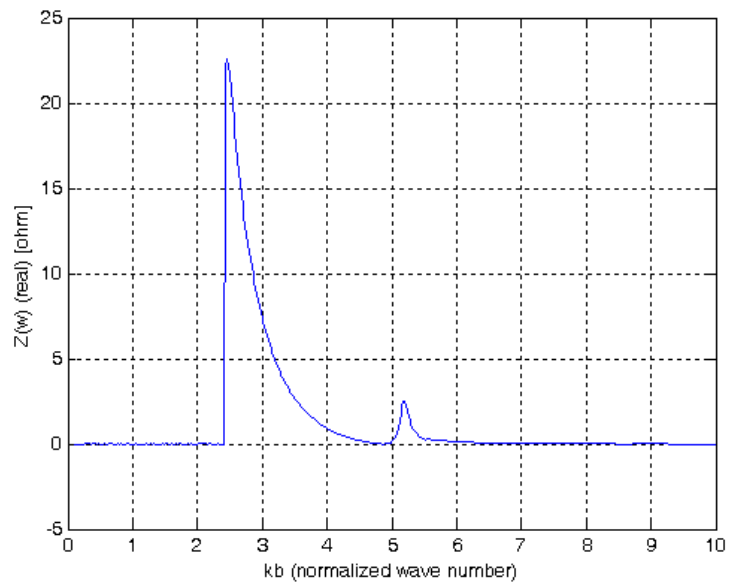


Fig. 3-18. Longitudinal Coupling Impedance, real part:  $\beta\gamma = 1$ ,  $c/b = 0.6$ ,  $L/b = 0.25$ .

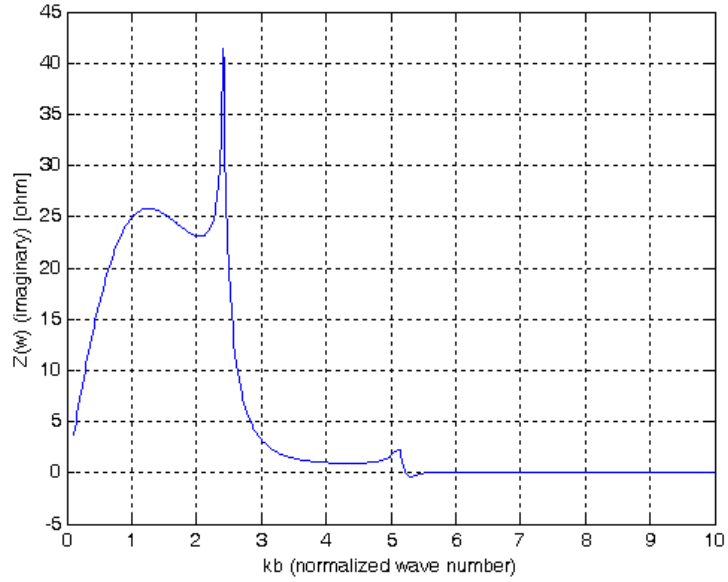


Fig. 3-19. Longitudinal Coupling Impedance, imaginary part:  $\beta\gamma = 1$ ,  $c/b = 0.6$ ,  $L/b = 0.25$ .

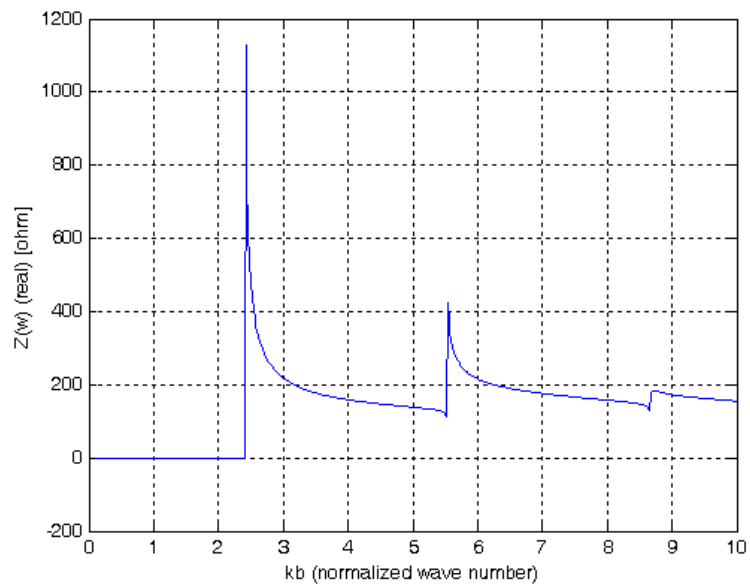


Fig. 3-20. Longitudinal Coupling Impedance, real part:  $\beta\gamma = 10$ ,  $c/b = 0.2$ ,  $L/b = 0.25$ .

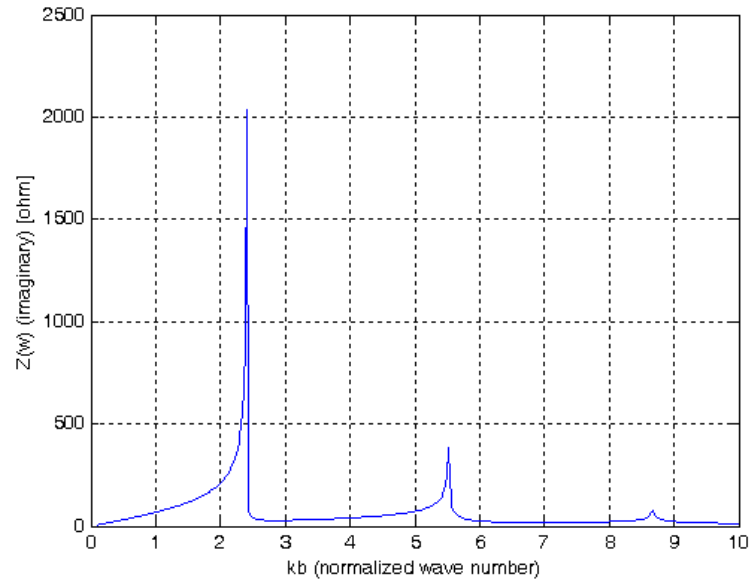


Fig. 3-21. Longitudinal Coupling Impedance, imaginary part:  $\beta\gamma = 10$ ,  $c/b = 0.2$ ,  $L/b = 0.25$ .

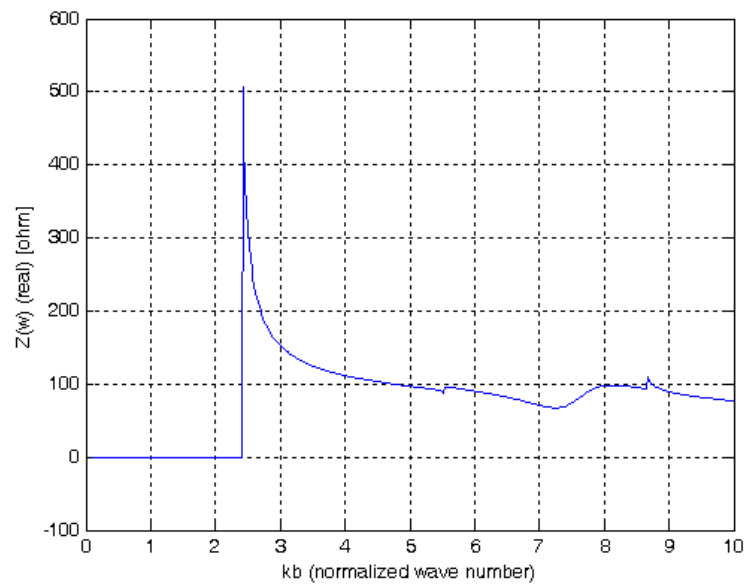


Fig. 3-22. Longitudinal Coupling Impedance, real part:  $\beta\gamma = 10$ ,  $c/b = 0.4$ ,  $L/b = 0.25$ .

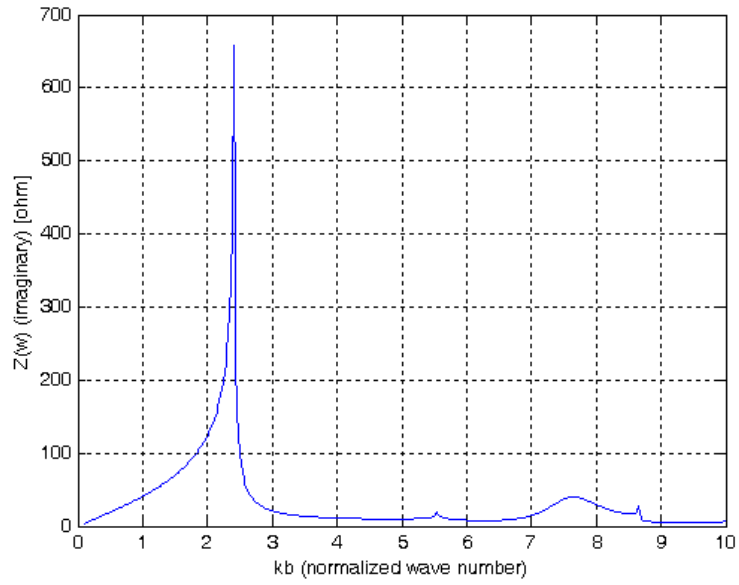


Fig. 3-23. Longitudinal Coupling Impedance, imaginary part:  $\beta\gamma = 10$ ,  $c/b = 0.4$ ,  $L/b = 0.25$ .

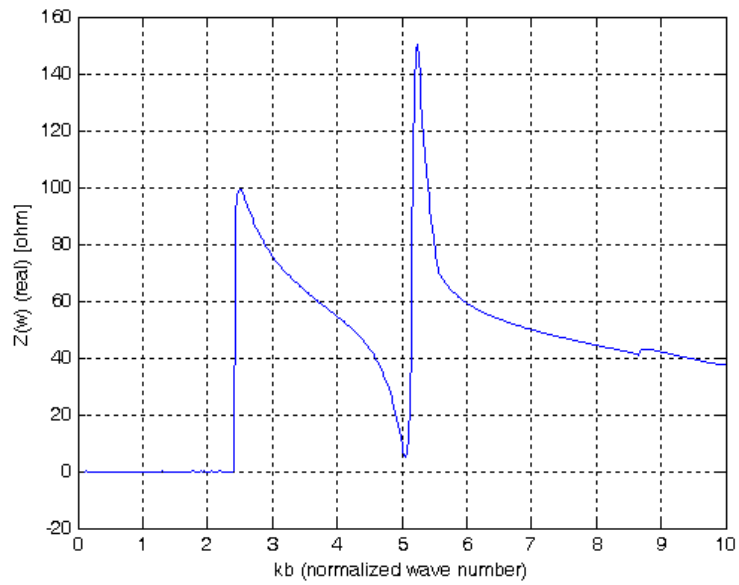


Fig. 3-24. Longitudinal Coupling Impedance, real part:  $\beta\gamma = 10$ ,  $c/b = 0.6$ ,  $L/b = 0.25$ .

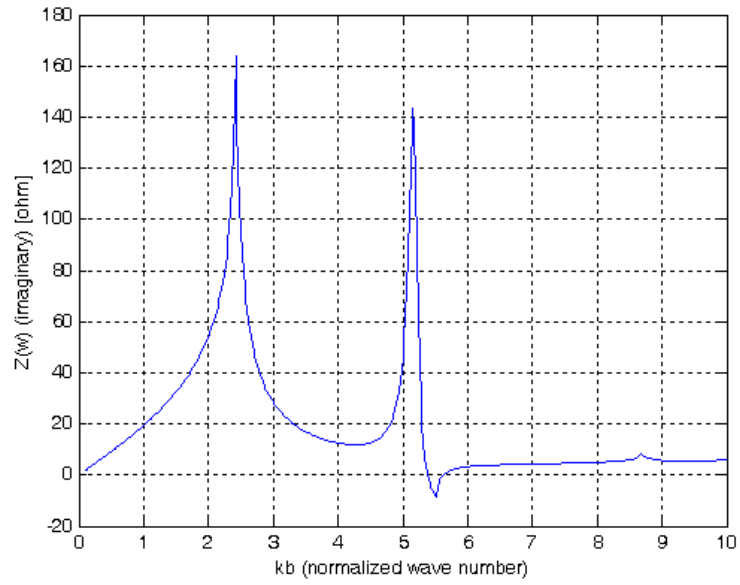


Fig. 3-25. Longitudinal Coupling Impedance, imaginary part:  $\beta\gamma = 10$ ,  $c/b = 0.6$ ,  $L/b = 0.25$ .

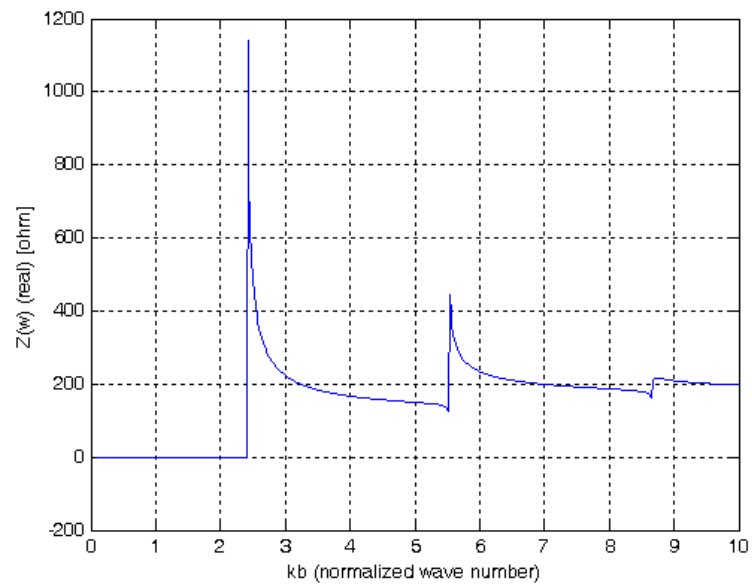


Fig. 3-26. Longitudinal Coupling Impedance, real part:  $\beta\gamma = 100$ ,  $c/b = 0.2$ ,  $L/b = 0.25$ .

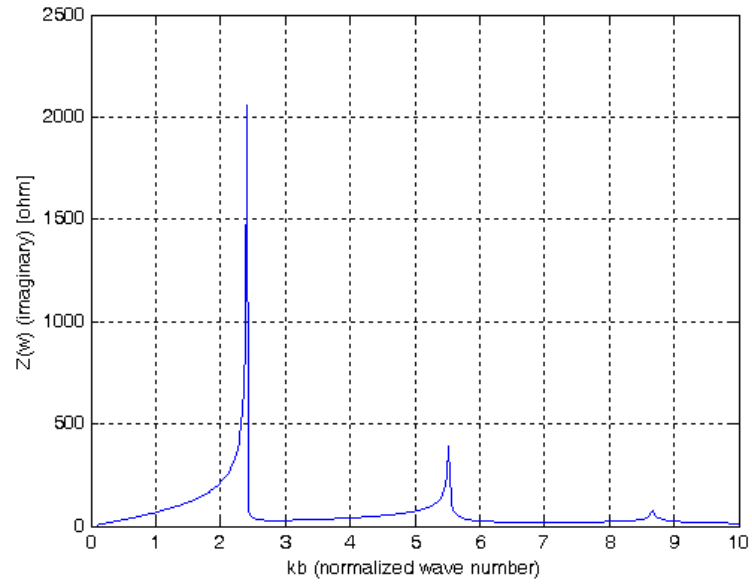


Fig. 3-27. Longitudinal Coupling Impedance, imaginary part:  $\beta\gamma = 100$ ,  $c/b = 0.2$ ,  $L/b = 0.25$ .

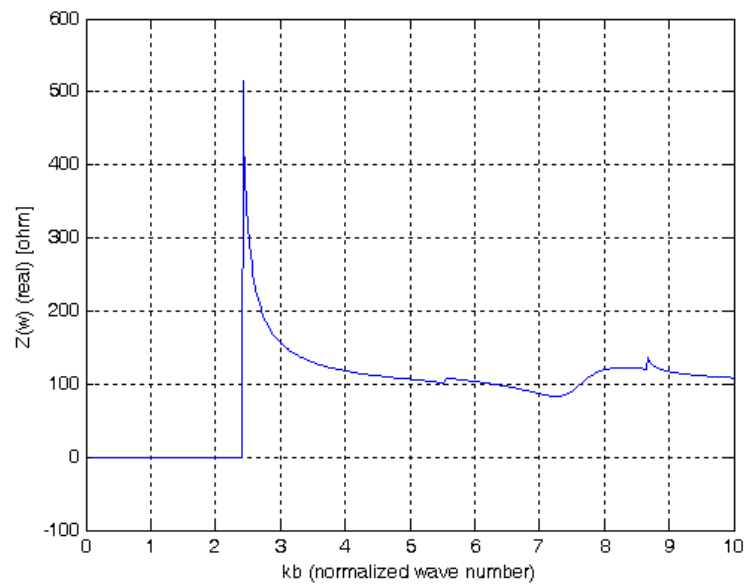


Fig. 3-28. Longitudinal Coupling Impedance, real part:  $\beta\gamma = 100$ ,  $c/b = 0.4$ ,  $L/b = 0.25$ .

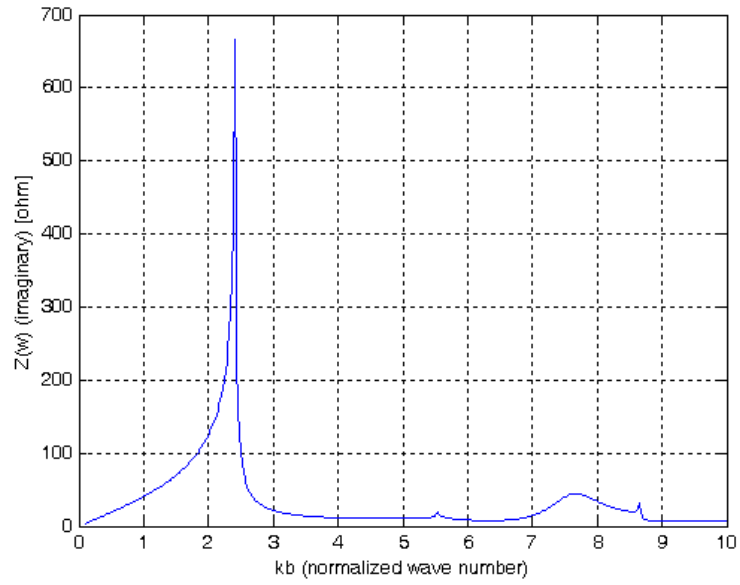


Fig. 3-29. Longitudinal Coupling Impedance, imaginary part:  $\beta\gamma = 100$ ,  $c/b = 0.4$ ,  $L/b = 0.25$ .

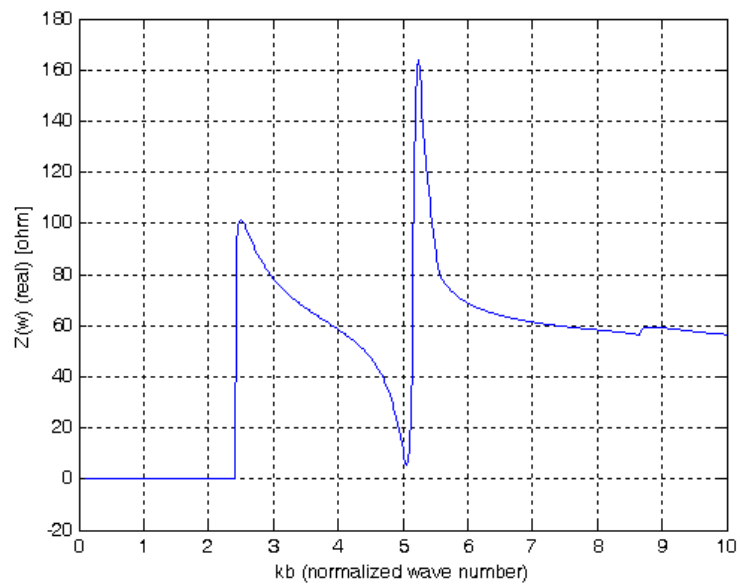


Fig. 3-30. Longitudinal Coupling Impedance, real part:  $\beta\gamma = 100$ ,  $c/b = 0.6$ ,  $L/b = 0.25$ .

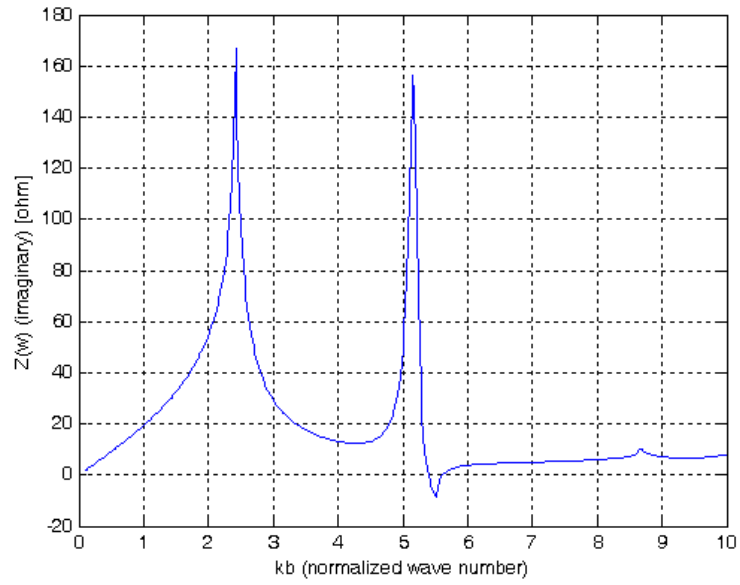


Fig. 3-31. Longitudinal Coupling Impedance, imaginary part:  $\beta\gamma = 100$ ,  $c/b = 0.6$ ,  $L/b = 0.25$ .

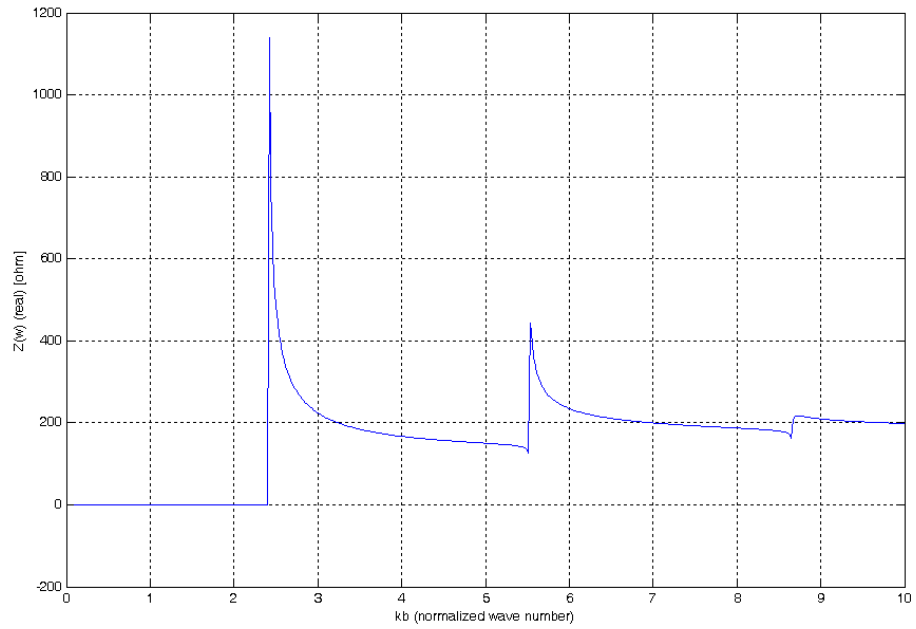


Fig. 3-32. Longitudinal Coupling Impedance, real part:  $\beta\gamma = \infty$ ,  $c/b = 0.2$ ,  $L/b = 0.25$ .

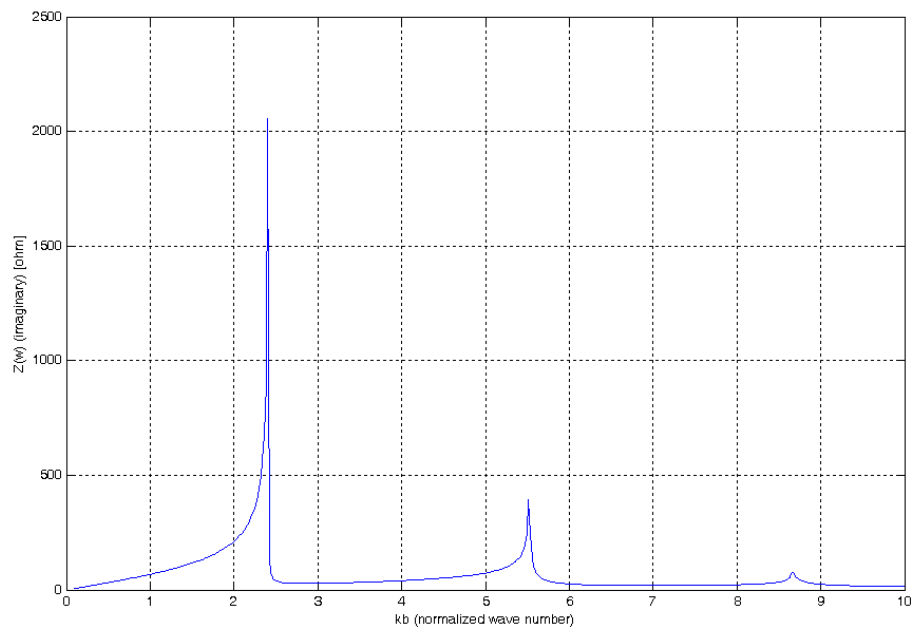


Fig. 3-33. Longitudinal Coupling Impedance, imaginary part:  $\beta\gamma = \infty$ ,  $c/b = 0.2$ ,  $L/b = 0.25$ .

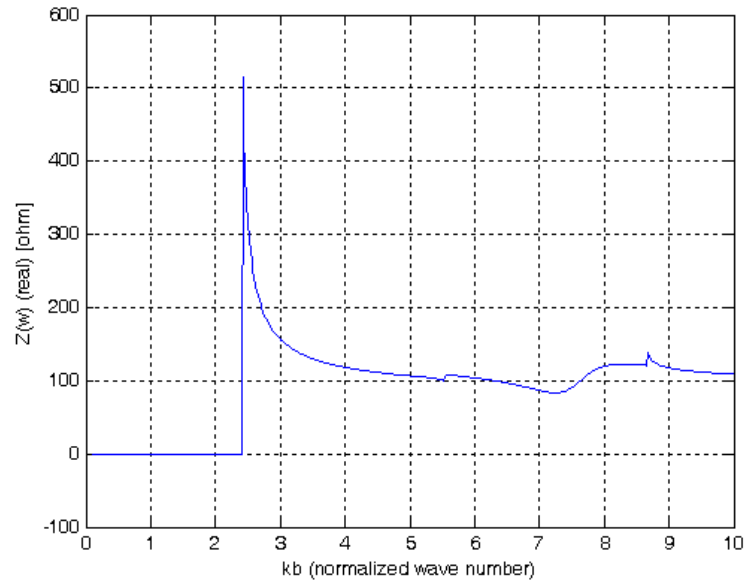


Fig. 3-34. Longitudinal Coupling Impedance, real part:  $\beta\gamma = \infty$ ,  $c/b = 0.4$ ,  $L/b = 0.25$ .

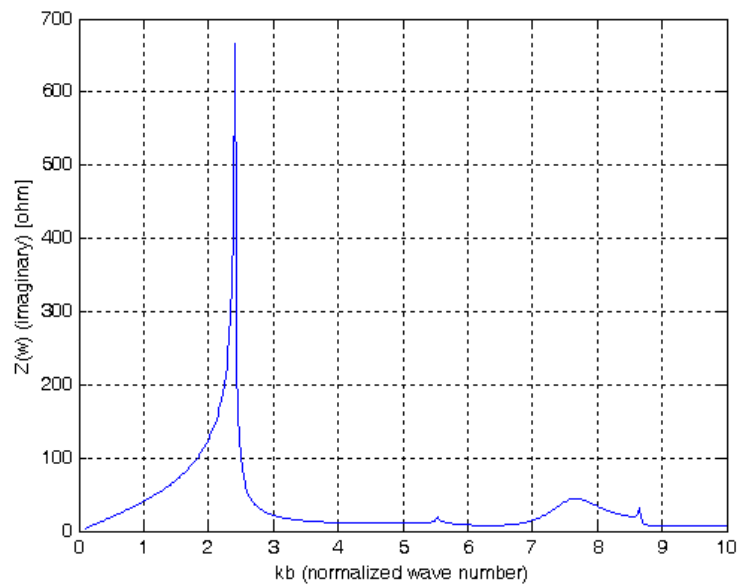


Fig. 3-35. Longitudinal Coupling Impedance, imaginary part:  $\beta\gamma = \infty$ ,  $c/b = 0.4$ ,  $L/b = 0.25$ .

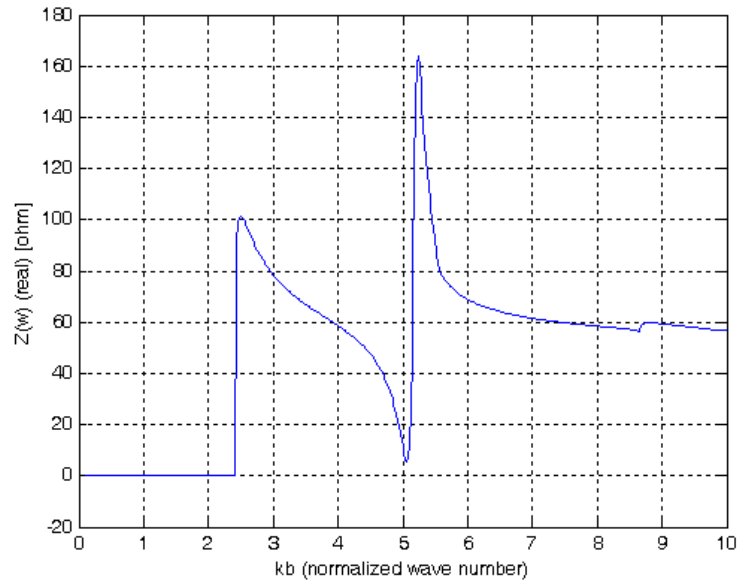


Fig. 3-36. Longitudinal Coupling Impedance, real part:  $\beta\gamma = \infty$ ,  $c/b = 0.6$ ,  $L/b = 0.25$ .

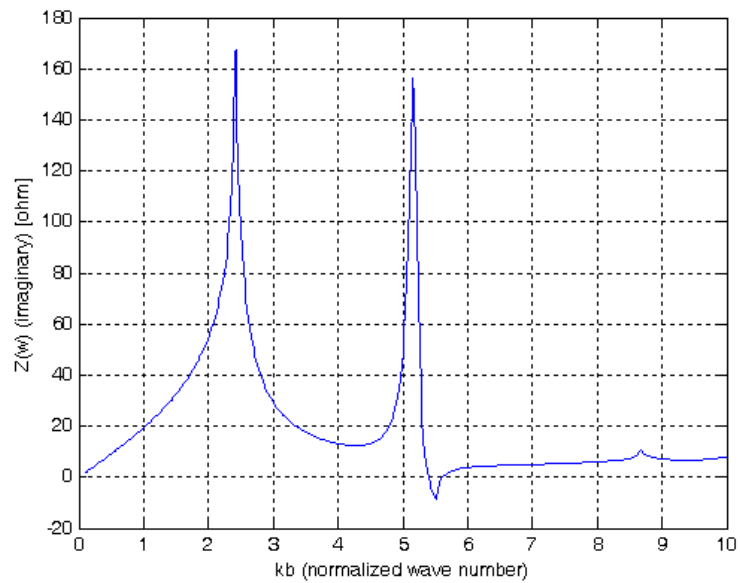


Fig. 3-37. Longitudinal Coupling Impedance, imaginary part:  $\beta\gamma = \infty$ ,  $c/b = 0.6$ ,  $L/b = 0.25$ .

One can see that for  $\beta\gamma = 0.1$ , or  $\beta \approx 0.1$  little Impedance spectra are reached (**fig.3.8-3.13**). This is due to the transit time of the charge through the iris. In fact, the lesser is the velocity the longer will be the transit time and consequently the shorter will be the spectrum.

Moreover, for little values of  $\beta\gamma$ , the interaction between particle and iris is at minimum, and the very little real part value of the obtained impedance confirms this assertion. It is worth of note that when the ratio  $c/b \approx 1$  the impedance amplitude decreases to very little values, as expected. In case of  $\beta\gamma = \infty$ , meaning  $\beta = 1$  (the charge moves with light speed), an infinite spectrum is obtained, with the real part of the impedance that never vanish.

# **Chapter 4:**

## **The Coaxial Setup**

### **4.1 Generalities and Fields Expression**

In this chapter, we will apply the mode matching technique to a device that consists of a pillbox with an inner wire stretched along its z-axis. The problem and, therefore, its solution are different with respect to the previous cases, first because of the absence of the beam: as a forcing term, we may consider a traveling waveguide mode. It is worth of note that, since the coaxial configuration has a multiple connection of first order, it can support at least one TEM mode: it is quite natural to take this mode as the forcing source. In this case, we will find the scattering parameters first, and then we will use them to determine the coupling impedance.

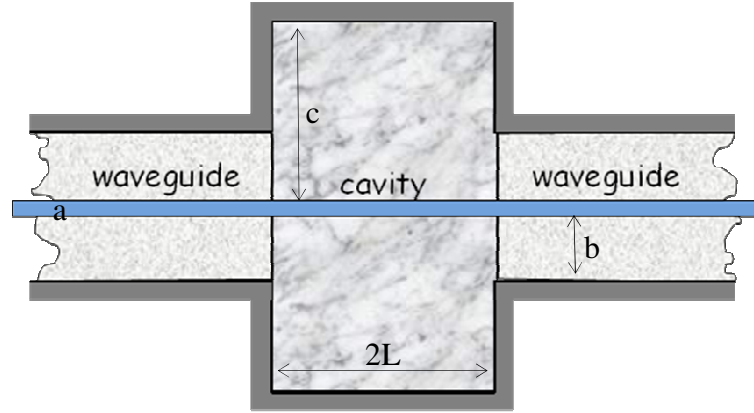


**Fig. 4-1.** Scheme of the pillbox with the stretched wire on  $z$  axis.  $a$  = wire radius;  $b$  = waveguide radius;  $c$  = cavity radius;  $2L$  = cavity length.

In addition, the presence of the wire changes the Device Under Test (DUT) characteristics. Inserting the wire, the waveguides behave like coaxial cables (with minor and major radii  $a$  and  $b$  respectively as designed in **Fig.4-1**) and the cavity is treated as a coaxial cavity. Therefore, the cavity modes and the waveguide waves are different from the previous cases. The functional expressions of modes in coaxial cables are as follows:

$$\Phi_{0_t}^g(k, r) = \begin{cases} 0 & t = 1 \\ \frac{\alpha_t \sqrt{\pi}}{2a} \frac{J_0(r\alpha_t/a)Y_0(\alpha_t) - J_0(\alpha_t)Y_0(r\alpha_t/a)}{\sqrt{J_0^2(\alpha_t)/J_0^2(g\alpha_t/a) - 1}} & t = 2, 3, \dots \end{cases} \quad (4.1)$$

where  $\alpha_t$  is solution of the equation  $\alpha[J_0(\alpha x)Y_0(\alpha) - Y_0(\alpha x)J_0(\alpha)] = 0$

with  $x = b/a$  e  $x = c/a$  respectively, and

$$\Phi_{it}^s(k_t r) = \begin{cases} \frac{1}{r\sqrt{2\pi\ln(g/a)}} & t=1 \\ \frac{\alpha_t\sqrt{\pi}}{2a} \frac{J_1(r\alpha_t/a)Y_0(\alpha_t) - J_0(\alpha_t)Y_1(r\alpha_t/a)}{\sqrt{J_0^2(\alpha_t)/J_0^2(g\alpha_t/a) - 1}} & t=2,3,\dots \end{cases} \quad (4.2)$$

The details are given in **Appendix D**.

For a cylindrical cavity of radius  $\mathbf{c}$  and length  $\mathbf{2L}$ , the expression of the normalized eigenmodes is given by [3]

$$\begin{aligned} \vec{e}_{ps}(r, z) &= e_{ps}(r, z)\hat{r} + e_{ps}^z(r, z)\hat{z} = \\ &= \frac{1}{k_{ps}} \sqrt{\frac{\epsilon_s}{2L}} \left[ -k_s \sin(k_s z) \Phi_{1p}^c(k_p r) \hat{r} + k_p \cos(k_s z) \Phi_{0p}^c(k_p r) \hat{z} \right] \end{aligned} \quad (4.3)$$

$$\vec{h}_{ps}(r, z) = h_{ps}(r, z)\hat{\phi} = \sqrt{\frac{\epsilon_s}{2L}} \cos(k_s z) \Phi_p^c(k_p r) \hat{\phi}$$

where the transverse modal functions  $\Phi_p^c(k_p r)$  are the same functions which represent the coaxial cable modes, and  $\epsilon_s$  is the Neumann symbol ( $\epsilon_s=1$  if  $s=1$ ,  $\epsilon_s=2$  else).

The expression of the fields as an expansion of the eigenmodes weighted with the expansion coefficients  $\mathbf{I}_{ps}$  and  $\mathbf{V}_t$  in the cavities and in the waveguides are

$$\left\{ \begin{array}{l} E_{1z}(r, z) = j \sum_t \frac{k_t Y_t^b}{k} \Phi_{0t}^b(k_t r) [V_{1t}^+(z) + V_{1t}^-(z)] \\ E_{1r}(r, z) = \sum_t \Phi_{1t}^b(k_t r) [V_{1t}^+(z) + V_{1t}^-(z)] \\ H_{1\phi}(r, z) = - \sum_t \frac{Y_t^b}{Z_0} \Phi_{1t}^b(k_t r) [V_{1t}^+(z) - V_{1t}^-(z)] \end{array} \right. \quad z < 0 \quad (4.3)$$

$$\left\{ \begin{array}{l} E_z^c(r, z) = -jZ_0 \sum_{p,s} \frac{k_p}{k} \sqrt{\frac{\epsilon_s}{2L}} \cos(k_s z) \Phi_{0p}^c(k_p r) I_{ps} \\ E_r^c(r, z) = -Z_0 \sum_{p,s} \sqrt{\frac{\epsilon_s}{2L}} k_s \sin(k_s z) \Phi_{1p}^c(k_p r) I_{ps} \\ H_\phi^c(r, z) = \sum_{p,s} \sqrt{\frac{\epsilon_s}{2L}} \cos(k_s z) \Phi_{1p}^c(k_p r) I_{ps} \end{array} \right. \quad 0 < z < 2L \quad (4.4)$$

$$\left\{ \begin{array}{l} E_{2z}(r, z) = -j \sum_t \frac{k_t Y_t^b}{k} \Phi_{0t}^b(k_t r) [V_{2t}^-(z-2L) + V_{2t}^+(z-2L)] \\ E_{2r}(r, z) = \sum_t \Phi_{1t}^b(k_t r) [V_{2t}^-(z-2L) + V_{2t}^+(z-2L)] \\ H_{2\phi}(r, z) = \sum_t \frac{Y_t^b}{Z_0} \Phi_{1t}^b(k_t r) [-V_{2t}^-(z-2L) + V_{2t}^+(z-2L)] \end{array} \right. \quad 2L < z \quad (4.5)$$

where

$$V_{1t}^{+/-}(z) = V_{1t}^{+/-} \exp(\mp jz\sqrt{k^2 - k_t^2})$$

$$V_{2t}^{+/-}(z) = V_{2t}^{+/-} \exp(\pm jz\sqrt{k^2 - k_t^2})$$

The only difference is that the expression of the modal radial functions is the one given by **eq.(4.1)**.

## 4.2 Matching the Magnetic Field

Let us allow for the coupling between the cylindrical cavity and the waveguides, which represent the vacuum chamber. A wire is stretched inside the vacuum chamber in order to model the situation that appears when we deal with measurements of the scattering matrix. We take into account the coupling between the cylindrical cavity and waveguides.

As already mentioned in **Chapter 2**, in which we have the same Perfect Electric Conductor boundary conditions, we may only consider the continuity of the magnetic field tangential component on the two ports connecting the waveguides and the cavity.

On the surfaces 1,2 the continuity

$$\begin{cases} H_{\varphi}(r,0^{-})=H_{\varphi}(r,0^{+}) & a \leq r \leq b \\ H_{\varphi}(r,2L^{-})=H_{\varphi}(r,2L^{+}) & a \leq r \leq b \end{cases} \quad (4.6)$$

It is assumed that in the waveguides there are traveling waves in both directions. We underline the convention adopted for the scattering matrices, which attributes the positive sign to the incoming wave with respect to the DUT. From **eq.(4.6)** and using the expressions of the transverse modes we get the explicit expression of the continuity:

$$\left\{ \begin{array}{l} \sum_p \Phi_p^c(k_p r) \left( \sum_s \sqrt{\frac{\epsilon_s}{2L}} I_{ps} \right) = Y_0 \sum_t Y_t^b (V_{1t}^+ - V_{1t}^-) \Phi_t^b(k_t r) \quad a \leq r \leq b \\ \sum_p \Phi_p^c(k_p r) \left( \sum_s (-1)^s \sqrt{\frac{\epsilon_s}{2L}} I_{ps} \right) = Y_0 \sum_t Y_t^b (V_{2t}^- - V_{2t}^+) \Phi_t^b(k_t r) \quad a \leq r \leq b \end{array} \right. \quad (4.7)$$

where indices  $b$  and  $c$  respectively indicate guide and cavity and for brevity sake it has been set  $V_t^{+/-}(z=0) = V_{1t}^{+/-}$  and  $V_t^{+/-}(z=2L) = V_{2t}^{+/-}$ .

As in the previous cases it is not needed to get  $I_{ps}$  but only the sums  $I_{1p}$  e  $I_{2p}$  defined as:

$$I_{1p} = \sum_s \sqrt{\frac{\epsilon_s}{2L}} I_{ps} \quad (4.8)$$

$$I_{2p} = \sum_s (-1)^s \sqrt{\frac{\epsilon_s}{2L}} I_{ps} \quad (4.9)$$

this will introduce a simplification because one index has been “saturated”.

By projecting **eq.(4.7)** on the eigenfunctions  $\Phi_i^b(k_i r)$  the following system is obtained:

$$\begin{cases} Z_0 \underline{\underline{M}}^T \underline{I}_1 = \underline{Y}^b (\underline{V}_1^+ - \underline{V}_1^-) \\ Z_0 \underline{\underline{M}}^T \underline{I}_2 = \underline{Y}^b (\underline{V}_2^- - \underline{V}_2^+) \end{cases} \quad (4.10)$$

where the matrix  $M_{pi}$  is defined as

$$M_{pi} = 2\pi \int_0^b \Phi_{1p}^c(k_p r) \Phi_{1i}^b(k_i r) r dr \quad (4.11)$$

and its explicit expression is given in **Appendix C**.

### 4.3 The excitation coefficients (PEC)

Following the same procedure already seen for the Thick Iris and the Pillbox we have:

$$\zeta_0 I_{ps} = \frac{jk}{k^2 - k_p^2 - k_s^2} \int_S \hat{n} \times \vec{E} \cdot \vec{h}_{ps}^* dS \quad (4.12)$$

where,  $n$  is the outgoing unit vector orthogonal to the cavity surface  $S$ .

Here we follow the procedure already adopted in the previous Chapters and we obtain the matrix representation for the unknown excitation currents  $I_{1p}$  and  $I_{2p}$ :

$$\begin{aligned} Z_0 I_1 &= j\underline{Y}^c \csc(2kL\underline{Z}^c) \underline{M}(\underline{V}_2^+ + \underline{V}_2^-) - j\underline{Y}^c \cot(2kL\underline{Z}^c) \underline{M}(\underline{V}_1^+ + \underline{V}_1^-) \\ Z_0 I_2 &= j\underline{Y}^c \cot(2kL\underline{Z}^c) \underline{M}(\underline{V}_2^+ + \underline{V}_2^-) - j\underline{Y}^c \csc(2kL\underline{Z}^c) \underline{M}(\underline{V}_1^+ + \underline{V}_1^-) \end{aligned} \quad (4.13)$$

Equating this expression with **eq.(4.10)** we get the system:

$$\begin{cases} \underline{Y}^b(\underline{V}_1^+ - \underline{V}_1^-) = j\underline{M}^T \underline{Y}^c \left[ \csc(2kL\underline{Z}^c) \underline{M}(\underline{V}_2^+ + \underline{V}_2^-) - \cot(2kL\underline{Z}^c) \underline{M}(\underline{V}_1^+ + \underline{V}_1^-) \right] \\ \underline{Y}^b(\underline{V}_2^- - \underline{V}_2^+) = j\underline{M}^T \underline{Y}^c \left[ \cot(2kL\underline{Z}^c) \underline{M}(\underline{V}_2^+ + \underline{V}_2^-) - \csc(2kL\underline{Z}^c) \underline{M}(\underline{V}_1^+ + \underline{V}_1^-) \right] \end{cases} \quad (4.14)$$

In order to give a simple expression of the scattering matrix for this DUT we introduce the following matrices:

$$\underline{\underline{A}} = j \underline{\underline{M}}^T \underline{\underline{Y}}^c \cot(2kLZ^c) \underline{\underline{M}}$$

$$\underline{\underline{B}} = j \underline{\underline{M}}^T \underline{\underline{Y}}^c \csc(2kLZ^c) \underline{\underline{M}}$$

hence the system in **eq.(4.14)** became as follows:

$$\begin{cases} \underline{\underline{B}}(\underline{\underline{V}}_2^+ + \underline{\underline{V}}_2^-) - \underline{\underline{A}}(\underline{\underline{V}}_1^+ + \underline{\underline{V}}_1^-) = \underline{\underline{Y}}^b (\underline{\underline{V}}_1^+ - \underline{\underline{V}}_1^-) \\ \underline{\underline{B}}(\underline{\underline{V}}_1^+ + \underline{\underline{V}}_1^-) - \underline{\underline{A}}(\underline{\underline{V}}_2^+ + \underline{\underline{V}}_2^-) = \underline{\underline{Y}}^b (\underline{\underline{V}}_2^+ - \underline{\underline{V}}_2^-) \end{cases} \quad (4.15)$$

The explicit expression of the scattering parameters is:

$$\underline{\underline{S}}_{11} = \left[ \underline{\underline{Y}}^b - \underline{\underline{A}} - \underline{\underline{B}}(\underline{\underline{Y}}^b - \underline{\underline{A}})^{-1} \underline{\underline{B}} \right]^{-1} \left[ \underline{\underline{Y}}^b + \underline{\underline{A}} + \underline{\underline{B}}(\underline{\underline{Y}}^b - \underline{\underline{A}})^{-1} \underline{\underline{B}} \right] \quad (4.16)$$

$$\underline{\underline{S}}_{21} = \left[ \underline{\underline{B}}(\underline{\underline{Y}}^b - \underline{\underline{A}})^{-1} \underline{\underline{B}} + \underline{\underline{A}} - \underline{\underline{Y}}^b \right]^{-1} \underline{\underline{B}} \left[ \underline{\underline{I}} + (\underline{\underline{Y}}^b - \underline{\underline{A}})^{-1} (\underline{\underline{Y}}^b + \underline{\underline{A}}) \right]$$

Because of the symmetry, the remaining parameters satisfy the following identities

$$\underline{\underline{S}}_{22} \equiv \underline{\underline{S}}_{11} \quad ; \quad \underline{\underline{S}}_{21} \equiv \underline{\underline{S}}_{12}$$

## 4.4 The excitation coefficients (Lossy)

In the case of the Wire Method is not necessary to introduce losses due to finite conductivity of the walls indeed, below cutoff the power lost because of the TEM wave is so larger than the one dissipated in the cavity that the quality factor  $Q$  is dominated by the former ones. Above cutoff frequency, the above statement is a fortiori valid.

## 4.5 The Longitudinal Coupling Impedance

We have used the mode matching technique to simulate an experimental setup for wire method measurements of the scattering parameters of a pillbox cavity [9]. This way to proceed implies that we need to use the same formula used for the experimental measurements case, to obtain the Longitudinal Coupling Impedance from the scattering parameters. This formula gives the real part of the longitudinal coupling impedance, which is sufficient to reach requested informations about the device under test

$$|Z_{//}| = -2Z_o \ln(|S_{21}|) = -2Z_o \ln(10) \log(|S_{21}|) \quad (4.17)$$

or in a more compact expression

$$|Z_{//}| = -Z_o \frac{\ln(10)}{10} |S_{21}|_{dB} \quad (4.18)$$

## 4.6 Numerical results

Eq.(4.16) involves infinite matrices. To allow a good convergence it is necessary to truncate the infinite matrices without detriment of the results validity. As already seen for the pillbox and for the iris, through the Relative Convergence phenomenon, it is possible to reach a different result for different matrix truncation.

Following the scheme reported on Lee and Mittra book [6] we imposed a relation between the number of modes of different zones in order to respect the Meixner condition [7]. We proceed in a similar way as done in the previous Chapters. The only difference is that the first component (namely the one relevant to the TEM mode) of the scattering parameters  $S_{\underline{21}}$  is sufficient to characterize the coupling impedance.

It will be represented the Longitudinal Coupling Impedance, as a fundamental parameter for accelerators project, subdivided in real and imaginary parts and for different values of geometrical parameters. The number of points is chosen as a simulation constant,  $n = 500$ , and the same is done for the waveguide radius ( $b = 12$  mm). We used very few modes ( $N = 20$ ) if compared to other cases already seen, inasmuch the exceptionally good convergence for the wire method. On the other

side, a little number of modes is necessary through the extreme slowness of the computing time associated to the wire method that cannot perform a direct calculus of the Coupling Impedance. Some examples of Mode Matching Technique used to simulate the wire method is shown in the following pictures.

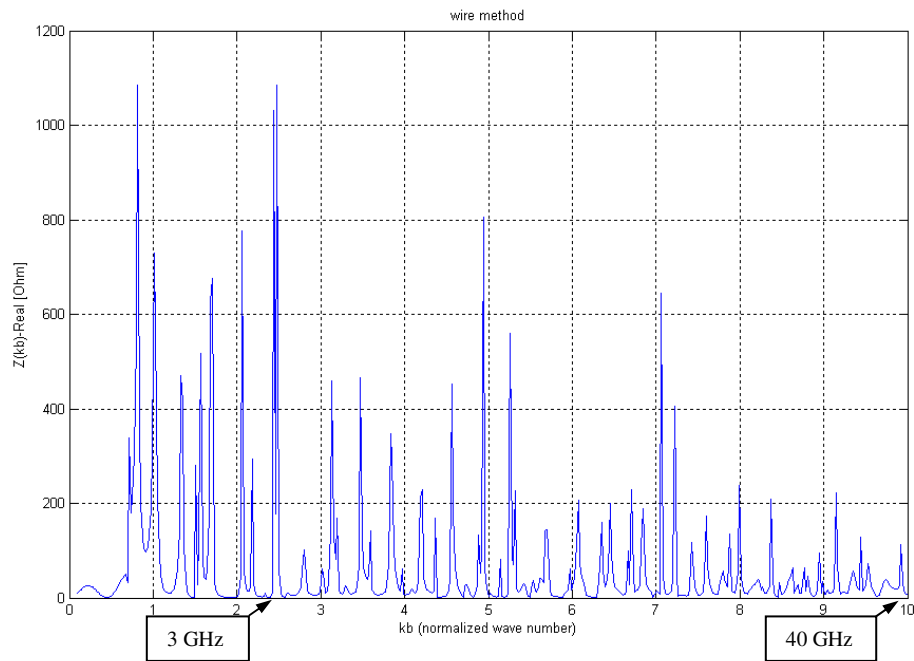


**Fig. 4-2. Longitudinal Coupling Impedance, real part:  $b=12\text{mm}$ ,  $c/b = 4$ ,  $L/b = 4$ .**

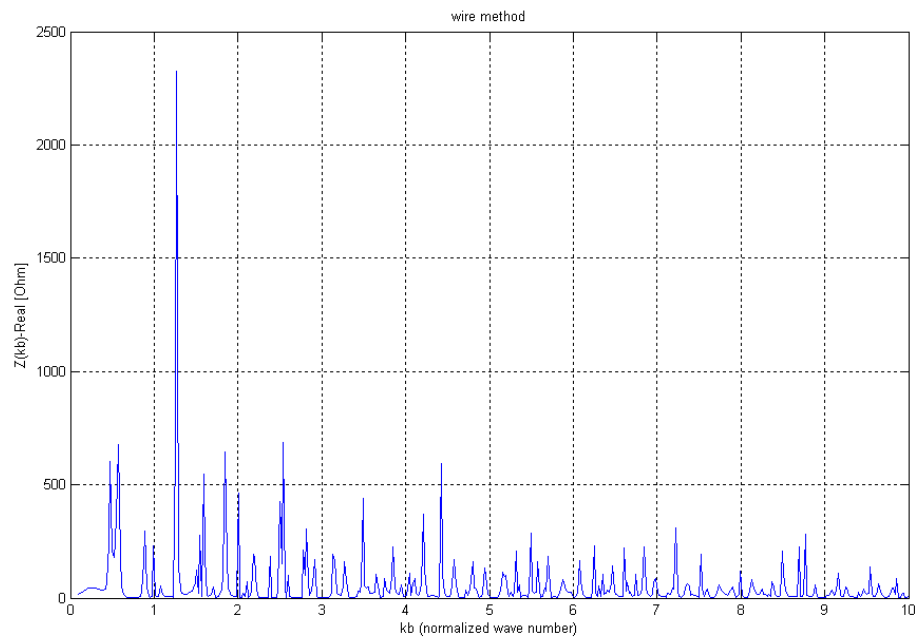


**Fig. 4-3. Longitudinal Coupling Impedance, real part:  $b=12\text{mm}$   $c/b = 6$ ,  $L/b = 4$ .**

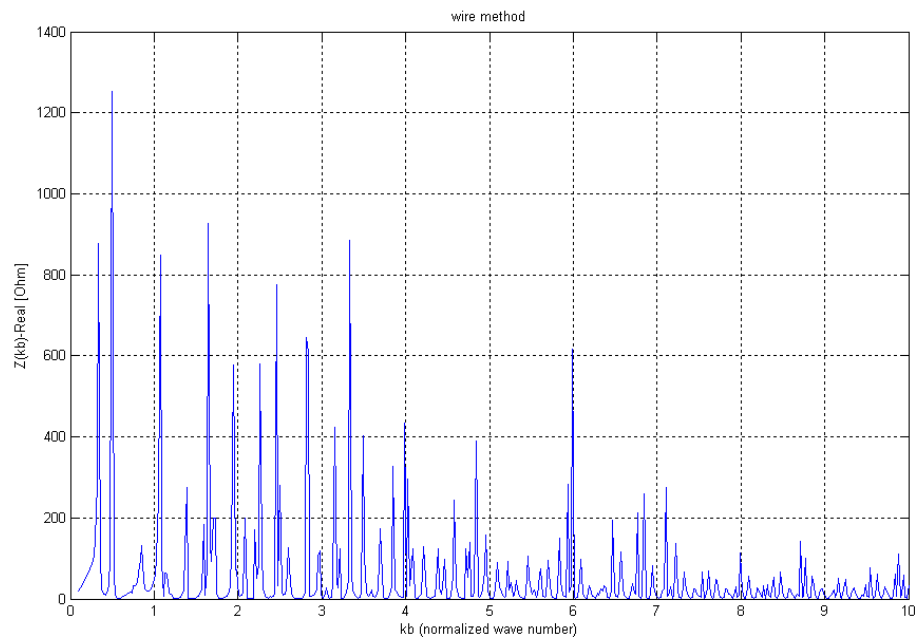


**Fig. 4-4. Coupling Impedance, real part:  $b=12\text{mm}$   $c/b = 8$ ,  $L/b = 4$ .**

By means of the **eq(4.18)**, the wire method simulations present a real part of the coupling impedance every time over zero. In the mode matching simulations, the real part of the C.I. under zero can be seen as a signal of bad convergence and thus it means the necessity to increase the number of the employed modes.



# Chapter 5:

## Comparisons among Results of Various Codes

### 5.1 Generalities

We have learned that the behaviour of any passive device inserted in a cylindrical vacuum tank dramatically changes passing from below to above the cutoff of the vacuum tank. It is worth of note that this frequency is connected only to the dimensions of the vacuum tank cross section and that below this frequency no wave is allowed to propagate in this pipe.

**Below cutoff**, in case of a PEC device, the real part of the Coupling Impedance (C.I.) must vanish at all the frequencies. A different behaviour would conflict with the energy conservation principle. Allowing for the energy released by the beam into the room delimited by the inserted device, this energy “must be entirely given back” again to the beam itself. Since we are below cutoff, no energy is indeed allowed to freely flow inside the pipes. Therefore, the real part of Coupling Impedance must be zero because no energy is delivered and propagated into the vacuum chamber, neither is lost by ohmic dissipation inside the device. By

converse, the imaginary part is certainly different from zero since there is a balanced exchange of energy between the beam and the room inside the device. We expect that the real part of the C.I. will not vanish when the walls of the inserted device have a finite conductivity, since the current impressed into the device dissipates on the walls a certain amount of the energy stored in the device: the exchange of power with the beam will be no longer balanced. We expect that in this case at some frequencies (related to the device resonances) it will appear a significant real part in the Coupling Impedance.

**Above cutoff**, the real part the coupling may be different from zero: a certain amount of the energy, released by the beam into the room delimited by the discontinuity of the device, is allowed to flow into the beam pipes. Since the phase velocity of its EM field is larger than the particle velocity, the mean power exchange between the beam and the field is zero: in sum, this energy is irreversibly lost for the beam and a non-zero real part appears in the Coupling Impedance, even in the case of a device with PEC walls. In the case of walls of finite conductivity, there will be additional losses which will lower the Quality Factor of the resonance which appears in the Coupling Impedance: this lowering is always rather small and sometimes is negligible. In general we expect high Q resonances below cutoff and low Q resonances above cutoff. These latter have a large degree of superposition and generate the so-called Broad Band Impedance.

The stretched wire method is since long (1969) largely used for measuring the Coupling Impedance. Since then, various improvements of the measuring technique

were introduced; however, from what said before hand, it is clear that the stretched wire method introduces an intrinsic perturbation to the behaviour of the electromagnetic field. The presence of the wire changes the device topology from simple connection to multiple-connection. This perturbation introduces a TEM wave which has zero Cutoff Frequency. This TEM wave is able to remove a certain amount of the energy stored into the inserted device and bring it to infinity without interacting with the beam. Therefore, the beam will be given back only a certain amount of the power previously released to the device. This will produce a more or less large discrepancy between the true Coupling Impedance and the measured by means of the Wire Method, whatever is the manipulation of the measured parameters (scattering parameters). Above the cutoff frequency of the original configuration, the perturbation introduced by the stretched wire is expected to be less significant than below cutoff.

## **5.2 Analysis of the Pillbox Long. Coupling Impedance.**

As an example we examine the results of the C.I. of a PEC pillbox as calculated from our code. The results are depicted in **Fig.5-1**, where the real and imaginary part of the C.I. are reported.

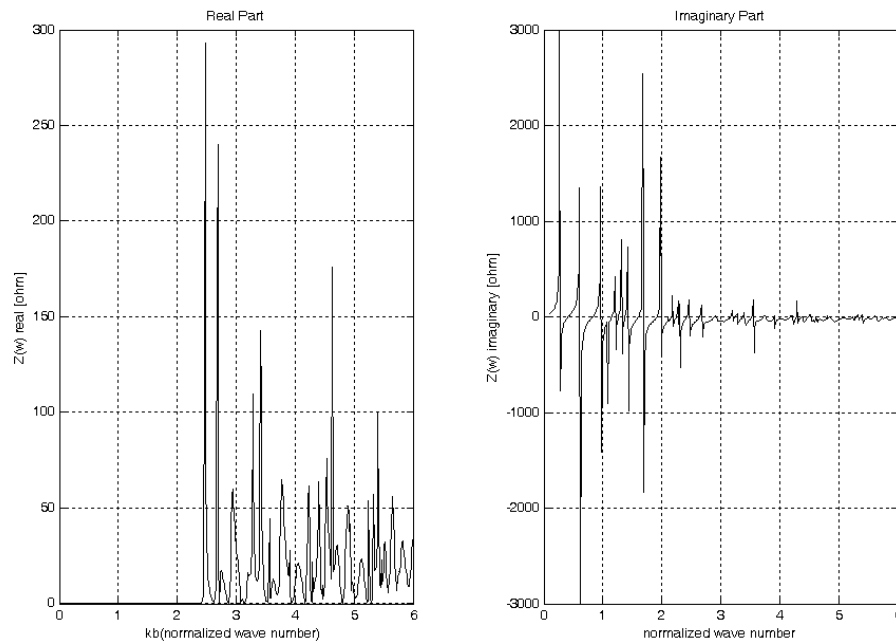


**Fig. 5-1. PEC. C. I. for a pillbox cavity:  $b = 4$  mm;  $c = 36$  mm;  $2L = 12$  mm;  $\beta\gamma > 1000$ ;**

One can notice that the real part is strictly zero below the cutoff frequency corresponding to the normalized wave number **2.4**. Inside this range the imaginary part is, however, different from zero and exhibits a large number of resonances.

This behaviour is just what we expected. In **Fig.5-2** are reported the results for a lossy pillbox and in **Fig.5-3** they are overlaid on those of the lossless pillbox.

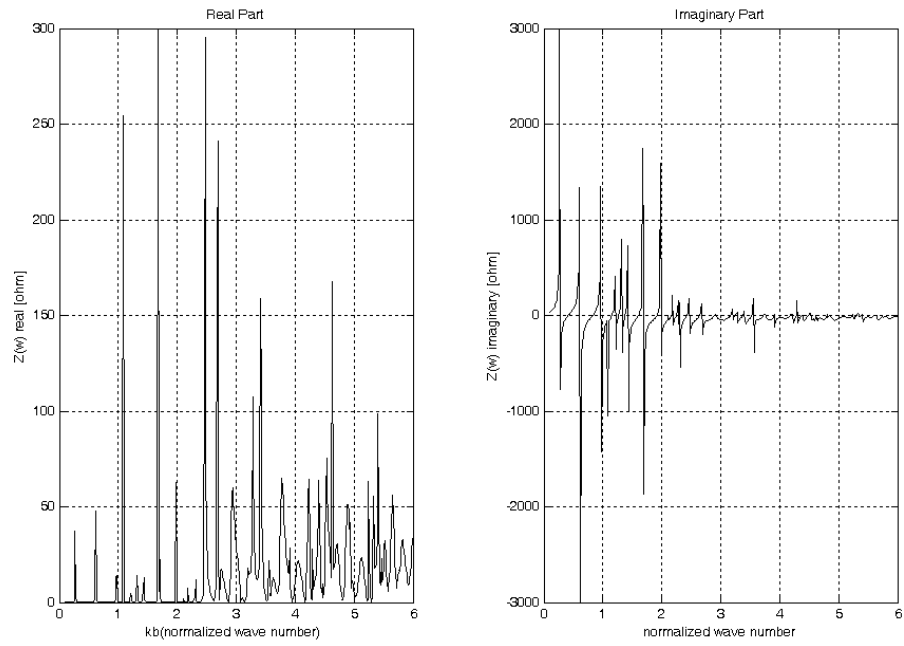


Fig. 5-2. Copper. C.I. for a pillbox cavity:  $b = 4$  mm;  $c = 36$  mm;  $2L = 12$  mm;  $\beta\gamma > 1000$ ;

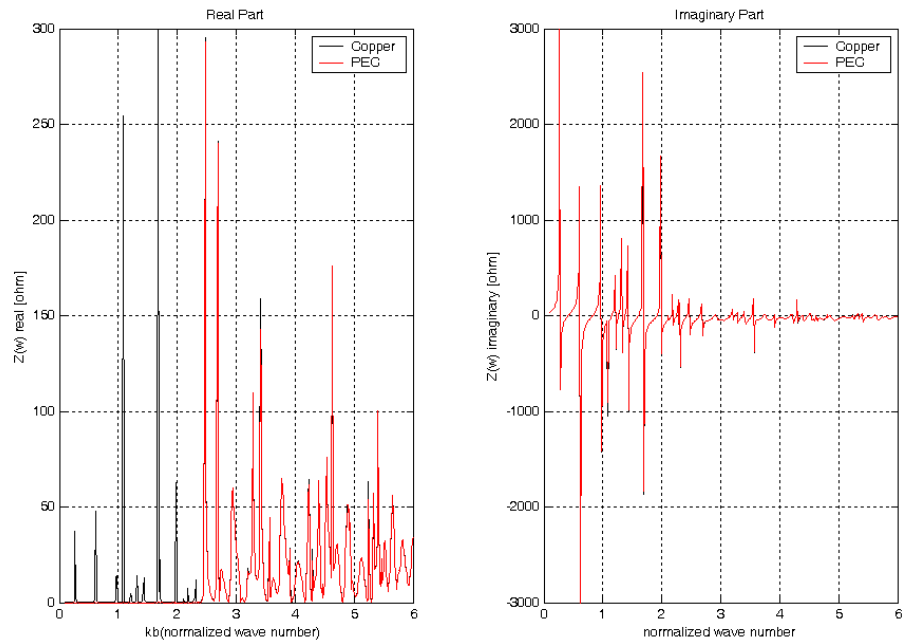


Fig. 5-3. Comparison between Copper and PEC. C.I. for a pillbox cavity:  $b = 4$  mm;  $c = 36$  mm;  $2L = 12$  mm;  $\beta\gamma > 1000$ ;

One can notice that below the cutoff the real part of the C.I. exhibits non-zero values at the same resonant frequencies as the imaginary part, while it is apparent that above cutoff it is not possible to appreciate any difference between copper and PEC behaviour. The representation system in **Fig.5-3** foresees that where the two curves coincide, red curve covers the black one.

Above the cutoff frequency, the results for steel coincide with the once of copper and PEC. So therefore is not interesting to show any picture for this case. Below cutoff there are differences which cannot be appreciated in such wide frequency range: therefore, it is worthwhile to compare them in a narrow frequency bandwidth, around the first resonance at 3.2GHz. This has been done in **Fig.5-4** and **Fig.5-5**.

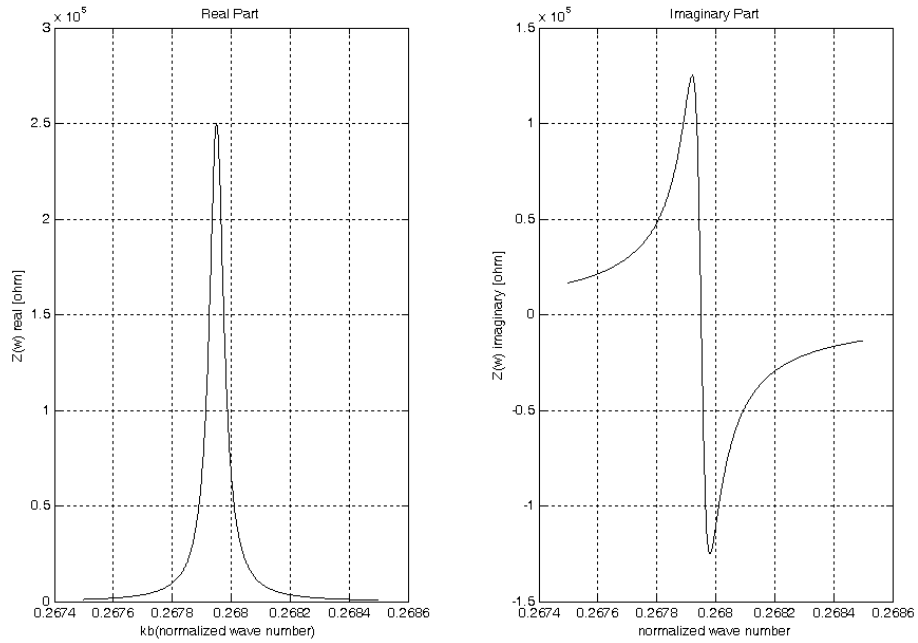


Fig. 5-4. Copper. C.I. for a pillbox:  $b = 4$  mm;  $c = 36$  mm;  $2L = 12$  mm;  $\beta\gamma > 1000$ ;

$$f_0 \approx 3.2 \text{ GHz.}$$

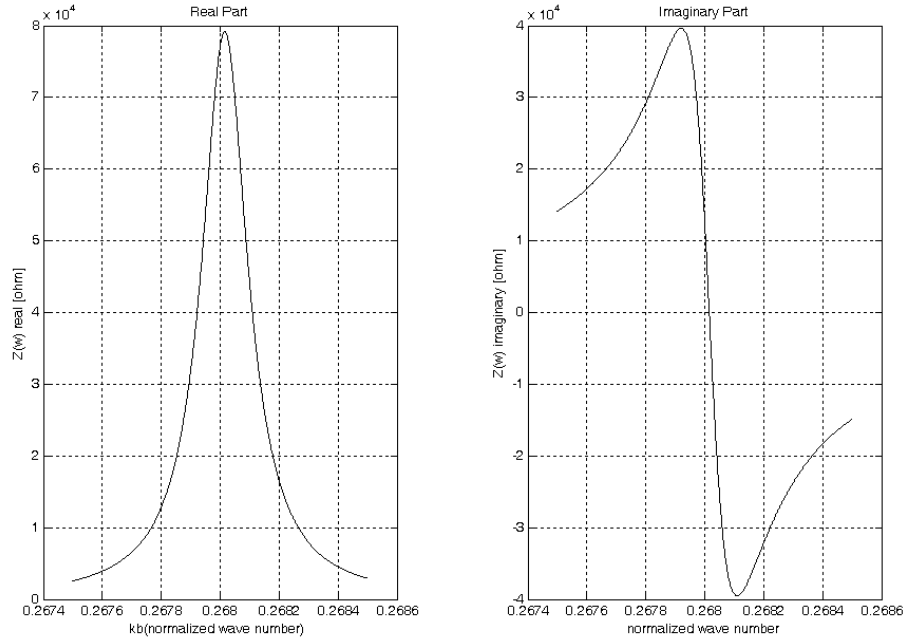


Fig. 5-5. Steel. C.I. for a pillbox:  $b = 4$  mm;  $c = 36$  mm;  $2L = 12$  mm;  $\beta\gamma > 1000$ ;  $f_0 \approx 3.2$  GHz.

Both resonances have a typical Lorentzian behaviour. It is remarkable the high value of the impedance even with stainless steel walls. The main parameters found are listed in **Table 1**.

MATERIAL	Re( $Z_c$ ) [k $\Omega$ ]	Q	$Q_{SF}$	Re( $Z_c/Q$ ) [ $\Omega$ ]	$f$ [GHz]	$f_{SF}$ [GHz]
Copper	250	8920	7689	28.0	3.196	3.196
Stainless Steel	79	2820	2500	28.1	3.197	3.196

**Table 1. fundamental parameters for two well-known materials, Copper and Steel, determined by Mode Matching Technique and SuperFish code applied to a pillbox cavity:  $b = 4$  mm;  $c = 36$  mm;  $2L = 12$  mm;  $\beta\gamma > 1000$**

It is worth of note that the value of  $Z_c$  and Q decrease as the square root of the relevant conductance ratio ( $\sqrt{10}$ ) which is just the ratio of the surface impedance of the two metals. The quantity  $Z_c/Q$  stays constant. The table reports also the Quality Factors and the resonant frequency calculated by means of the computer code SuperFish. The agreement is quite satisfactory.

The results of the calculations for a different pillbox cavity are represented in **Fig.6**, where we compare PEC and copper pillboxes.

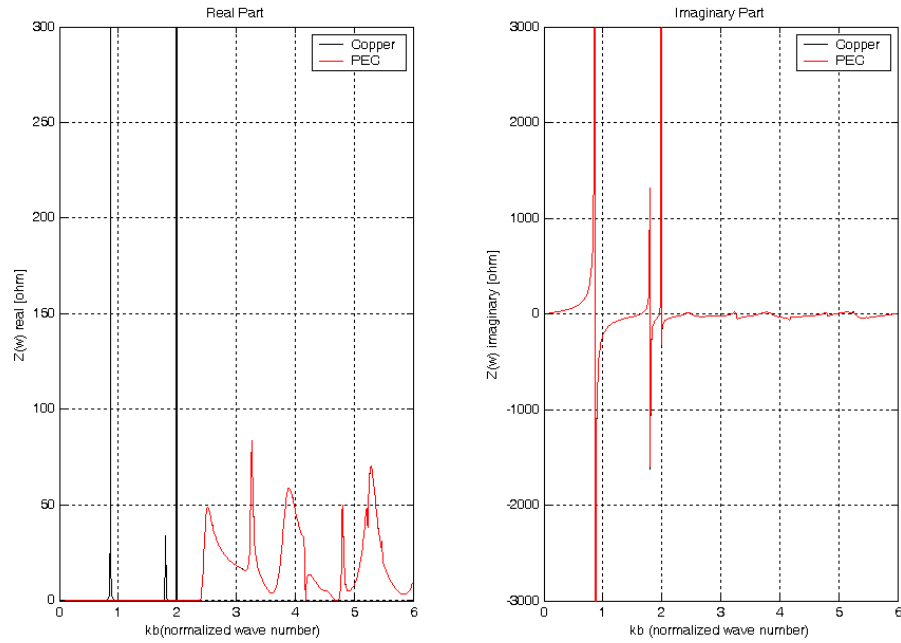


**Fig. 5-6. Comparison between Copper and PEC. C.I. for a pillbox cavity:  $b = 15$  mm;  $c = 43$  mm;  $2L = 30$  mm;  $\beta\gamma > 1000$ ;**

The narrow band investigation for copper and steel are reported in **Fig.5.7** and **Fig.5.8**.

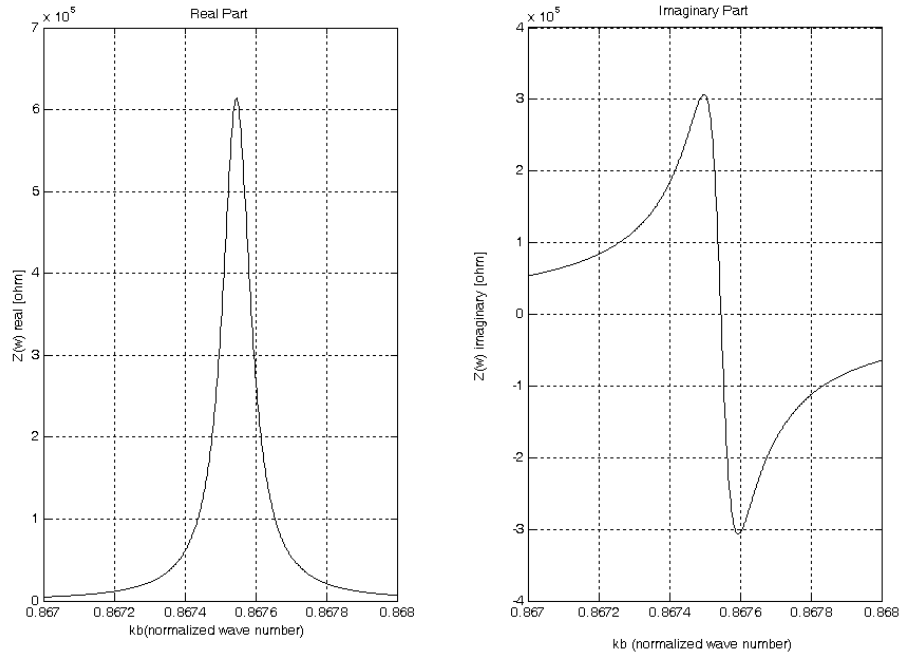


Fig. 5-7. Copper. C.I. for a pillbox:  $b = 15$  mm;  $c = 43$  mm;  $2L = 30$  mm;  $\beta\gamma > 1000$ ;  $f_0 \approx 2.8$  GHz.

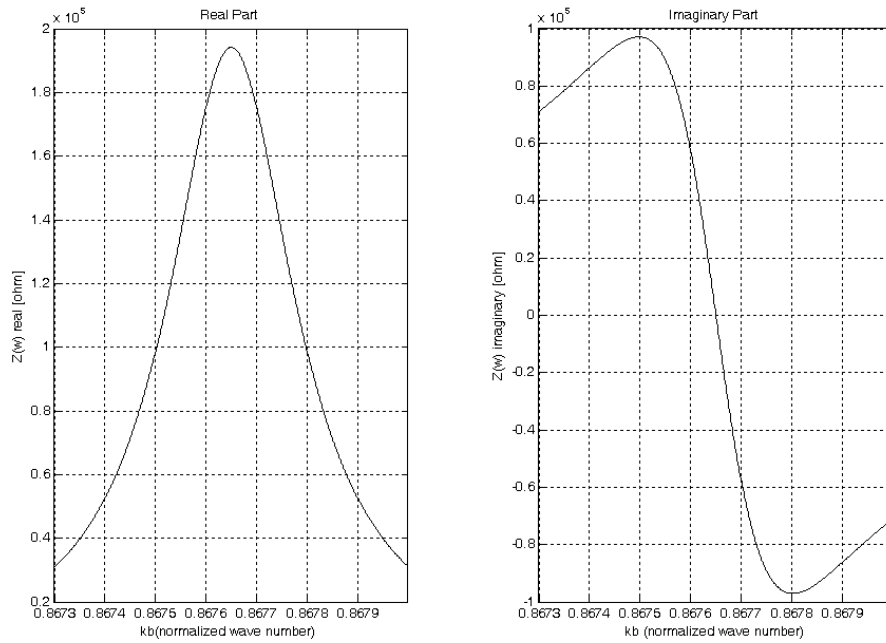


Fig. 5-8. Steel. C.I. for a pillbox:  $b = 15$  mm;  $c = 43$  mm;  $2L = 30$  mm;  $\beta\gamma > 1000$ ;  $f_0 \approx 2.8$  GHz.

In **Table 2** the most important parameters are listed.

MATERIAL	Re( $Z_c$ ) [k $\Omega$ ]	Q	Q <sub>SF</sub>	Re( $Z_c/Q$ ) [ $\Omega$ ]	$f$ [GHz]	$f_{SF}$ [GHz]
Copper	614	17670	13992	34.7	2.760	2.680
Stainless Steel	194	5674	4579	34.2	2.760	2.760

**Table 2. fundamental parameters for two well-known materials, Copper and Steel, determined by Mode Matching Technique and SuperFish code applied to a pillbox cavity:  $b = 15$  mm;  $c = 43$  mm;  $2L = 30$  mm;  $\beta\gamma > 1000$**

All the comments done for the first structures apply to this case.

In general, in the lossless case, it is very difficult to pick up the resonances below cutoff. These can be built only as the limit for the conductivity going to infinity. In this case, at resonant frequencies will appear impedance represented by a delta function of the form

$$Z_c(f_i) = \frac{f_i}{2\pi} \left[ \lim_{\sigma \rightarrow \infty} \frac{Z_c(f_i, \sigma)}{Q(f_i, \sigma)} \right] \delta(f - f_i) = Z_d(f_i) \delta(f - f_i)$$

Where  $\delta(f - f_i)$  is the Dirac impulsive function.

As an example, the quantities  $Z_c(f_i)$  and  $Z_d(f_i)$ , the latter indicated with arrows, are reported in the following picture:

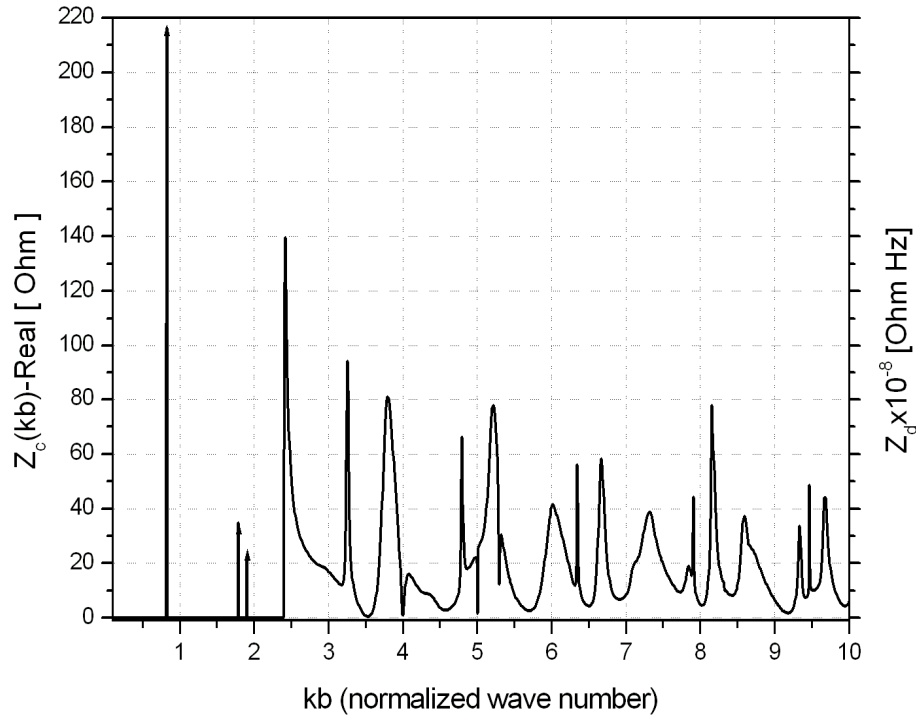
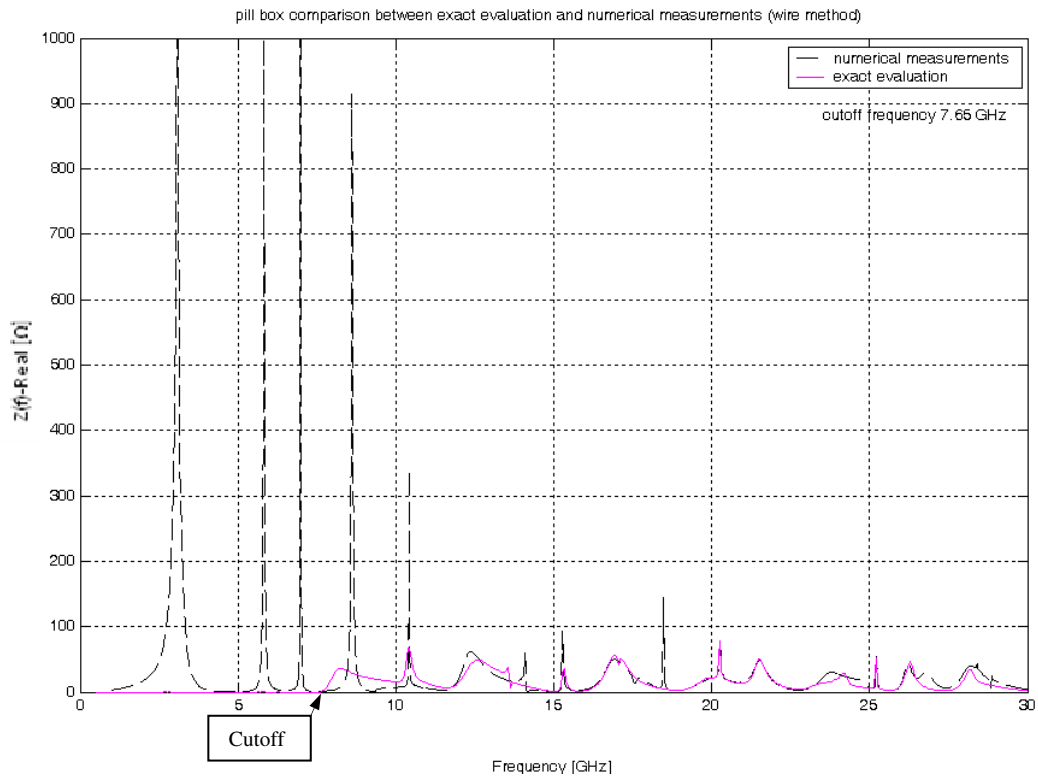


Fig. 5-9. PEC. C.I. for a pillbox:  $b = 10$  mm;  $c = 30$  mm;  $2L = 20$  mm;  $\beta\gamma > 1000$ .

### 5.3 Comparison with the Results of Wire Method.

Now we want to compare the results just discussed, with those given by the simulation of measurements obtained by means of the Stretched Wire Method. In **Fig.5-10** it is reported, for a lossless Pillbox, this comparison up to a frequency of 30 GHz well above the cutoff frequency. According to fundamental arguments on physical behaviour we expect some discrepancies. We need a more detailed view of



**Fig. 5-10.** Comparison between the “numerical experiment” based on the Wire Method and the Mode Matching exact evaluation in a wide range of frequencies. C.I. for a PEC pillbox:  $b = 10$  mm;  $c = 60$  mm;  $2L = 80$  mm;  $\beta\gamma > 1000$ .

this behaviour and therefore we split the frequency range in two parts: the first one (Fig.5.11) from zero up to cutoff frequency increased of about 30%. The second one (Fig.5.12) up to 30 GHz.

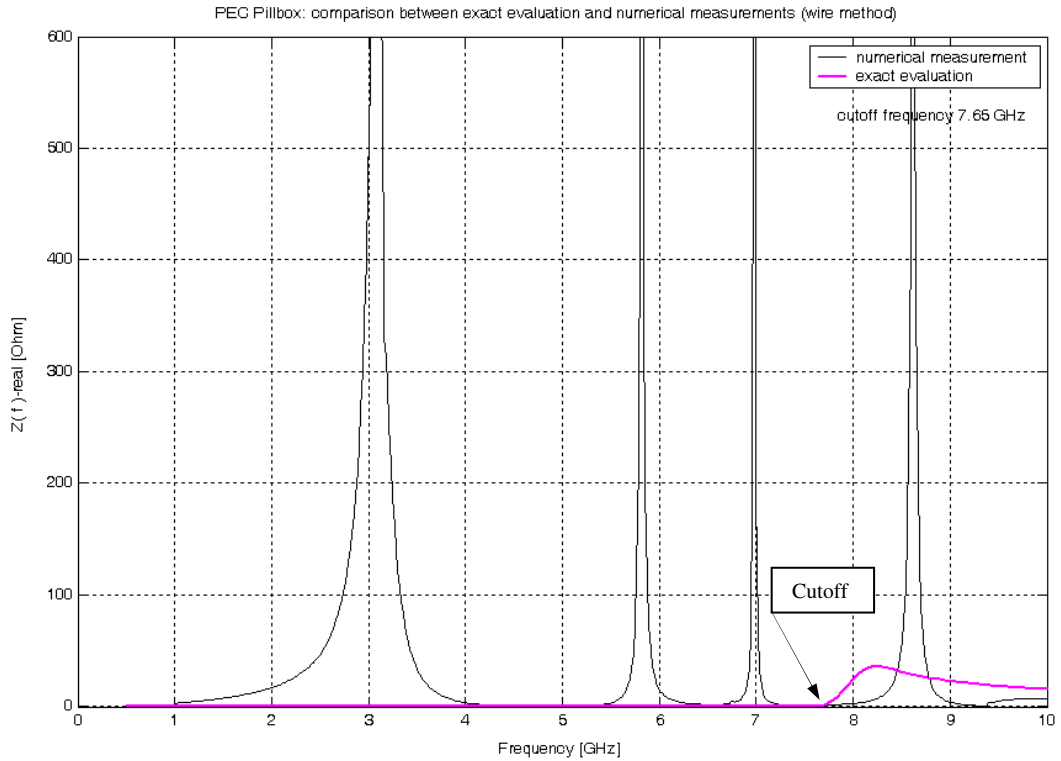


**Fig. 5-11. Comparison between the “numerical experiment” based on the Wire Method and the Mode Matching exact evaluation. C.I. for a PEC pillbox:  $b = 10$  mm;  $c = 60$  mm;  $2L = 80$  mm;  $\beta\gamma > 1000$ .**

It is clear that the wire method shows a very bad agreement below the cutoff frequency. This phenomenon is to be ascribed to the presence of the wire which perturbs the measurement making uncertain some results. The presence of the wire, indeed, shifts the cutoff frequency to zero by introducing a TEM mode (the TEM mode is allowed to propagate because coaxial cables support it). This implies an additional loss of energy from the resonant cavity and a consequent depletion of the quality factor: broadband impedance behaviour appears in the forbidden region.

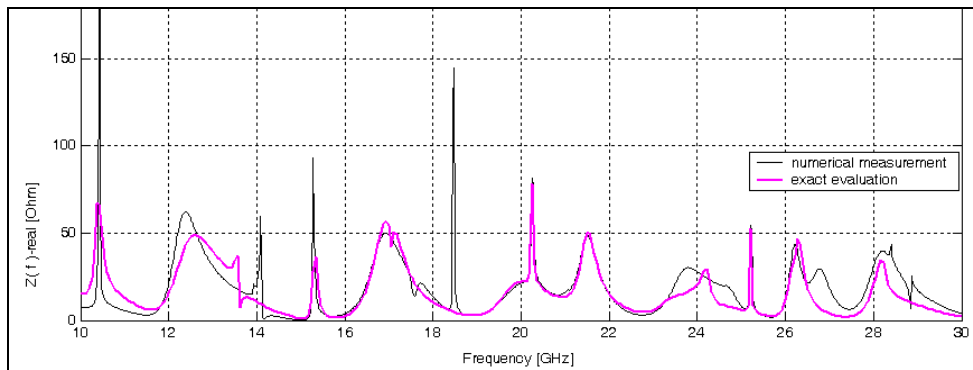


**Fig. 5-12. Comparison between the “numerical experiment” based on the Wire Method and the Mode Matching exact evaluation. C.I. for a PEC pillbox:  $b = 10$  mm;  $c = 60$  mm;  $2L = 80$  mm;  $\beta\gamma > 1000$ .**

In the range of frequencies 30% larger than the cutoff (10-30 GHz) it is quite striking the agreement between the behaviour of the wire measurement and the exact evaluation. Negligible perturbations appear in this range.

Below cutoff we want to compare the behaviour of the impedances calculated with the two methods taking into account the losses (e.g. copper). This is done for the same set of parameters as in **Fig.5-4**.

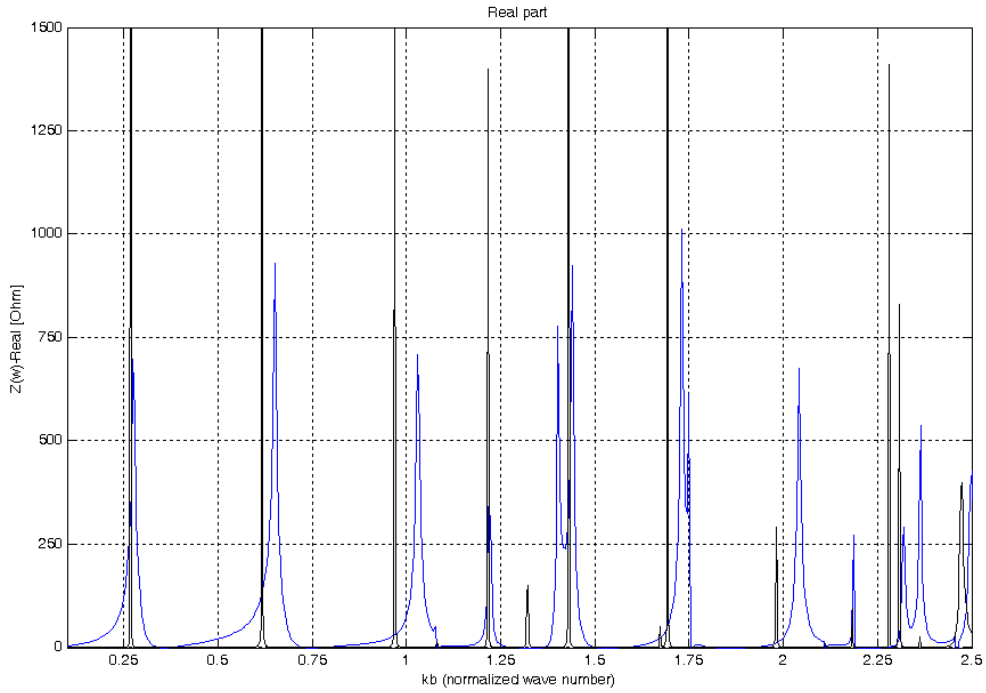


**Fig. 5-13.** Comparison between the “numerical experiment” based on the Wire Method and the Mode Matching exact evaluation. Copper. C.I. for a pillbox:  $b = 4$  mm;  $c = 36$  mm;  $2L = 12$  mm;  $\beta\gamma > 1000$ .

The relevant resonances do not correctly overlap as the first one. However, there are differences which cannot be appreciated in such wide frequency range: therefore, it is worthwhile to compare them in a narrow frequency bandwidth, around the first resonance at 3.3GHz, and it is reported in **Fig.5-14**.

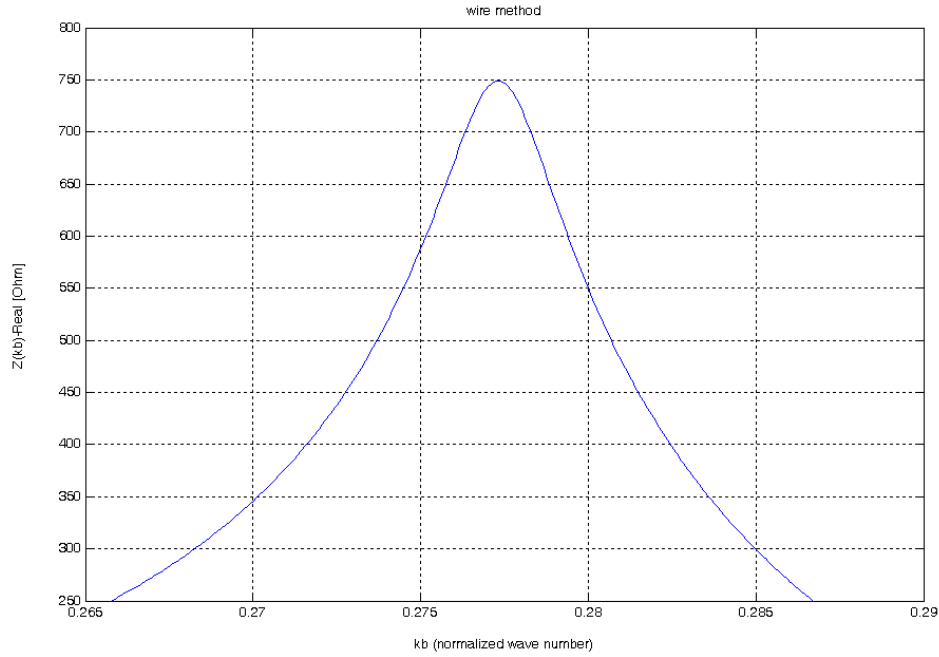


**Fig. 5-14.** C.I. for a pillbox:  $b = 4 \text{ mm}$ ;  $c = 36 \text{ mm}$ ;  $2L = 12 \text{ mm}$ ;  $\beta\gamma > 1000$ ;  $f_0=3.3 \text{ GHz}$ ; as from the “numerical experiment” based on the Wire Method.

The peak of the Coupling Impedance is almost two hundred times smaller than the one calculated by MM, and there is also a drastic reduction of the Quality Factor (see **Fig.5-14**). This is due to the foreseen loss of power channelled by the TEM mode present because of the wire. The results are summarized in the **Table 3**.

Method	Re( $Z_c$ ) [k $\Omega$ ]	Q	Re( $Z_c/Q$ ) [ $\Omega$ ]
Exact evaluation	250	8920	28.0
Wire Method	1.27	300	4.25

**Table 3.** Comparison between the main parameters obtained by Numerical Wire Measurements and Exact Evaluation applied to a pillbox cavity:  $b = 15 \text{ mm}$ ;  $c = 43 \text{ mm}$ ;  $2L = 30 \text{ mm}$ ;  $\beta\gamma > 1000$

## 5.4 Comparison of the results with a commercial code.

The comparison between the Mode Matching and a commercial code, in this case Particle Studio, for a PEC pillbox cavity is reported in **Fig.5-15**.

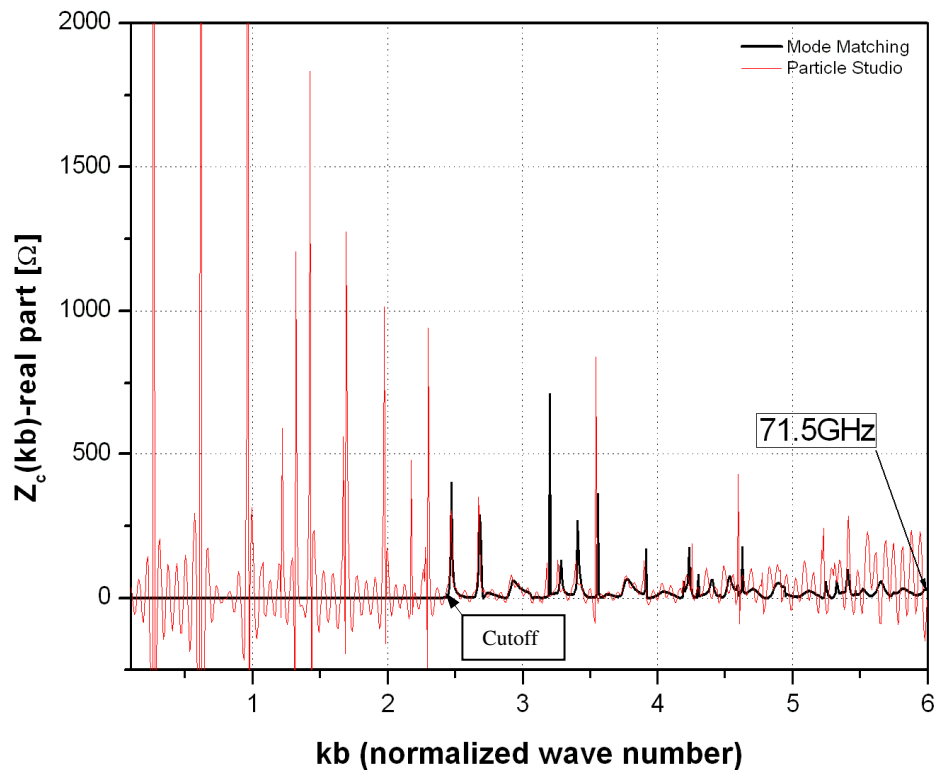


**Fig. 5-15. Comparison between the Mode Matching exact evaluation and the commercial code Particle Studio. C.I. for a PEC pillbox:  $b = 4$  mm;  $c = 36$  mm;  $2L = 12$  mm;  $\beta\gamma > 1000$ .**

As a first evaluation, it is evident that the Particle Studio simulation is very noisy. It means a very rough representation of the coupling impedance, with values not strictly above zero, a clear sign of bad accuracy, in spite of the long time needed by

the simulation. As already seen for the Wire Method, the coupling Impedance assume values different from zero in the forbidden region below the cutoff frequency. It is noticeable a good agreement with mode matching technique for the resonances above the cutoff, up to normalized wave number 4.5. For higher frequencies, the agreement is acceptable only for resonance frequencies of high amplitude. Then the results are becoming more and more noisy. For a lossy pillbox,

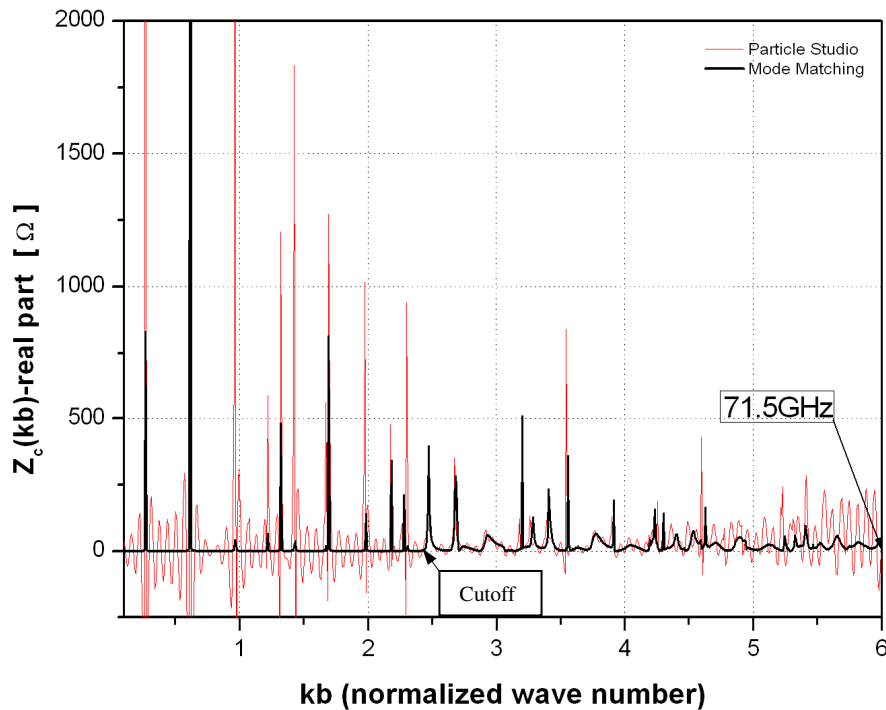


**Fig. 5-16. Comparison between the Mode Matching exact evaluation and the commercial code Particle Studio. C.I. for a Copper pillbox:  $b = 4$  mm;  $c = 36$  mm;  $2L = 12$  mm;  $\beta\gamma > 1000$ .**

above cutoff there is no difference with the previous considerations. Below cutoff the results of Particle Studio seems to be quite insensitive to the conductivity. It is

impossible to recognize any correspondence between the resonance shown by the Mode Matching and one of the Particle Studio.

## Conclusions

There is no doubt that computer codes have some limitation in their performances mainly in the range of frequencies below cutoff and up to a certain extent. We may interpret at least the behaviour of Particle Studio as a consequence of the procedure adopted in this electromagnetic CAD. The problem is solved in the time domain and then an inverse Fourier Transform is performed in order to get the Coupling Impedance from the Wake Field. This implies that high Q resonances need very long computing time in order to let the resonance to damp down. We have seen in our analysis that below cutoff the Coupling Impedance at resonances is very high and also the quality factor Q. Therefore, for these resonances the length of the damping time is unacceptable for inverse Fourier Transform and a truncation introduces remarkable errors in computation, even more magnified by the high value of the Coupling Impedance. As a consequence we get large noise below cutoff. Another important accomplishment of this work was the understanding of the limitations of bench measurements by means of the stretched wire method. It has been demonstrated that this method intrinsically will give wrong results below cutoff. The presence of the wire introduces a TEM wave which intrinsically has a zero cutoff frequency. All the resonant frequencies are depleted because of power drained in the pipes by the TEM mode. Above frequency 30% larger than the cutoff, there are indications that this method may give fairly good results.

**A proposal for future developments**

Even if the mode matching in its various forms is quite powerful and efficient, it is restricted to a limited number of canonical cases which may be treated analytically. Therefore, it cannot be used for insertions of arbitrary shapes. However, it is suggested to still use MM method by resorting to hybrid techniques in order to surmount this inconvenient:

Apart for exceptional cases, the vacuum tank is formed by pipes of standard cross sections (rectangular, circular, and elliptical) so that the waveguide modes can be represented analytically. Allowing for the exotic shape inserts, one may resort to the modal expansions which can be found by means of commercial codes (e.g. Eigenmode Solver by Microwave Studio CST), after then Mode Matching Technique can be use numerically to match the boundary conditions on the surfaces of the adjacent domains (waveguides-inserts). In this way we can profit from the flexibility of the Eigenmode Solvers and the precision and velocity of MM techniques. It is worth of note that in this way, one can introduce the power losses due to the finite conductivity of the inserts.



## Appendix A

### Particle in an infinite pipe

In this appendix we will deliver an expression for the EM field generated by a particle travelling with constant velocity  $\mathbf{v} = \beta\mathbf{c}$  in an infinite cylindrical pipe (**Fig. A-1**).

An ultrarelativistic particle field is confined in an angular region of aperture  $\approx 1/\gamma$ , where

$$\gamma = \frac{1}{\sqrt{1-\beta^2}}$$

is called Lorentz Factor. It represent the particle energy measured in rest mass units. The radiation phenomenon is due to the image charges on the lateral surfaces of the pipe.

A particle of charge  $q$ , travelling in free space with constant velocity  $\mathbf{v}=\beta\mathbf{c}$ , feed an electromagnetic field of only TM modes

$$\vec{E}_v = \zeta_0 \frac{q\kappa}{2\pi} [yK_1(\kappa r)\hat{r} + jK_0(\kappa r)\hat{z}] \exp\left(-j\frac{kz}{\beta}\right) \quad (\text{A.1})$$

$$\vec{H}_v = \frac{q\kappa}{2\pi} K_1(\kappa r) \exp\left(-j\frac{kz}{\beta}\right) \hat{\phi} \quad (\text{A.2})$$

where  $v$  indicates vacuum medium and  $K_0(x)$  e  $K_1(x)$  are the modified Bessel Functions of order zero and one respectively.

Every Electromagnetic entity can be represented as a superposition of two terms: the first term is due to a charge moving uniformly in a free space; the second term is the same kind, but fed by the induced surface current flowing on pipe walls ( $r=a$ , where  $a$  is the pipe radius)

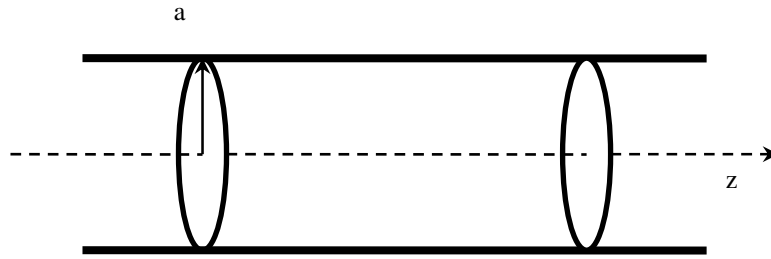


Fig. A-1. A cylindrical pipe of radius  $a$

$$\vec{J}(z, \omega) = J(z, \omega) \hat{z} \tag{A.3}$$

and ever directed along the axis maintaining a TM propagation. Therefore, the unknown of the problem is the spatial Fourier Transform of the just mentioned current density  $J(z, \omega)$ , in wave number domain

$$F(u) = \frac{1}{2\pi} \int_{-\infty}^{+\infty} J(z) \exp(jzu) dz \tag{A.4}$$

where we have omitted  $\omega$  for brevity.

Let us begin writing the potential vector as a function of the chosen unknown. By means of the azimuthal symmetry of the problem, one can write

$$\vec{A}(r,z) = A_z(r,z)\hat{z} = \hat{z} \frac{\mu a}{2} \int_{-\infty}^{+\infty} J(z_0) \left( \int_0^{2\pi} \frac{\exp(-jkR)}{R} d\varphi_0 \right) dz_0 \quad (\text{A.5})$$

where  $R$  is the distance between a generic reference point  $P(r,\varphi,z)$  and the source point  $P_0(r,\varphi_0,z_0)$

$$R^2 = r^2 + a^2 - 2ar \cos(\varphi - \varphi_0) + (z - z_0)^2 = D^2 + (z - z_0)^2 \quad (\text{A.6})$$

where  $D$  is the distance on the transverse plane, introduced for notation easiness. It is possible to write the Green Function as a spatial integral of Bessel Functions

$$\frac{\exp(-jkR)}{R} = \frac{1}{\pi} \int_{-\infty}^{+\infty} K_0\left(D\sqrt{u^2 - k^2}\right) \exp[-ju(z - z_0)] du \quad (\text{A.7})$$

It is interesting to notice that the convergence of the above integral requests a negative  $k$  imaginary component. This implies the presence of losses, even little, in the medium that fills the pipe, and implies the sign assignment to the root function

to obtain  $\text{Im}(\sqrt{k^2 - u^2}) \leq 0$ , that is an appropriate cut in the complex plane in order to avoid the “polidromy” of this function.

The (A.7) allows to write

$$\int_0^{2\pi} \frac{\exp(-jkR)}{R} d\varphi_0 = 2 \int_{-\infty}^{+\infty} G(u,r) \exp[-ju(z-z_0)] du \quad (\text{A.8})$$

where the  $G(u,r)$  function, depending only on the transverse coordinate  $r$ , can be easily simplified applying the addition formulas of Bessel Functions

$$K_0\left(m\sqrt{r^2 - \rho^2 - 2r\rho \cos x}\right) = \begin{cases} \sum_{n=0}^{\infty} \varepsilon_n I_n(m\rho) K_n(mr) \cos(nx) & \rho \leq r \\ \sum_{n=0}^{\infty} \varepsilon_n I_n(mr) K_n(m\rho) \cos(nx) & \rho \geq r \end{cases} \quad (\text{A.9})$$

where  $\varepsilon_n$  is the Neumann symbol, defined as

$$\varepsilon_n = \begin{cases} 1 & n = 0 \\ 2 & n = 1, 2, 3, \dots \end{cases}$$

And executing the integration on  $\varphi_0$ , we reach

$$G(u,r) = \begin{cases} I_0(r\sqrt{u^2 - k^2})K_0(a\sqrt{u^2 - k^2}) & r \leq a \\ I_0(a\sqrt{u^2 - k^2})K_0(r\sqrt{u^2 - k^2}) & r \geq a \end{cases} \quad (\text{A.10})$$

The knowledge of the  $G(u,r)$  function allow us to write simple integral relations that relate the Potential and the Fields to the unknown  $F(u)$ . This way it will be easy to obtain an integral equation for  $F(u)$ , bringing the liaison between Potential and Fields spectra of algebraic type.

Returning to the vector Potential (A.5), one can write

$$A_z(r,z) = \zeta \frac{a}{c} \int_{-\infty}^{+\infty} G(u,r) F(u) \exp(-juz) du \quad (\text{A.11})$$

where  $\zeta$  is the impedance of the medium that fills the pipe (usually vacuum).

From the last expression, it is possible to obtain the electric field fed by the induced current

$$\begin{cases} H_\varphi(r,z) = -\frac{c}{\zeta} \frac{\partial A_z}{\partial r} = -a \int_{-\infty}^{+\infty} \frac{\partial G(u,r)}{\partial r} F(u) e^{-juz} du \\ E_r(r,z) = \frac{c}{jk} \frac{\partial^2 A_z}{\partial r \partial z} = -\frac{a\zeta}{k} \int_{-\infty}^{+\infty} u \frac{\partial G(u,r)}{\partial r} F(u) e^{-juz} du \\ E_z(r,z) = \frac{c}{jk} \left( \frac{\partial^2 A_z}{\partial z^2} + k^2 A_z \right) = j \frac{a\zeta}{k} \int_{-\infty}^{+\infty} (u^2 - k^2) G(u,r) F(u) e^{-juz} du \end{cases} \quad (\text{A.12})$$

where the longitudinal component of the electric field must satisfy the boundary conditions on the perfect conducting pipe.

In fact, imposing the nullifying of the tangential component of the electric field on pipe edges ( $r = a$ ), it is possible to bring the integral equation for the current spectrum

$$\int_{-\infty}^{+\infty} F(u)T(u)\exp(-juz)du = -\frac{q\kappa^2}{\pi} K_0(\kappa a)\exp(-jzk/\beta z) \quad \forall z \quad (\text{A.13})$$

That is a integral equation on the unknown  $F(u)$ , whose kernel is

$$T(u) = 2a(u^2 - k^2)I_0(a\sqrt{u^2 - k^2})K_0(a\sqrt{u^2 - k^2}) \quad (\text{A.14})$$

Since it is needed to develop such kind of integrals, it is useful to explicit the real and imaginary parts.

Reminding the choice on imaginary part of the root  $\text{Im}\sqrt{k^2 - u^2} \leq 0$ , it is possible to explicit the two cases

$$T(u) = \begin{cases} 2a(u^2 - k^2)I_0(a\sqrt{u^2 - k^2})K_0(a\sqrt{u^2 - k^2}), & |u| \geq k \\ a\pi(k^2 - u^2)J_0(a\sqrt{k^2 - u^2})\left[Y_0(a\sqrt{k^2 - u^2}) + jJ_0(a\sqrt{k^2 - u^2})\right], & |u| \leq k \end{cases} \quad (\text{A.15})$$

The integral equation (A.13) does not show calculus difficulties because, being valid for every  $z$ , it is possible to read it as a Fourier Transform. So that

$$F(u) = -\frac{q\delta(u - k/\beta)}{2\pi a I_0(\kappa a)} \quad (\text{A.16})$$

where  $\delta(x)$  is the  $\delta$ -Dirac function.

The knowledge of  $F(u)$  function is enough to calculate the entire electromagnetic field. The formula of the current density is obtained anti-transforming the **eq.(A.4)**

$$J(z) = \int_{-\infty}^{+\infty} F(u) \exp(-juz) du = -\frac{q \exp(-jkz/\beta)}{2\pi a I_0(\kappa a)} \quad (\text{A.17})$$

The current flowing along pipe lateral surface can be expressed as vector  $\mathbf{J}$  flux and it is  $I(z) = 2\pi a J(z)$ , so

$$I(z) = -\frac{q \exp(-jkz/\beta)}{I_0(\kappa a)}. \quad (\text{A.18})$$

The current  $I(z)$  is a Fourier transform  $I(z, \omega)$ ; it represents the temporal Fourier Transform of the current  $i(z, t)$  that flows along the edges of the cylindrical

conductor. To obtain the  $i(z,t)$  one should perform a further inverse Fourier transformation. It is possible but useless to our goals.

We get at last, the expression of electromagnetic fields substituting the **eq.(A.10)** and **eq.(A.16)** in the **eq.(A.13)**.

The total field is defined as

$$\vec{E}_t = \vec{E}_0 + \vec{E}$$

where  $\vec{E}_0$  represents the field of a single particle moving in a vacuum medium.

The field results null for  $r > a$ , and for  $0 \leq r \leq a$ , and using the **eq.(A.1)** it is represented by the formulas

$$E_{tz}(r,z) = \frac{jq\zeta}{2\pi\beta} \left[ K_0(\kappa r) - \frac{I_0(\kappa r)}{I_0(\kappa a)} K_0(\kappa a) \right] \exp\left(-j\frac{kz}{\beta}\right) \quad (\text{A.19})$$

$$E_{tr}(r,z) = \frac{q\zeta\kappa}{2\pi} \left[ K_1(\kappa r) + \frac{I_1(\kappa r)}{I_0(\kappa a)} K_0(\kappa a) \right] \exp\left(-j\frac{kz}{\beta}\right) \quad (\text{A.20})$$

Adopting the same procedure for the magnetic field, (using the **eq.(A.2)**), one obtains

$$H_{i\varphi}(r,z) = \frac{q\kappa}{2\pi} \left[ K_1(\kappa r) + \frac{I_1(\kappa r)}{I_0(\kappa a)} K_0(\kappa a) \right] \exp\left(-j \frac{kz}{\beta}\right) \quad (\text{A.21})$$

where  $\kappa = k/\beta\gamma$ .

If the particle is moving with light velocity, the fields became independent from the waveguide radius, so:

$$E_{tz}(r,z) = 0$$

$$E_r(r,z) = \frac{q\zeta}{2\pi r} \exp(-jkz) \quad (\text{A.22})$$

$$H_{i\varphi}(r,z) = \frac{q}{2\pi a} \exp(-jkz)$$



## Appendix B

### Eigenfunctions of Helmholtz Equation for a cylindrical pipe, with Dirichlet conditions.

The purpose of this appendix is to give the expression of the modal functions of a circular cross section waveguide with radius  $a$ , as showed in **Fig.B-1**.

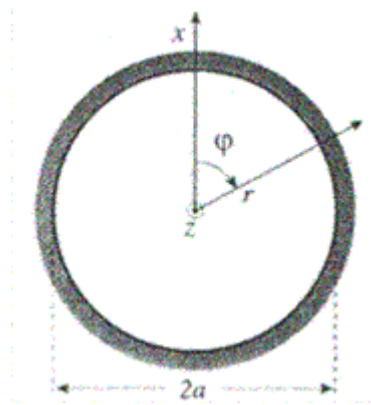


**Fig. B-17.** Cross section of a cylindrical waveguide.

We assume a symmetrical azimuthal TM propagation in the waveguide. The Helmholtz equation in a cylindrical frame is

$$\nabla_t \Phi + k_t^2 \Phi = 0 \quad (\text{B.1})$$

The explicit expression of  $\nabla_t$  is

$$\nabla_t \rightarrow \frac{1}{r} \frac{\partial}{\partial r} r \frac{\partial}{\partial r} + \frac{1}{r^2} \frac{\partial^2}{\partial \varphi^2}$$

Thus the **eq.(B.1)** becomes

$$\frac{1}{r} \frac{\partial}{\partial r} r \frac{\partial \Phi}{\partial r} + \frac{1}{r^2} \frac{\partial^2 \Phi}{\partial \varphi^2} + k_t^2 \Phi = 0 \quad (\text{B.2})$$

where  $\Phi$  is a function of  $\mathbf{r}$  and  $\varphi$ . Splitting  $\Phi$  in two functions, each one depending on a variable only, as

$$\Phi(\mathbf{r}, \varphi) = \Phi_1(\mathbf{r}) \Phi_2(\varphi)$$

and substituting in **eq.(B.2)** we obtain

$$\begin{cases} \frac{1}{r} \frac{\partial}{\partial r} r \frac{\partial \Phi_1}{\partial r} + \left( k_t^2 - \frac{n^2}{r^2} \right) \Phi_1(\mathbf{r}) = 0 \\ \frac{1}{r^2} \frac{\partial^2 \Phi_2}{\partial \varphi^2} + n^2 \Phi_2(\varphi) = 0 \end{cases} \quad (\text{B.3})$$

with the Dirichlet condition  $\Phi(\mathbf{r} = a) = 0$ .

The solutions of the just written **eq.(B.2)** are

$$\begin{cases} \Phi_1(r) = AJ_n(k_t r) + BY_n(k_t r) \\ \Phi_2(\varphi) = C \exp(jn\varphi) \end{cases} \quad (\text{B.4})$$

In the case of  $n = 0$ , we have

$$\frac{1}{r} \frac{\partial}{\partial r} r \frac{\partial \Phi}{\partial r} + k_t^2 \Phi = 0 \quad (\text{B.5})$$

and its solution

$$\Phi(r) = AJ_0(k_t r) + BY_0(k_t r) \quad (\text{B.6})$$

It is worth of note that in this case  $\Phi_2(\varphi)$  becomes a constant, and it can be put as unity. Since  $r \rightarrow 0$  implies that  $Y_0(r) \rightarrow -\infty$ , we need  $B = 0$  to have finite fields, besides we impose the Dirichlet condition  $\Phi(r = a) = 0$ , so we reach the following modes expression

$$\Phi_m(r) = AJ_0\left(p_m \frac{r}{a}\right) \quad (\text{B.7})$$

where  $k_{im} = \frac{p_m}{a}$ ;  $p_m \forall m \in N$  is the  $m^{\text{th}}$  zero  $J_0(x)$  (Bessel Function of first kind and zero order) and the propagation constants can be expressed as

$$k_{zm} a = \begin{cases} \sqrt{(ka)^2 - p_m^2} & |ka| > p_m \\ -j\sqrt{p_m^2 - (ka)^2} & |ka| < p_m \end{cases} \quad (\text{B.8})$$

where we have taken into account the identity  $(ak)^2 = (ak_{im})^2 + (ak_{zm})^2$ .

The imaginary part sign of the propagation constants must be chosen negative to satisfy the condition of radiation to infinite. Substituting  $r = a$  in the **eq.(B.7)** it is evident that the Dirichlet condition is satisfied.

The modes must be orthonormal, that is

$$\iint_S |\Phi_m(r)|^2 dS = 1 \quad (\text{B.9})$$

where S is the waveguide cross section.

The explicit expression of **eq.(B.9)** is

$$\int_0^a r J_n\left(p_{nm} \frac{r}{a}\right) J_n\left(p_{nm'} \frac{r}{a}\right) dr = \frac{a^2}{r} [J_n'(p_{nm})]^2 \delta_{mm'}$$

where  $\delta_{mm'} = \begin{cases} 1 & m = m' \\ 0 & m \neq m' \end{cases}$ .

In case of  $n = 0$ , we must reach this result

$$\int_0^a \int_0^{2\pi} A^2 \left[ J_0 \left( p_{0m} \frac{r}{a} \right) \right]^2 r dr d\theta = A^2 a^2 \pi [-J_1(p_{0m})]^2 = 1$$

where we resort to the property  $J_0'(x) = -J_1(x)$ .

Taking into account **eq.(B.9)** we have

$$A = \frac{1}{a\sqrt{\pi}} \frac{1}{J_1(p_{0m})} \tag{B.10}$$

where the minus sign is included to respect the radiation condition.

Substituting the **eq.(B.10)** in the **eq.(B.7)** we reach

$$\Phi_m(r) = \frac{1}{a\sqrt{\pi}} \frac{J_0(p_{0m} r/a)}{J_1(p_{0m})} \tag{B.11}$$

which is the modes expression commonly used (without writing  $p_{0m}$  but only  $p_m$  to have a more compact expression).

## Appendix C

### Coefficients Calculation

The purpose of this appendix is to calculate the coefficients introduced in the problems formulation. Even if there are little differences between the iris coefficients and the pillbox ones, we will report both the expressions, to be clearer.

#### IN IRIS CASE:

recalling the definition of  $A_i$  in **eq.(2.11)**

$$A_{1t} = \int_S E_r^0(r, 0^-) \Phi_{1t}^b(k_t r) dS - \left[ \int_S E_r^0(r, 0^+) \Phi_{1t}^b(k_t r) dS \right] \tilde{H}(c-r) \quad (\text{C.1})$$

$$A_{2t} = A_{1t} e^{\frac{-jk2L}{\beta}}$$

From **eq.(2.3)** we have

$$\Phi_{1t}^b(\alpha_t r/b) = \frac{J_1(\alpha_t r/b)}{b\sqrt{\pi}J_1(\alpha_t)}$$

and from Primary Fields expression in **eq.(2.1)** we have on the waveguide side of the left interface:

$$E_r^0(r, z = 0^-) = \frac{qZ_0\kappa}{2\pi|\beta|} \left[ K_1(\kappa r) + \frac{I_1(\kappa r)}{I_0(\kappa b)} K_0(\kappa b) \right]$$

and on the cavity side of the left interface:

$$E_r^0(r, z = 0^+) = \frac{qZ_0\kappa}{2\pi|\beta|} \left[ K_1(\kappa r) + \frac{I_1(\kappa r)}{I_0(\kappa c)} K_0(\kappa c) \right]$$

substituting in **eq.(C.1)** we obtain

$$A_{1r} = \frac{Z_0\kappa}{|\beta|} \left\{ \int_0^b \left[ K_1(\kappa r) + \frac{I_1(\kappa r)}{I_0(\kappa b)} K_0(\kappa b) \right] \frac{J_1(\alpha_i r/b)}{b\sqrt{\pi}J_1(\alpha_i)} r dr + \right. \\ \left. - \int_0^c \left[ K_1(\kappa r) + \frac{I_1(\kappa r)}{I_0(\kappa c)} K_0(\kappa c) \right] \frac{J_1(\alpha_i r/b)}{b\sqrt{\pi}J_1(\alpha_i)} r dr \right\} \quad (\text{C.2})$$

it is easily resolvable using integrals of this type [8]

$$\int_0^a r J_1(\alpha r) K_1(\beta r) dr = \frac{-\alpha a J_0(\alpha a) K_1(\beta a) - \beta a J_1(\alpha a) K_0(\beta a) + \alpha/\beta}{\alpha^2 + \beta^2} \quad (\text{C.3})$$

$$\int_0^a r J_1(\alpha r) I_1(\beta r) dr = \frac{\beta a J_1(\alpha a) I_0(\beta a) - \alpha a J_0(\alpha a) I_1(\beta a)}{\alpha^2 + \beta^2}, \quad (\text{C.4})$$

whence we have after some simplifications

$$A_{1t} = \frac{Z_0 \alpha_i}{\beta \sqrt{\pi} J_1(\alpha_i) (b^2 \kappa^2 + \alpha_i^2)} \left[ \frac{I_0(\kappa b) - J_0(\alpha_i)}{I_0(\kappa b)} - \frac{I_0(\kappa c) - J_0(\alpha_i c/b)}{I_0(\kappa c)} \right] \quad (\text{C.5})$$

The first term in square brackets is = 1 because  $J_0(\alpha_i) = 0$  inasmuch  $\alpha_i$  is a zero of the just written equation, so:

$$A_{1t} = \frac{Z_0 \alpha_i J_0(\alpha_i c/b)}{\beta \sqrt{\pi} J_1(\alpha_i) I_0(\kappa c) (b^2 \kappa^2 + \alpha_i^2)} \quad (\text{C.6})$$

Since the  $A_i$  vectors differ of an exponential only, the calculus for  $A_{2t}$  is omitted.

To complete the description of the vectors and matrices existing in the continuity system, we need now to calculate the  $M_{pt}$  matrix

$$M_{pt} = \int_S \Phi_{1p}^c(k_p r) \Phi_{1t}^b(k_t r) dS \quad (\text{C.14})$$

where  $S$  is the iris aperture. According to the definition of  $\Phi_{1q}^g(k_q r)$  in **eq.(2.3)**, we can summarize this formula for the waveguide and the cavity as

$$\Phi_{1p}^c(\alpha_p r/c) = \frac{J_1(\alpha_p r/c)}{c\sqrt{\pi}J_1(\alpha_p)}, \quad \Phi_{1t}^b(\alpha_t r/b) = \frac{J_1(\alpha_t r/b)}{b\sqrt{\pi}J_1(\alpha_t)}$$

Then eq.(C.14) becomes

$$M_{pt} = \frac{2}{cbJ_1(\alpha_p)J_1(\alpha_t)} \int_0^c J_1(\alpha_p r/c) J_1(\alpha_t r/b) r dr \quad (C.15)$$

Resorting to the well known integral [8]

$$\int_0^a r J_1(\alpha r) J_1(\beta r) dr = \frac{\beta \alpha J_1(\alpha a) J_0(\beta a) - \alpha a J_0(\alpha a) J_1(\beta a)}{\alpha^2 - \beta^2} \quad (C.16)$$

we obtain

$$M_{pt} = \frac{2c^2 \alpha_p J_0(\alpha_t) J_1(c \alpha_t / b) - 2cb \alpha_t J_0(c \alpha_t / b) J_1(\alpha_p)}{J_1(\alpha_t) J_1(\alpha_p) (b^2 \alpha_p^2 - c^2 \alpha_t^2)}$$

the first addendum is zero because  $J_0(\alpha_t) = 0$  inasmuch  $\alpha_t$  is a zero of the just written identity. Therefore, we have

$$M_{pt} = \frac{2c^2 \alpha_t J_0\left(\alpha_t \frac{c}{b}\right)}{J_1(\alpha_t) (b^2 \alpha_p^2 - c^2 \alpha_t^2)} \quad (\text{C.17})$$

For what concerns the calculation of the excitation coefficients  $V_{ps}$  and  $F_{ps}$  we need the explicit expression of its vectors:

$$N_{1p} = -2\pi \int_0^c [H_\varphi(r, z=0^-) - H_\varphi(r, z=0^+)] \cdot \Phi_p^c(k_p r) r dr \quad (\text{C.18})$$

$$N_{2p} = N_{1p} e^{\frac{-jk2L}{\beta}}$$

From the primary fields in **eq.(2.1)** and the definition of  $\Phi_{1q}^a(k_q r)$  in **eq.(3.3)** we have

$$\Phi_{1p}^c(\alpha_p r/c) = \frac{J_1(\alpha_p r/c)}{c\sqrt{\pi}J_1(\alpha_p)}$$

$$H_\varphi^0(r, z=0^-) = \frac{q\kappa}{2\pi} \left[ K_1(\kappa r) + \frac{I_1(\kappa r)}{I_0(\kappa b)} \cdot K_0(\kappa b) \right]$$

$$H_\varphi^0(r, z=0^+) = \frac{q\kappa}{2\pi} \left[ K_1(\kappa r) + \frac{I_1(\kappa r)}{I_0(\kappa c)} \cdot K_0(\kappa c) \right]$$

Substituting in eq.(C.18), it results

$$N_{1p} = \frac{\beta\kappa}{c\sqrt{\pi}J_1(\alpha_p)} \left[ \frac{K_0(\kappa b)}{I_0(\kappa b)} - \frac{K_0(\kappa c)}{I_0(\kappa c)} \right] \int_0^c r J_1(\alpha_p r/c) I_1(\kappa r) dr \quad (C.10)$$

Using the integral (C.4) we attain

$$N_{1p} = \left[ \frac{K_0(\kappa b)}{I_0(\kappa b)} - \frac{K_0(\kappa c)}{I_0(\kappa c)} \right] \frac{c\kappa [c\kappa I_2(\kappa c)J_1(\alpha_p) + I_1(\kappa c)J_2(\alpha_p)\alpha_p]}{\sqrt{\pi}J_1(\alpha_p)(c^2\kappa^2 + \alpha_p^2)}$$

To decrease the order of the  $I_2$  and  $J_2$  Bessel Functions, it is useful to use the following recurrence relations [8]:

$$J_{\nu+1}(z) = \frac{2\nu}{z} J_{\nu}(z) - J_{\nu-1}(z)$$

$$I_{\nu+1}(z) = I_{\nu-1}(z) - \frac{2\nu}{z} I_{\nu}(z)$$

Besides, taking into account that  $J_0(\alpha_t) = 0$  we have

$$N_{1p} = \frac{c^2\kappa^2 [I_0(\kappa c)K_0(\kappa b) - I_0(\kappa b)K_0(\kappa c)]}{\sqrt{\pi}I_0(\kappa b)(c^2\kappa^2 + \alpha_p^2)} \quad (C.11)$$

**IN PILLBOX CASE:**

To obtain the homonymous coefficients of the iris case we will follow the same procedure. Therefore, we will report only the definitions and the results.

$$A_{1t} = \int_S H_\varphi^0(r, 0^-) \Phi_{1t}^b(k_t r) dS - \left[ \int_S H_\varphi^0(r, 0^+) \Phi_{1t}^b(k_t r) dS \right] \tilde{H}(b-r)$$

$$A_{2t} = A_{1t} e^{\frac{-jk2L}{\beta}}$$

Resorting to the primary Magnetic Field definition in **eq.(3.1)**, after some algebra we can write

$$A_{1t} = \kappa \int_0^b \left[ \frac{I_1(\kappa r)}{I_0(\kappa b)} K_0(\kappa b) - \frac{I_1(\kappa r)}{I_0(\kappa c)} K_0(\kappa c) \right] \Phi_{1t}^b(k_t r) r dr$$

Solving the above integral, we obtain:

$$\boxed{A_{1t} = \frac{b^2 \kappa^2 [I_0(c\kappa)K_0(b\kappa) - I_0(b\kappa)K_0(c\kappa)]}{\sqrt{\pi} I_0(c\kappa) (b^2 \kappa^2 + \alpha_t^2)}} \quad (C.12)$$

Since the  $A_i$  vectors differ of an exponential only, the calculus for  $A_{2t}$  is omitted.

The  $M_{pt}$  matrix in pillbox case differs from iris case by the integration path only:

$$M_{pt} = \frac{2}{cbJ_1(\alpha_p)J_1(\alpha_t)} \int_0^b J_1(\alpha_p r/c) J_1(\alpha_t r/b) r dr$$

Thus, following the same procedure as iris we obtain:

$$M_{pt} = -\frac{2b^2 \alpha_p J_0\left(\alpha_p \frac{b}{c}\right)}{J_1(\alpha_p)(b^2 \alpha_p^2 - c^2 \alpha_t^2)} \quad (\text{C.13})$$

For what concerns  $N_{1p}$  and  $N_{2p}$

$$N_{1p} = -2\pi \int_0^c \left[ E_r^0(r, z=0^-) \cdot \tilde{H}(b-r) - E_r^0(r, z=0^+) \right] \cdot \Phi_p^c(k_p r) r dr$$

$$N_{2p} = N_{1p} e^{\frac{-jk2L}{\beta}}$$

$$N_{1p} = -\frac{J_0\left(\alpha_p \frac{b}{c}\right) \alpha_p Z_0}{\sqrt{\pi} |\beta| I_0(b\kappa) J_1(\alpha_p)(c^2 \kappa^2 + \alpha_p^2)} \quad (\text{C.14})$$

### PILLBOX CAVITY WITH FINITE CONDUCTIVITY:

in **Chapter 2** we got the following equation

$$I_{ps} = \frac{jkY_0}{(k^2 - k_{ps}^2)} \int_{S_1+S_2} (\vec{E}_{tot} \times \vec{h}_{ps}^*) \cdot \hat{n} dS - \frac{jkY_0 Z_s}{k^2 - k_{ps}^2} I_{ps} \frac{\epsilon_s}{2L} \int_S [\cos(k_s z) \Phi_p^c(k_p r)]^2 dS \quad (C.15)$$

The integration on  $S$  is performed as follows:

$$\begin{aligned} & \int_S [\cos(k_s z) \Phi_p^c(k_p r)]^2 dS = \\ & = \int_{S_1} [\cos(k_s 0) \Phi_p^c(k_p r)]^2 dS + \int_{S_2} [\cos(k_s 2L) \Phi_p^c(k_p r)]^2 dS + \int_{S_3} [\cos(k_s z) \Phi_p^c(k_p r)]^2 dS = \\ & = 2\pi \int_0^c [\Phi_p^c(k_p r)]^2 r dr + 2\pi \int_0^c [\Phi_p^c(k_p r)]^2 r dr + \frac{2}{c} \int_0^{2L} \cos^2(k_s z) dz = \\ & = 2 + \frac{4L}{c\epsilon_s} \end{aligned}$$

By inserting the previous result in **eq.(C.15)** we obtain

$$I_{ps} = \frac{jkY_0}{(k^2 - k_{ps}^2)} \int_{S_1+S_2} (\vec{E}_{tot} \times \vec{h}_{ps}^*) \cdot \hat{n} dS - \frac{jkY_0 Z_s}{k^2 - k_{ps}^2} I_{ps} \left( \frac{\epsilon_s}{L} + \frac{2}{c} \right)$$

and, after some algebra, finally

$$I_{ps} = \frac{jkY_0}{(k^2 - k_{ps}^2) + jkY_0 Z_s \left( \frac{2}{c} + \frac{\epsilon_s}{L} \right)} \int_{S_1+S_2} (\vec{E}_{tot} \times \vec{h}_{ps}^*) \cdot \hat{n} dS \quad (C.16)$$

Resorting to the expressions in **eq.(3.9)**, we may write

$$I_{1p} = \sum_s \sqrt{\frac{\epsilon_s}{2L}} \frac{jkY_0}{(k^2 - k_{ps}^2) + jkY_0Z_s \left( \frac{2}{c} + \frac{\epsilon_s}{L} \right)} \int_{S_1+S_2} (\vec{E}_{tot} \times \vec{h}_{ps}^*) \cdot \hat{n} dS$$

$$I_{2p} = \sum_s \sqrt{\frac{\epsilon_s}{2L}} \frac{(-1)^s jkY_0}{(k^2 - k_{ps}^2) + jkY_0Z_s \left( \frac{2}{c} + \frac{\epsilon_s}{L} \right)} \int_{S_1+S_2} (\vec{E}_{tot} \times \vec{h}_{ps}^*) \cdot \hat{n} dS$$
(C.17)

In order to express the sums in a closed form we must perform the integrations which give a result similar to **eq.(3.19)**:

$$I_{1p} = \sum_{s=0}^{\infty} \frac{jk\epsilon_s Y_0 \left[ (-1)^s \left( -N_{2p} + \sum_t M_{pt} V_{2t}^+ \right) - \left( -N_{1p} + \sum_t M_{pt} V_{1t}^- \right) \right]}{2L \left[ (k^2 - k_{ps}^2) + jkY_0Z_s \left( \frac{2}{c} + \frac{\epsilon_s}{L} \right) \right]}$$

$$I_{2p} = \sum_{s=0}^{\infty} \frac{jk\epsilon_s Y_0 \left[ \left( -N_{2p} + \sum_t M_{pt} V_{2t}^+ \right) - (-1)^s \left( -N_{1p} + \sum_t M_{pt} V_{1t}^- \right) \right]}{2L \left[ (k^2 - k_{ps}^2) + jkY_0Z_s \left( \frac{2}{c} + \frac{\epsilon_s}{L} \right) \right]}$$
(C.18)

The sums in a closed form it is not so simple as done for **eq.(3.19)** because of the Neumann symbol present in the denominator. The sums are therefore slightly different, namely

$$\begin{aligned} \sum_{s=0}^{\infty} \frac{\epsilon_s}{\left[ (k^2 - k_{ps}^2) + jkY_0Z_s \left( \frac{2}{c} + \frac{\epsilon_s}{L} \right) \right]} &= \delta_p + \sum_{s=0}^{\infty} \frac{\epsilon_s}{(k^2 - k_{ps}^2) + \Delta} = \\ &= \frac{2L}{k} \delta_p + \frac{2L \cot(2L\sqrt{k^2 - k_p^2 + \Delta})}{\sqrt{k^2 - k_p^2 + \Delta}} \end{aligned}$$

Where

$$\Delta = jkY_0Z_s \left( \frac{2}{c} + \frac{2}{L} \right)$$

$$\delta_p = \frac{j2Y_0Z_s}{\left[ (k^2 - k_p^2) + \Delta \right] \left[ (k^2 - k_p^2) + \Delta - jkY_0Z_s/L \right]}$$

Similarly we obtain for  $I_{2p}$  :

$$\sum_{s=0}^{\infty} \frac{\epsilon_s (-1)^s}{\left[ (k^2 - k_{ps}^2) + jkY_0Z_s \left( \frac{2}{c} + \frac{\epsilon_s}{L} \right) \right]} = \frac{2L}{k} \delta_p + \frac{2L \csc(2L\sqrt{k^2 - k_p^2 + \Delta})}{\sqrt{k^2 - k_p^2 + \Delta}}$$

Defining a new modal impedance as:

$$Z_p^c = \frac{\sqrt{k^2 - k_p^2 + \Delta}}{k}$$

We obtain for the **eq.(C.18)**

$$I_{1p} = jY_0 \left\{ \left[ \delta_p + Y_p^c \csc(2kLZ_p^c) \right] \left( \sum_t M_{pt} V_{2t}^+ - N_{2p} \right) - \left[ \delta_p + Y_p^c \cot(2kLZ_p^c) \right] \left( \sum_t M_{pt} V_{1t}^- - N_{1p} \right) \right\}$$

$$I_{2p} = jY_0 \left\{ \left[ \delta_p + Y_p^c \cot(2kLZ_p^c) \right] \left( \sum_t M_{pt} V_{2t}^+ - N_{2p} \right) - \left[ \delta_p + Y_p^c \csc(2kLZ_p^c) \right] \left( \sum_t M_{pt} V_{1t}^- - N_{1p} \right) \right\}$$

This can be written in the matrix formalism as:

$$\underline{I}_1 = jY_0 \left\{ \left[ \underline{\delta} + \underline{Y}^c \csc(2kL\underline{Z}^c) \right] \cdot \left( \underline{M} \underline{V}_2^+ - \underline{N}_2 \right) - \left[ \underline{\delta} + \underline{Y}^c \cot(2kL\underline{Z}^c) \right] \cdot \left( \underline{M} \underline{V}_1^- - \underline{N}_1 \right) \right\} \quad (\text{C.19})$$

$$\underline{I}_2 = jY_0 \left\{ \left[ \underline{\delta} + \underline{Y}^c \cot(2kL\underline{Z}^c) \right] \cdot \left( \underline{M} \underline{V}_2^+ - \underline{N}_2 \right) - \left[ \underline{\delta} + \underline{Y}^c \csc(2kL\underline{Z}^c) \right] \cdot \left( \underline{M} \underline{V}_1^- - \underline{N}_1 \right) \right\}$$



## Appendix D

### Modes of a Coaxial Cable

In this appendix we will give the expression of the Fields inside a coaxial waveguide. We will mainly discuss about the EM field transverse components ( $\vec{E}_t$  ed  $\vec{H}_t$ ) on which will be imposed the continuity condition. We will deal with a PEC waveguide, so we will not consider wall losses. It is possible to express the EM field separating the longitudinal components from the transverse ones:

$$\vec{E}(P) = \vec{E}_t(P) + E_z(P)\hat{z} \quad , \quad \vec{H}(P) = \vec{H}_t(P) + H_z(P)\hat{z} \quad (\text{D.1})$$

We can introduce a transverse cylindrical frame, which is perfectly suitable to the treated structure. Furthermore, we will use only TM modes ( $H_z=0$ ) which are the mainly excited modes in a particle accelerating machine. In this case we can express the EM field as follows [9,10]:

$$\begin{aligned} \vec{E}_t(P) &= \sum_n V_n(z)\vec{e}_n(r, \varphi) \\ \vec{H}_t(P) &= \sum_n I_n(z)\vec{h}_n(r, \varphi) \end{aligned} \quad (\text{D.2})$$

$$\begin{aligned} E_z(P) &= \frac{\zeta_0}{jk} \sum_n k_n I_n(z)\Phi_n(r, \varphi) \\ H_z(P) &= 0 \end{aligned} \quad (\text{D.3})$$

where  $\vec{e}_n(r, \varphi)$  e  $\vec{h}_n(r, \varphi)$  are the vector modal functions and  $V_n(z)$  e  $I_n(z)$  are the scalar excitation coefficients (scalar modal functions),  $k_n$  is the transverse eigenvalue,  $k$  is the propagation constant and  $\zeta_0$  is the characteristic impedance of the medium that fills the waveguide.

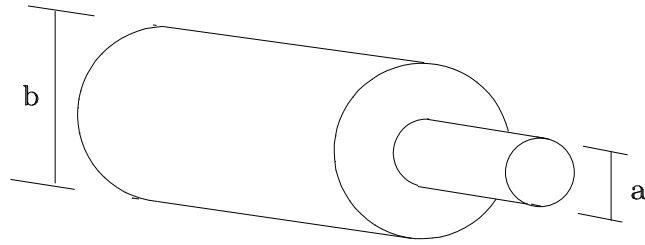


Fig. D-18. A coaxial cable

The excitation coefficients obey to the telegraphers Equations and can be expressed as a sum of a travelling wave and a scattering wave:

$$\begin{cases} \vec{E}_t(P) = \sum_n [V_n^+(z) + V_n^-(z)] \vec{e}_n(r, \varphi) \\ \vec{H}_t(P) = \frac{1}{\zeta_0} \sum_n \left[ \frac{V_n^+(z) - V_n^-(z)}{\zeta_n^w} \right] \vec{h}_n(r, \varphi) \end{cases} \quad (D.4)$$

The  $\zeta_n^w$  are the normalized modal impedances, and in a coaxial cable of external radius and internal radius 'b' and 'a' respectively, they are:

$$\zeta_n^w = \frac{\sqrt{(ka)^2 - w_n^2}}{ka} \quad w_n \leq ka \quad , \quad \zeta_n^w = -j \frac{\sqrt{w_n^2 - (ka)^2}}{ka} \quad w_n \geq ka \quad (\text{D.5})$$

where  $w_n$  are the zeros of the following equation:

$$x[J_0(\alpha x)Y_0(x) - J_0(x)Y_0(\alpha x)] = 0 \quad , \quad \alpha = \frac{b}{a} \quad (\text{D.6})$$

Resorting to the orthonormality property of the vector functions:

$$\int_{\Sigma} \hat{z} \cdot \vec{e}_n \times \vec{h}_m^* dS = \begin{cases} 1 & n = m \\ 0 & n \neq m \end{cases}$$

It is possible to express them as:

$$\vec{e}_m(r) = \hat{r} Z_1^w(k_m r) \quad , \quad \vec{h}_m(r) = \hat{\phi} Z_1^w(k_m r) \quad (\text{D.7})$$

where  $Z_1^w(k_m r)$  are linear combinations of Bessel Functions and  $w$  indicates the feeding guide [9]:

$$Z_1^w(k_m r) = \begin{cases} \frac{1}{r\sqrt{2\pi \ln(b/a)}} & m = 1 \\ \frac{w_m \sqrt{\pi} J_1(rw_m/a)Y_0(w_m) - J_0(w_m)Y_1(rw_m/a)}{2a \sqrt{J_0^2(w_m)/J_0^2(bw_m/a) - 1}} & m = 2, 3, \dots \end{cases} \quad (\text{D.8})$$

$Z_1^w(k_1 r)$  is the fundamental mode of the coaxial cable and it is a TEM mode. The modes corresponding to the others  $m$  are TM type modes.



## Bibliography

- [1] L. Palumbo, V. G. Vaccaro, M. Zobov, *Wake fields and impedance, LNF-94/041 Preprint*
- [2] Andrea Argan: *L'impedenza longitudinale negli acceleratori: Teoria e misura* 1996/1997.
- [3] G. Franceschetti: *Campi elettromagnetici*, Boringhieri 1988.
- [4] J.Van Bladel. *Electromagnetic Fields*, McGraw-Hill Book Company, 1964.
- [5] L. S. Gradshtein, I.M. Ryzhik; *Table of Integrals, Series and Products*; Academic press, 1980.
- [6] R. Mittra, W.W. Lee; *Analytical techniques in the theory of guided waves*; Macmillan, New York, 1971.
- [7] J. Meixner; *The behaviour of electromagnetic fields at edges*; IEEE Transactions on antennas and propagation 20, pp. 442 - 446, 1972.
- [8] M. Abramowitz, A. Stegun; *Handbook of Mathematical Functions*; Dover Publications, INC., New York.1970
- [9] D.Davino: *Analisi modale di una cavità a soppressione dei modi*, a.a. 1995/96
- [10] D.Davino, M. R. Masullo, V.G. Vaccaro, L. Verolino: *Coaxial-wire technique: A comparison between theory and experiment*, IL NUOVO CIMENTO, 1999

- [11] V. G. Vaccaro, *Coupling Impedance Measurements: An Improved Wire Method*, INFN/TC-94/023, 1994.
- [12] N. Marcuvitz, *Waveguide handbook*, IEE 1986